Thermohaline variability of AAIW in the Atlantic sector of the Southern Ocean investigated using an Altimetry Gravest Empirical Mode

Katherine Hutchinson

Dissertation presented for the co-badged degree of Masters of Science shared between the University of Cape Town and l'Université de Bretagne Occidentale

August 2013

Abstract.

The southeast Atlantic sector of the Southern Ocean connects the Atlantic with the Indian Ocean and the Antarctic Circumpolar Current, thereby acting as a major conduit within global ocean circulation. Thermohaline transports in this region are widely thought to have a critical influence on global climate. Yet magnitudes of the associated heat and salt content variations are poorly understood due to a lack of hydrographic observations and model limitations. An improved Gravest Empirical Mode (GEM) is set up for the Southern Ocean south of Africa using the updated store of hydrographic measurements obtained from CTD transects for the area, combined with the available Argo profiles sampled in the region. Satellite altimetry is combined with the GEM relationships to create an Altimetry GEM (AGEM), thereby generating 20 years of temperature and salinity fields. These thermohaline sections for the region of the ocean south of Africa are found to be proficient at reproducing observations, with associated RMS errors being two orders of magnitude smaller than those reported by other comparable Southern Ocean GEM studies. Confident in the accuracy of the AGEM produced fields, an examination of the temporal evolution of Antarctic Intermediate Water (AAIW) is undertaken. The fluctuation and trends in heat and salt content anomalies and budgets is presented for each Southern Ocean frontal zone, along with the examination of the change in position of the isopycnal limits and resultant water mass thickness. So as to better understand one of the factors that may be influencing some of the changes detected within AAIW, property alterations of eddies identified in the region from 1992 to 2010 are investigated. A general decrease in magnitude and frequency of cyclones, coupled with an increase in absolute dynamic topography (ADT) of anticyclones, designates elevated injection of warm, saline water into the area. The connection identified between eddy property variations and AAIW modification in the region of the ocean south of Africa indicates that the water mass experiences ventilation with the mixed layer at latitudes further north than previously thought to occur. Obtaining an improved image of the magnitudes and variability of AAIW thermohaline properties in the Atlantic sector of the Southern Ocean greatly improves our understanding of its role in the ocean-climate system.

Table of Contents

1. Introduction.

The Atlantic sector of the Southern Ocean plays an essential role in global ocean circulation and climate regulation, hosting the interaction between Indian, South Atlantic and Southern Ocean waters. The subsequent promotion of high levels of water mass mixing and transformation render this area to be globally one of the most dynamic ocean domains (Lutjeharms, 1996; Swart and Speich, 2010; Rintoul et al., 2010; Rimaud et el., 2012). The principal current flowing within the Southern Ocean is the Antarctic Circumpolar Current (ACC), which is the worldôs largest current (Rintoul et al., 2001; Killworth and Hughes, 2002). The area of the Southern Ocean south of Africa is where the ACC is found to experience the highest levels of variability (Swart et al., 2008). Despite the importance of this region within the global ocean-climate system, changes in thermohaline properties and water mass evolution in this sector are poorly understood. This is largely due to the scarcity of high resolution data and difficulties that exist when attempting to model such a dynamic arrangement (Ansorge et al., 2005; Speich and Arhan, 2007).

Antarctic Intermediate Water (AAIW) is widely thought to have a critical influence on ocean circulation and climate regulation. This water mass facilitates important transports of heat, freshwater, and biogeochemical tracers both vertically from the surface to the interior ocean, and meridionally from the Southern Ocean to the tropics (Sloyan and Rintoul, 2001; Pahnke et al., 2008). In the South Atlantic Ocean, AAIW forms an essential component of the upper limb of the Meridional Overturning Circulation (MOC), thereby implying global repercussions from local water mass alteration (Banks et al., 2000; Rimaud et al., 2012;)

The large scale variability experienced in the Atlantic sector of the Southern Ocean is thought to have a significant impact on the properties of AAIW located in the region (Sloyan and Rintoul, 2001; Rusciano et al., 2012). The water mass undergoes significant modification of its properties as it experiences high levels of mixing crossing from the South Atlantic to the South Indian Ocean (Rimaud et al., 2012). Warming has been detected within the AAIW layer throughout the worldôs oceans, however due to the scarcity of high resolution data for

the southeast Atlantic, the extent of water mass transformation in this area is poorly understood (Banks et al., 2000; Pahnke et al., 2008). The contribution of the Atlantic sector of the Southern Ocean to regulating climate, coupled with the influence of AAIW on the stability of the ocean circulation system, make obtaining a better view of the extent of property evolution in the area is of the utmost importance. Filling this gap in understanding is essential if we are to adequately inform and prepare ourselves for the impacts of a changing climate (Boning et al., 2008; Rintoul et al., 2010).

The traditional approach to observing the thermohaline properties within the ACC is through *in situ* hydrographic measurements. This process of data acquisition, however, is very resource intensive in the hostile environment of the Southern Ocean, and limited to short periods of the year. An investigation of the ACC density field, with sufficient resolution to avoid aliasing, is therefore very challenging (Sokolov et al., 2004). An alternative to this traditional observation method is to develop a proxy technique that establishes the relationships between the thermohaline properties and a variable that can be measured at a higher temporal and spatial resolution, in a way that requires fewer resources (Watts et al., 2001; Sokolov et al., 2004). This can be done via the creation of a Gravest Empirical Mode (GEM), and the subsequent generation of an Altimetry GEM (AGEM) via the coupling of the GEM relationships with satellite obtained sea surface dynamic height measurements (Swart et al., 2010). The ACC is ideal for the implementation of such a proxy relation due to its strongly baroclinic nature and associated steep meridional density gradients. This prescribes that columns of water largely maintain their vertical structure during horizontal displacements (Meijers et al., 2011b).

An AGEM has been established for the southeast Atlantic by Swart et al. (2010), however this technique was based on hydrographic data from only 7 CTD transects of the ACC. Since the launch of the Array for Real-time Geostrophic Oceanography (ARGO: Roemich and Owens 2000; Roemich et al. 2004) profiling float project in 2000, there has been an enormous augmentation of thermohaline measurements available for the global ocean. Data availability for the region of the Southern Ocean south of Africa has been subsequently greatly improved post-2004 due to the float deployments undertaken under the auspices of the GoodHope CLIVAR project. Via the inclusion of updated cruise CTD data, and the

introduction of Argo float measurements, along with the implementation of various improvements to the GEM method, an ñupgradedò GEM can be created for the Atlantic sector of the Southern Ocean. By coupling this GEM with 20 years of satellite sea surface height measurements, an AGEM can be obtained. The resultant AGEM produced temperature and salinity fields can be used to investigate the temporal evolution of AAIW, thereby greatly improving understanding of the changes this water mass has experienced over the past two decades.

2. Research Review.

2.1 The Southern Ocean.

The Southern Ocean is vital to Earthôs ocean-climate system as it plays a critical role in global ocean circulation and water mass transformation (Rintoul et al., 2002; Rintoul et al., 2010). The predominant flow situated within the Southern Ocean, is the worldôs largest current, the Antarctic Circumpolar Current (ACC) (Rintoul et al., 2001; Killworth and Hughes, 2002). The ACC flows uninterrupted around Antarctica, and in doing so is the primary means by which heat and salt are transported between the three main ocean basins. This current is therefore an essential limb of the ocean ñconveyor beltò- the global Meridional Overturning Circulation (MOC) (Rintoul et al., 2002; Swart et al., 2008). As the MOC is largely responsible for regulating Earthôs climate, any changes in the ACC and the Southern Ocean have dramatic global repercussions (Speich et al., 2001).

Recent studies have shown that there has been a significant warming of the worldôs oceans in the past 50 years. On a global scale, ocean heat content has increased by 2×10^{23} J from the mid-1950s to the mid-1990s (Levitus et al., 2000). It is thought that the Southern Ocean is warming at a rate faster than the global average, and that this warming is largely localized to the ACC (Gille, 2002; Gille, 2008). However, the high sea states and incredibly strong winds experienced in the Southern Ocean have hampered the acquisition of high-resolution hydrographical samples (Sokolov et al., 2004; Swart et al., 2010). The resultant large data gaps impede scientistsô ability to accurately assess the Southern Oceanôs response to and influence on changing climate.

Climate anomalies experienced at the surface of the Southern Ocean are transmitted into the interior via strongly sloping isopycnal surfaces associated with the ACC. This region thereby acts as a ñwindowò connecting the atmosphere with the deep ocean (Santoso and England, 2004). In doing so, the Southern Ocean not only sustains essential thermohaline transports, but allows for significant air-sea exchange of atmospheric gasses (Boning et al., 2008). Approximately 40% of anthropogenic CO_2 is sequestered by the Southern Ocean. However, as the water warms its ability to hold a dissolved gas is reduced thereby decreasing the CO_2 storage capacity (Gille, 2002; Lovenduski and Ito, 2009).

Due to the integral role of the Southern Ocean in global circulation, the recent changes experienced in this region are predicted to manifest themselves throughout the globeôs oceans in future years. The evolution of climate under increasing greenhouse gas emissions will be strongly influenced by conditions within the Southern Ocean (Boning et al., 2008; Rintoul et al., 2010). Obtaining a better view of these conditions is crucial if we are to accurately forecast, and in turn, adequately prepare ourselves for the impacts of climate change.

2.2 Use of proxy methods to observe the Southern Ocean.

The traditional observational methodology of the ACC density field is through the acquisition of temperature and salinity profiles via hydrographic sections from research vessels. The financial and human resource intensive nature of this data procurement means that it is highly challenging to monitor the current with sufficient resolution to avoid aliasing (Sokolov et al., 2004). An alternative approach to these customary methods is to develop a proxy technique based on a variable that can be measured at a higher spatial and temporal resolution, and in a manner that requires fewer resources (Watts et al., 2001; Sokolov et al., 2004). It may seem counter-intuitive to estimate the profile of a water column from one single proxy measurement, but in fact this approximation is based on correlations from numerous hydrocasts, and is thus highly representative of the variability encountered (Watts et al., 2001).

2.2.2 What is a proxy method?

The deduction of one variable that has not been sampled, through the knowledge of its relationship with another observed variable, is called a proxy technique (Watts et al., 2001;

Meinen, 2001). One of the first examples of using a proxy method in oceanography was the use of the Temperature-Salinity (T-S) correlation for dynamic height computations developed by Stommel (1947). In certain parts of the ocean, temperature and salinity are so tightly correlated, that salinity is a function of temperature. In these areas, where the T-S curve is well defined, dynamic height can be computed using temperature observations alone (Stommel, 1947).

2.2.3 Proxy methods within the ACC.

The regional T-S curve for the ACC is not well-defined, as temperature and salinity vary significantly with latitude (Rintoul et al., 1997). This is evident in the steep thermohaline gradients which dominate the ACC, thereby giving rise to the presence of baroclinic fronts (Sun and Watts, 2001). The strong meridional density gradient and the baroclinic nature of variability within the ACC make it ideal for the implementation of proxy methods (Meijers et al., 2011a). Particular contours of absolute sea surface height (SSH) can be regarded as ñstreamlinesò, and the location of these streamlines correlate strongly with the position of the frontal jets (Sokolov and Rintoul, 2007). The T-S curve can be considered to be regular along these streamlines as the T-S relation is steady with time (Sokolov et al., 2004). Consequently, it is possible to estimate dynamic height at a certain point using the temperature profile alone (Rintoul et al., 1997; Swart et al., 2008).

Rintoul et al. (1997) was the first to exploit the strong relation between temperature and dynamic height in the region of the ACC between Tasmania and Antarctica. Using 13 repeat hydrographic sections of the region occupied between 1991 and 1994, the relationship between the average temperature of the top 600m of the water column and the dynamic height at the sea surface relative to 2000m was obtained. This relationship is shown in Figure 2.1a. By projecting the hydrographic measurements onto a stream function coordinate, such as dynamic height, a temporal mean known as the ñmodalò field is produced (Sun and Watts, 2001).

One of the first proxy methods to produce data of sufficient time extent and continuity to allow the ACC variability to be appropriately examined was that developed by Rintoul et al. (2002). An empirical relationship between upper ocean temperature and baroclinic transport stream function was established using 31 XBT sections of the ACC south of Tasmania from

1993-1999. A second relation between altimeter SSH and cumulative transport produced an estimate of baroclinic transport through the Australian choke point at a temporal resolution of every 10 days (Rintoul et al., 2002).

The tight relationship between temperature and stream function throughout the whole Southern Ocean later allowed Sokolov et al. (2004) to use hydrographic sections across the ACC in the Drake Passage to obtain baroclinic transport estimates. In total, 4 transects of the segment of the ACC south of South America between 1993 and 2002 were used to attain transport measurements that, when cross referenced with observations, were found to be reliable with an error of under 4Sv (Sokolov et al., 2004).

Legeais et al. (2005) estimated the baroclinic transport of the ACC south of Africa using the same proxy relation between XBT temperature and transport that Rintoul et al. (2002) and Sokolov et al. (2004) used. Upon comparison of the transport results with those computed from geostrophy, the values inferred from the proxy relation were on average 1.3Sv too large, an overestimation well within the geostrophic error bars (Legeais et al., 2005). Swart et al. (2008) later established a relationship between temperature and dynamic height from CTD data also for the region of the ACC south of Africa. The proxy correlation used by Swart et al. (2008) was found to be very robust with a correlation coefficient of $r = 0.95$, significant at the 95% confidence level. This relationship can be seen in Figure 2.1b. These descriptions of the intensity of the ACC in the African choke point are valuable contributions to improving our understanding of the ACC dynamics and its role in thermohaline circulation.

The work of Baker-Yeboah et al. (2009) for the southeast South Atlantic is a another good example of the use of proxy techniques, albeit the investigation region was located north of the ACC. Variability in SSH was observed using measurements obtained by pressure sensor-equipped echo sounders (PIES) located along the Jason-1 ground track crossing the Agulhas leakage eddy corridor as part of the Agulhas South Atlantic Thermohaline Experiment (ASTTEX). The relative contributions of the baroclinic and barotropic changes to these SSH variations were then decomposed (Baker-Yeboah et al., 2009). The baroclinic portion was calculated from the measured vertical acoustic travel time converted to geopotential height using a lookup curve based on regional hydrography. The largest errors in the derived solution were found to stem from scatter in the lookup curve which is characteristic of areas where different water masses interact (Baker-Yeboah et al., 2009). This finding indicated the

importance of employing caution when using GEM type proxy techniques in areas where waters with very different properties converge and interleave, thereby contributing different temperature and salinity profiles corresponding to the same surface value of dynamic height.

a) b)

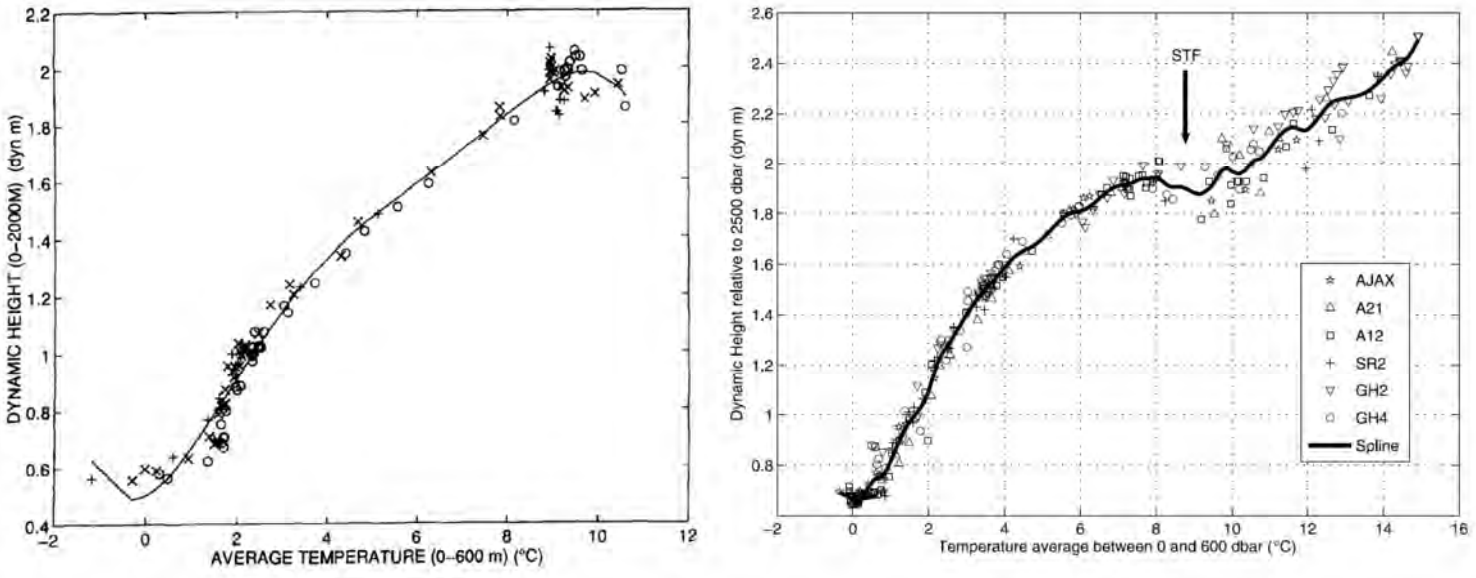

Figure 2.1 a) Dynamic height (0-2000m) plotted against vertically averaged temperature (0-600m) for the region of the ACC south of Tasmania. The solid curve shows a fifth order polynomial fit to the data. b) Dynamic height (0-2500m) plotted against vertically averaged temperature (0-600m) for the region of the ACC south of Africa. The solid curve depicts a smoothing spline fit to the data.
Source: a) Sokolov et al., 1997 ; b) Swart et al., 2008

2.3 The ACC as an equivalent-barotropic jet.

For geophysical flows of significantly large spatial scale, the meridional gradient of the Beta effect (planetary vorticity) provides a restoring force which works to organize the flow into persistent narrow jets (Sokolov and Rintoul, 2007). On earth, the oceanic flows that fall into the scale range that is conducive to the formation of jets are usually disrupted by land barriers. However, the ACC circumnavigates Antarctica uninterrupted by continental boundaries, therefore the zonation of the flow results in the production of jets known as fronts (Sokolov and Rintoul, 2007). These jets are found to be consistently aligned with particular SSH contours (streamlines), and therefore correspond to an almost constant value of dynamic height (Sokolov and Rintoul, 2002; Sokolov and Rintoul, 2009). The ACC takes an

equivalent-barotropic form as it is a strong flow where the velocity does not vary significantly with depth, and where all quantities are approximately constant along a characteristic streamline (Killworth and Hughes, 2002). Since the SSH contours approximate streamlines in the equivalent-barotropic flow of the ACC, and the streamlines also correspond to a particular water column structure in such a flow, the SSH value at a point can indicate the properties of the underlying water column and vice versa (Watts et al., 2001).

2.4 Development of a GEM for the ACC.

To represent the vertical structure of a continuously stratified ocean, the ñGravest Baroclinic Modeò is often used. However, in the Southern Ocean the basic state changes greatly, and thus the water column cannot be represented by projecting all variability onto a single vertical mode (Watts et al., 2001). The solution is to employ a technique developed by Meinen and Watts (2000) in the Newfoundland Basin. Meinen and Watts (2000) presented a method for obtaining a time series of full water column profiles of temperature and specific volume anomaly using historic acoustic travel time measurements. This method is named a ñGravest Empirical Modeò (GEM) as it makes no assumptions regarding the vertical structure of the water column, but rather uses an empirical fit of historical hydrographic data (Meinen and Watts, 2000). By using the GEM fields in conjunction with a time series of acoustic travel time measurements, synoptic and time averaged views of the current structure and temperature profile can be obtained. This time series is more valuable than one single snapshot of conditions provided by an individual CTD station or transect (Meinen and Watts, 2000; Sun and Watts, 2002a).

Watts et al. (2001) was the first to apply this GEM method to the ACC. This was done for the region south of Australia. In this area, the geopotential (dynamic) height at the sea surface was found to exhibit a tight empirical relationship with acoustic travel time, and in turn to temperature and salinity in this region (Watts et al., 2001). Measurements of acoustic travel time therefore allow for the proximate estimation of the thermohaline properties of the water column using a two dimensional (2D) GEM. The frontal and water mass features of varying spatial scales that characterize the ACC in this region provide a demanding test for the GEM proxy technique. The GEM however, proved its applicability, as a striking 96% of the variance was found to be captured in the depth range of 150-3000dbar of the GEM produced

fields (Watts et al., 2001). Figure 2.2 shows the two dimensional GEM fields produced for temperature and salinity.

Watts et al. (2001) suggested that GEM fields can be parameterized by geopotential thickness (a baroclinic stream function) instead of acoustic travel time. The success of this substitution indicates why the GEM ñworksò so well in the Southern Ocean. Using geopotential (dynamic) height coordinates takes advantage of the strong meridional gradients in the ACC, and its consequential equivalent barotropic form whereby columns of water maintain their vertical structure during horizontal movements (Meijers et al., 2011b). This however is subject to the assumption that the thickness of the water column is dominated by its baroclinic (steric) component, meaning that water properties and processes along a stream function have an almost identical vertical structure (Watts et al., 2001). As a result of this, the error in the GEM is highest in regions were different waters converge, thereby contributing different properties along the same streamline at different times (Swart et al., 2010).

The GEM dominance does not apply only to the ACC, but also to other mid and high-latitude baroclinic currents where geostrophy governs the dynamic balance (Sun and Watts, 2001). The GEM method has likewise been shown to work well in the North Atlantic current by Meinen (2001) and in the Kuroshio by Book (2002).

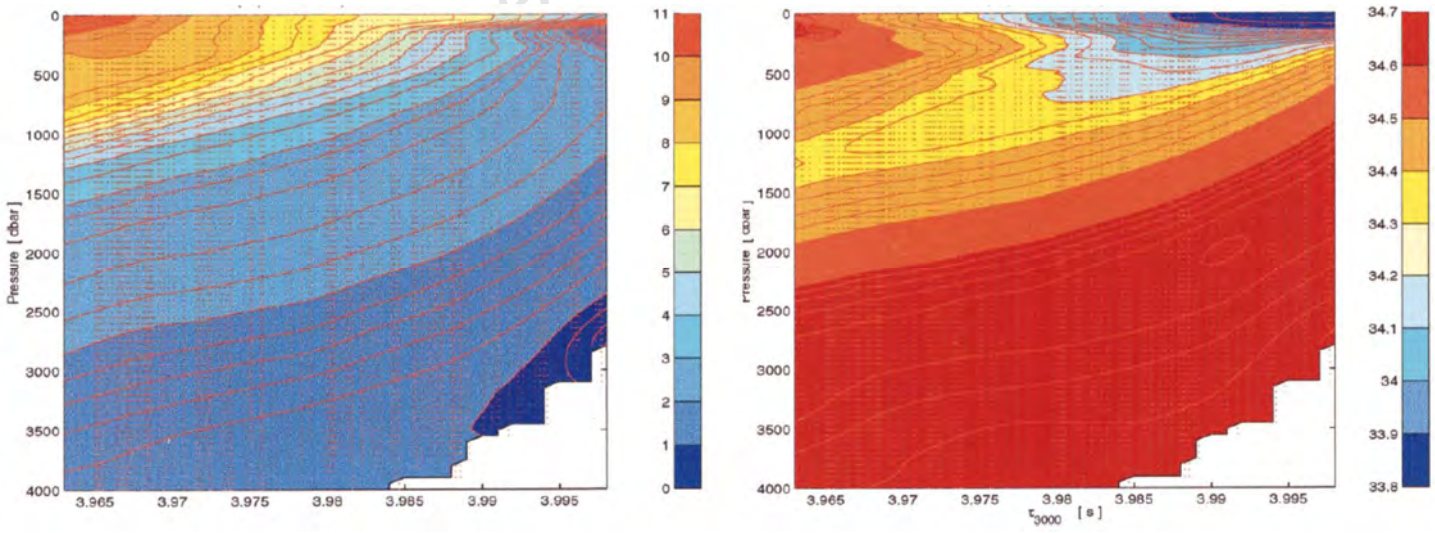

Figure 2.2 a) Temperature GEM field in ^{o}C, parameterized by pressure and acoustic travel time relative to 3000bar. Dots indicate the positions of the CTD data, but only at every 50dbar so as to avoid dominating the plot. b) Same as (a) but for Salinity in psu. Source: Watts et al., 2001.

2.4.1 Three dimensional GEM.

A three dimensional (3D) projection can be produced by a simple extension of the GEM technique in space. The first such example was established by Sun and Watts (2001) where a 3D Southern Ocean GEM was created by projecting hydrographic measurements into stream function space parameterized by pressure, geopotential height and longitude. The data used to set up the 3D GEM was a synthesis of all circumpolar hydrographic stations compiled by the Alfred Wegener Institute (Olbers et al., 1992). The data spans the time period of 1900-1990, with a strong seasonal summer bias and a spatial bias of the densest data located in the Drake Passage (Sun and Watts, 2002a). Despite these biases, the resultant 3D GEM is able to capture an astounding 97% of the total density variance of the ACC. The success of the GEM technique in the ACC region denotes that the thermohaline fields are nearly rigid in stream function space (Sun and Watts, 2002b). The resultant GEM temperature fields produced for 6 latitude sections of the ACC can be seen in Figure 2.3. These projections, along with their matching salinity counterparts, do not contain a temporal dimension and therefore represent the steady part of the ACC thermohaline field (Sun and Watts, 2001). To now add a time parameter to the field is quite a simple process of dimension decomposition. Once the time-invariant GEM field is known (as shown in Figure 2.3), the task of determining a time-dependent 3D field is reduced to a 2D one, i.e. the spatial distribution of the specific stream function (geopotential height) with time (Sun and Watts, 2001).

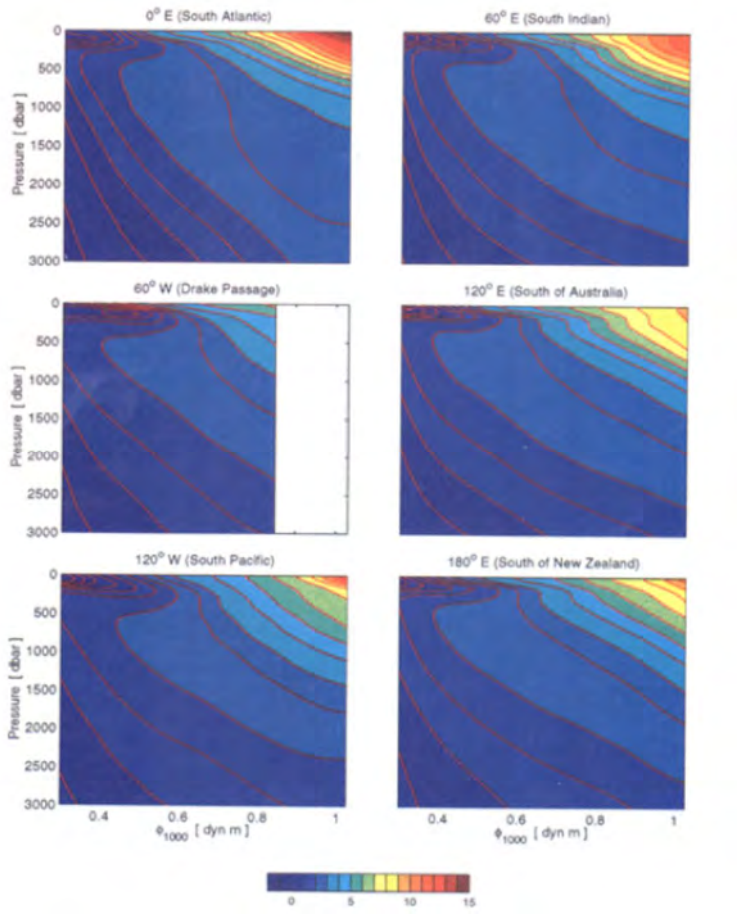

Figure 2.3 Meridional sections of the circumpolar GEM temperature (^{o}C) field parameterized by pressure and geopotential height at 100dbar relative to 1000dbar at six equally spaced longitudes around the Southern Ocean.
Source: Sun and Watts, 2001

2.4.2 Adding the dimension of time.

A four dimensional (4D) GEM can be produced by coupling the static circumpolar GEM with satellite altimetry, thereby creating an Altimetry GEM: ñAGEMò, or satellite GEM: ñsatGEMò, depending on which nomenclature is preferred. Meijers et al. (2011a) developed one such satGEM set up using historical hydrography combined with Argo profiling float data. Satellite data is available for the Southern Ocean since 1992. By combining this dynamic height data from 1992-2006 with GEM projections of temperature and salinity, Meijers et al. (2011a) produced thermohaline fields at weekly time intervals with a spatial resolution of 1/3^{o}, and 36 depths. These satellite derived fields were found to capture over 96% of the temperature variance, 90% of the salinity variance and with Root Mean Square (RMS) residuals of 0.45 ^{o}C and 0.05 psu below 500 dbar (Meijers et al., 2011a). The percentage variability captured by the satGEM fields is shown in Figure 2.4. The variability captured drops from the GEM to the satGEM due to errors introduced by instrument noise within the altimeter, data processing, sampling resolution, and interpolation (Meijers et al., 2011b). The high resolution of the SSH data enables the observation of filaments in fronts and eddy features from the GEM produced fieldsï this is extraordinarily valuable in improving our understanding of the 4D structure of the Southern Ocean. Even though errors exist in the satGEM projections, these fields are significantly more accurate than traditional climatology (Meijers et al., 2011a).

The GEM fields were subsequently used by Meijers et al. (2011a) to estimate full depth geostrophic velocity fields, and by Meijers et al. (2011b) to observe frontal movements and property fluxes. Meijers et al. (2011b) used the GEM and satGEM to separate observed trends into diabatic and adiabatic changes. The satGEM effectively laterally moves an entire column of water in response to a change in dynamic height, therefore trends detected using this mode can be attributed to adiabatic shifts in the circumpolar fronts. The residuals between the static GEM and the hydrography, on the other hand, provide an indication of the diabatic changes of water mass properties with time (Meijers et al., 2011b). By combining the

adiabatic and diabatic components, Meijers et al. (2011b) found a net increase in both heat and freshwater of 0.570 ± 0.099 $W.m^{-2}$, and 36.91 ± 0.72 $mm.yr^{-1}$ respectively. The adiabatic and diabatic portions of this warming and freshening trend are assessed separately and in significant detail thereby allowing, for the first time, the separate contributions of these components to be better understood (Meijers et al., 2011b).

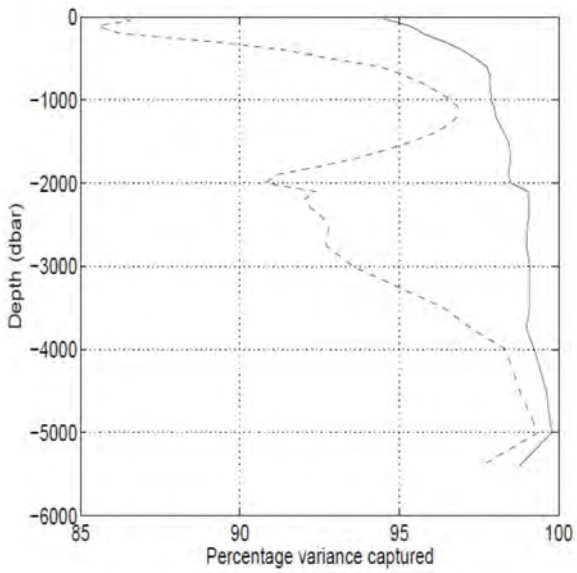

Figure 2.4. The percentage of circumpolar data variance with depth captured by the Southern Ocean satGEM fields for temperature (solid line) and salinity (dashed line).
Source: Meijers et al., 2011a

2.5 Benefits and restrictions of the GEM technique.

2.5.1 Advantages.

The GEM technique enables the use of any profile in the study region, regardless of whether it is an isolated cast or part of a synoptic section. This permits the synthesizing of many historic casts that have not been included in past Southern Ocean thermohaline studies as they were not located upon a repeat transect (Sun and Watts, 2002a). In doing so, the GEM has more reference points for the proxy relationship and thus can better represent the variability observed in the region (Watts et al., 2001). An additional advantage is that by using a circumpolar GEM, it is possible to observe thermohaline properties in regions that are seldom occupied by hydrographic surveys. Other oceanographic parameters can subsequently be

calculated from the GEM temperature and salinity fields, such as mass, heat and freshwater fluxes (Meijers et al., 2011).

The GEM is surprisingly successful in capturing the variability observed in the ACC as it is able to smooth over small, transient events but retains all hydrographic features that appear repeatedly in stream function space (Sun and Watts, 2002b). An example of this is the GEMôs ability to capture the persistent sharp, shallow thermocline below the surface mixed layer as seen by Watts et al. (2001). The resultant modal field, with the absence of transient features, is ideal for general circulation studies (Sun and Watts, 2002a; Swart et al., 2010)

As a projection, the GEM is by definition steady in stream function space, even though the streamline pattern changes with time. Furthermore, the geostrophic stream function is a vertically integrated property, therefore ensuring that the projected field is vertically coherent (Sun and Watts, 2002a).

2.5.2 Disadvantages.

A significant restriction of the GEM is its weakness in areas where waters converge and interleave (Meijers et al., 2011a). Regions such as the Cape Basin, for example, are therefore very challenging to represent in a GEM projection due to presence of mixing of many different water masses (Swart et al., 2010). The GEM proxy relation is founded on the principal that in equivalent barotropic flows, one single measurement of, say dynamic height, corresponds to set temperature and salinity profiles at that location. In areas of mixing of waters with significantly different properties, the GEM residuals are increased as different thermohaline signatures exist along the same streamline path at different times (Watts et al., 2001). Barotropic variations are also not captured in the GEM fields. The resultant temperature and salinity variability only reflect the baroclinic component, thereby somewhat restricting the GEM application (Meijers et al., 2011).

2.6 A GEM for the African choke point.

The southeast Atlantic sector of the Southern Ocean is thought to be one of the most dynamic ocean domains of the world as it hosts the convergence of Indian, South Atlantic and Southern Ocean waters (Swart and Speich, 2010; Rimaud et el., 2012). The segment of

the Southern Ocean to the south of Africa is also the most variable choke point of the ACC (Swart et al., 2008). The importance of this area to global ocean circulation is further highlighted by the widely accepted theory that the upper branch of the Atlantic MOC (AMOC) originates in the southeast Atlantic, where waters from the Agulhas Current mix with those of the South Atlantic Current (Rimaud et al., 2012). Despite its global significance, this area happens to be the least investigated of all the three passages to the south of the Southern Hemisphere continents (Legeais et al., 2005).

2.6.1 Developing a GEM south of Africa.

A two dimensional (2D) GEM parameterized by pressure and dynamic height was developed by Swart et al. (2010) for the region of the ACC south of Africa. The GEM itself is 2D, as the projection applies to only one longitudinal transect centered on the Good Hope line. However the projected temperature (T) and salinity (S) fields are time evolving as they are updated on a weekly basis using satellite altimetry, thereby creating what Swart et al. (2010) calls an Altimetry GEM (AGEM). A 16 year time series of thermohaline fields is produced which captures more than 97% of the density variance in the region (Swart et al., 2010). In total 8 CTD sections were used to set up the GEM projection, with 199 stations located within the ACC domain, spanning the time period 1984 to 2005. The dynamic height at the surface was referenced to 2500 dbar, as this is the depth of the mid-ocean ridge and allows for the use of non-full-depth data (Swart et al., 2010).

When compared with cruise data, the AGEM sections were found to be remarkably similar to the observations, as can be seen in Figure 2.5. The water mass boundaries are well captured and the major mesoscale features accurately represented. The RMS differences (Figure 2.5c) are highest in the surface layer (due to atmospheric interactions), and in the northern part of the transect (due to the influence of the Agulhas retroflection and resultant mixing of considerably different water masses) (Swart et al., 2010).

The weekly T and S fields produced by this AGEM were further exploited by Swart and Speich (2010) in order to better understand the dynamic nature of the Southern Ocean fronts south of Africa. The generated AGEM fields are the longest time series of thermohaline data available for the African sector of the Southern Ocean. This data is consequently very valuable in improving our knowledge of such a globally important and dynamic region.

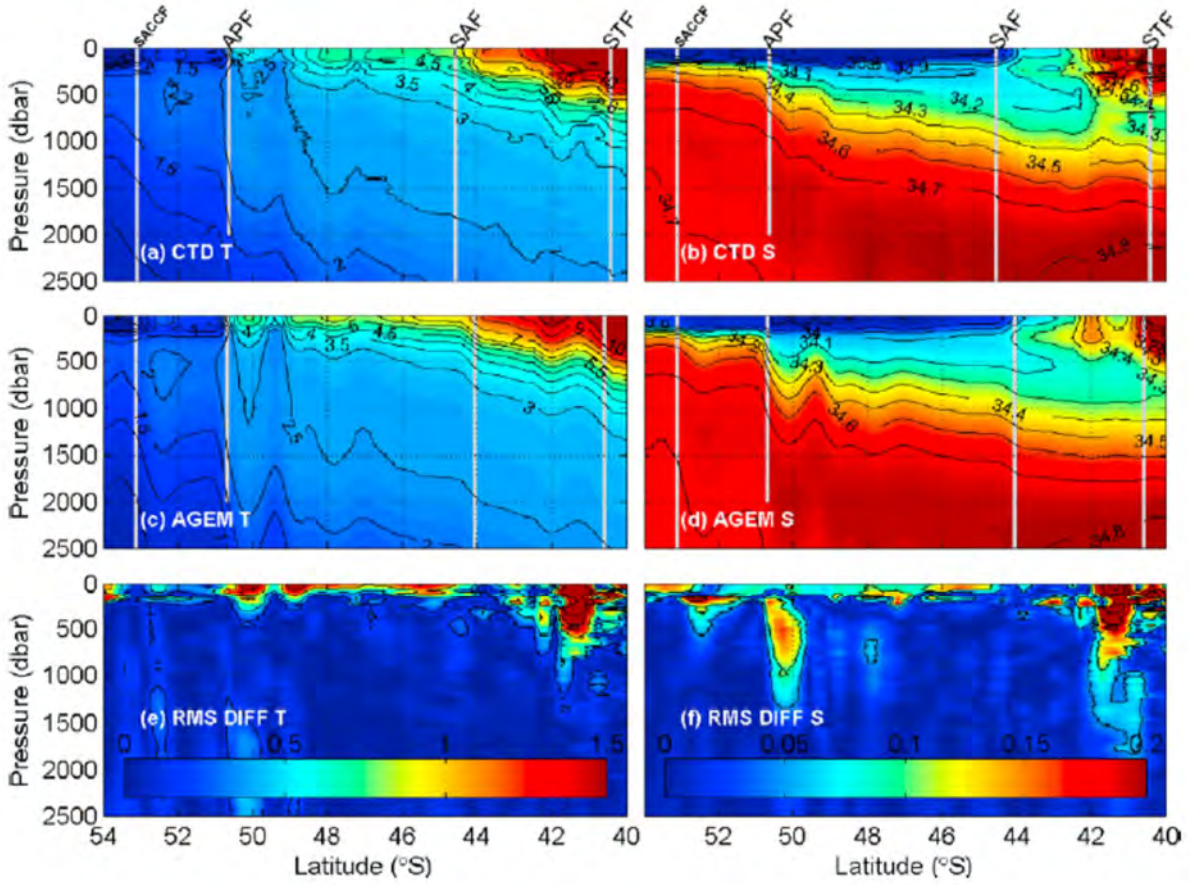

Figure 2.5. Comparison of the observed (a) temperature (^{o}C) and (b) salinity (psu) cruise sections with the AGEM produced (c) temperature and (d) salinity fields. The RMS difference between the cruise and AGEM fields are displayed for (e) temperature and (f) salinity. The ACC front locations determined using the Orsi et al. (1995) criteria, are indicated by the vertical grey lines.
Source: Swart et al., 2010.

2.6.2 Mesoscale variability in the southeast Atlantic.

The Agulhas Current has a volume transport of the same order as the Gulf Stream, with the entire current system exhibiting the highest ocean variability found in the Southern Hemisphere (Feron et al., 1992). At approximately 36^{o}S, the Agulhas splits from the continental shelf and develops oscillations of progressively increasing amplitude (Biastoch et al., 2009). A schematic of the region showing the dominant flow patterns of the upper and intermediate layers is presented in Figure 2.6. Between 16^{o}E and 20^{o}E, the current then reflects back toward the Indian Ocean in an almost opposite direction to its original flow, this current is named the Agulhas Return Current (Peterson and Stramma, 1991). During this

process, the current loop occasionally closes in on itself, thereby leaking some warm and saline Indian Ocean water into the Atlantic in the form of a pinched off Agulhas Ring (Feron et al., 1992; Dencausse et al., 2010a). These anti-cyclonic features and their concomitant cyclonic counterparts (formed within the Cape Basin along the continental shelf) are thought to be highly important for inter-ocean exchanges (Boebel et al., 2003; Biastoch et al., 2009; Rimaud et al., 2012). This mixing of water south of Africa is thought to play a key role in the ventilation of the Atlantic and Indian Ocean thermoclines (Lutjeharms and Ballegooyen, 1988).

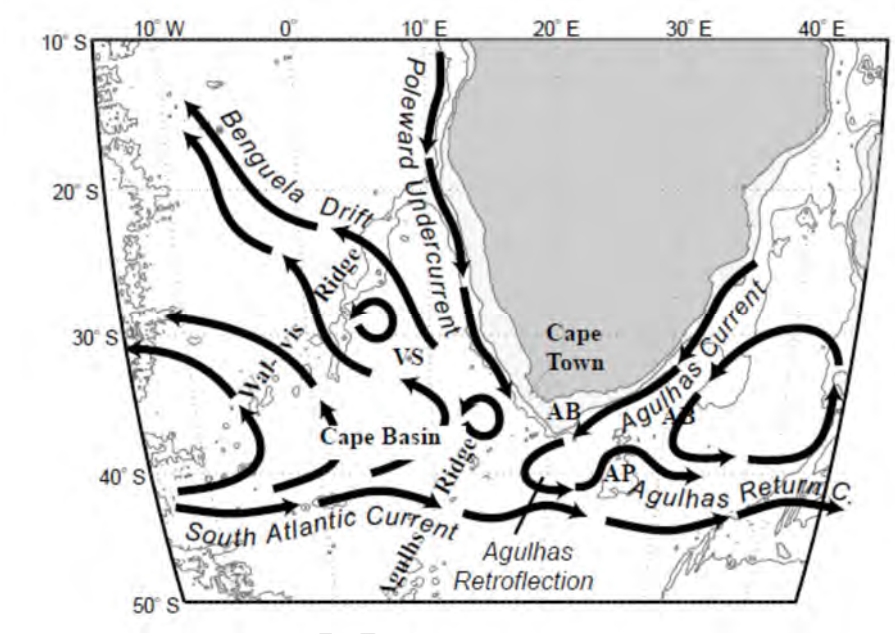

Figure 2.6 Diagram depicting the ocean flow patterns around southern Africa for upper and intermediate water layers.
Source: Boebel et al., 2003

Eddies found in the southeast Atlantic are thought to significantly influence the formation rates and properties of water masses that are critical to the MOC. Their values of available potential energy rate them amongst the most energetic ring features observed in the worldôs oceans (Goni et al., 1997). These rings are deep reaching, indicated by the ability of juvenile features to trap water to up to 1600m depth (Dencausse et al., 2010b). In addition to the actual fluid transported via these features from the Indian to the Atlantic Ocean, eddies act as diffusive systems through the production of filaments pulling fluid across the mean geostrophic contours in the region (Goni et al., 1997). Both cyclones and anti-cyclones are known to generally extend through the upper thermocline and into the intermediate depth

layer. Anti-cyclones are commonly known as Agulhas Rings and typically are 200km in diameter. These positive sea surface height anomalies are often observed to merge, split, deform and reconnect around the Agulhas retroflection (Boebel et al., 2003). The cyclones typical of the area, on the other hand, are slightly more numerous and smaller in diameter. They form inshore of the Agulhas current and drift south across the path of the Agulhas Rings. The interaction between cyclones and anti-cyclones promotes vigorous mixing processes, highly important for inter-ocean exchange (Beobel et al., 2003).

Eddies shed by the Agulhas Retroflection subsequently follow three routes: a northern path that enters the South Atlantic equatorward of the Erica seamount, a central one that passes between the seamount and the tip of the Agulhas ridge, and a southern trajectory. The southernmost rings of the central route are thought to reside at the approximate location of the Subtropical Front, while the rings of the southern path actually transit through to the Subantarctic domain (Dencausse et al., 2010b). Lutjeharms and Ballegooyen (1988) were the first to suggest that the meridional propagation of eddies across the STF is an essential mechanism for the transport of heat into the Southern Ocean. The poleward heat flux facilitated by these eddies, balances the heat lost to the atmosphere at higher latitudes. The longest and highest scales of variability within the Subantarctic Zone (SAZ) south of Africa are driven principally by the presence of Agulhas rings which penetrate the region approximately 2.7 times a year. In turn, the variability within the SAZ is responsible for over 50% and 60% of the respective heat and salt content variations within the ACC (Swart and Speich, 2010).

Poleward of the SAZ, the variability is largely dominated by frontal meandering, explained by the conservation of potential vorticity in response to the disturbance in flow caused by local topography. A large frontal meander can become an isolated ring system, thereby generating high levels of eddy kinetic energy (Meredith and Hogg, 2006). In the southeast Atlantic sector of the Southern Ocean, the Subantarctic Front (SAF) experiences fragmentation leading to the subsequent birth of meanders and eddies, due to the loss of topographic control downstream of the Mid-Ocean Ridge (Swart and Speich, 2010). Eddy genesis as a product of frontal meandering is vital in influencing local dynamics and meridional fluxes of heat and salt within the Southern Ocean (Swart and Speich, 2010).

The magnitude of variability in the region of the Southern Ocean south of Africa is clearly visible in Figure 2.7 which exposes the turbulent character of this area (Sokolov and Rintoul, 2009). The eddy kinetic energy in this region is higher than anywhere else in the Southern Hemisphere, with on average 6 to 9 eddies shed per year (Peterson and Stramma, 1991; Feron et al., 1992; Goni et al., 1997). These mesoscale eddies provide some of the largest rapid non-tidal variations in sea surface height (SSH) observed by altimeters (Baker-Yeboah et al., 2009). The Agulhas Current, the Retroflection, and the ensuing production of rings can be seen in the dark maroon shading of SSH gradient. The large amplitudes of the meanders of the Southern Ocean fronts can also be observed, along with the intermittent consequential creation of an eddy (Figure 2.7).

Recent observations have seen an enhancement of the Southern Ocean eddy field in response to increased zonal wind stress (Meredith and Hogg, 2006). Water mass transformation takes place throughout the southeast Atlantic oceanic domain, but is significantly intensified in regions of ubiquitous mesoscale activity (Garzoli and Matano, 2011). This area must therefore be considered an active region of water mass alteration, thereby implying global implications for the local variability (Rimaud et al., 2012).

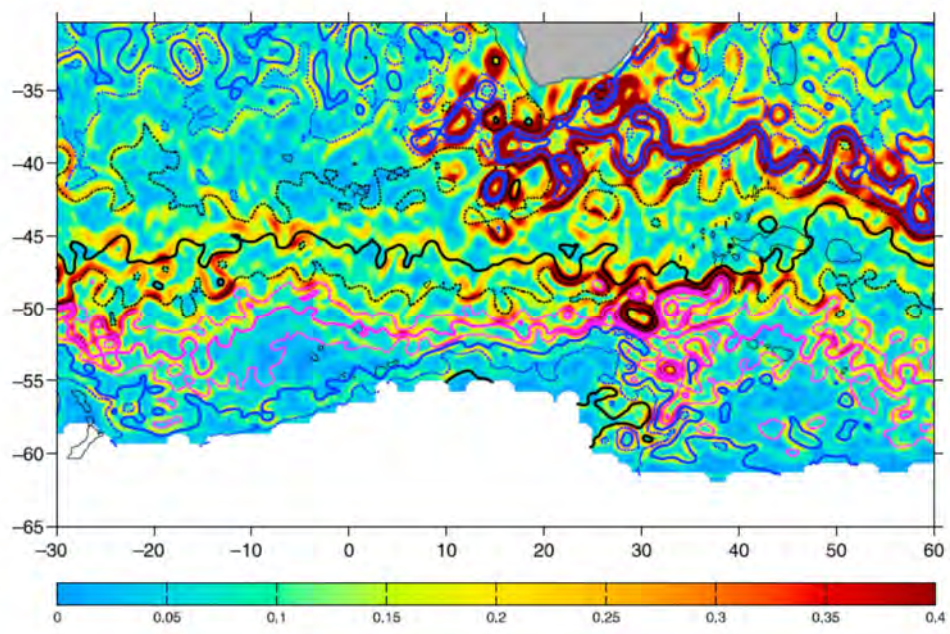

Figure 2.7 A typical SSH gradient field south of Africa (11 October 2000), overlaid with the synoptic positions of the SSH contours of each front derived from the 15 year time period of altimetry observations. The fronts are color coded from north to south as follows: STF (blue), SAF (black), APF (magenta), SACCF (blue), and SBdy (black).

Source: Sokolov and Rintoul, 2009

2.7 Antarctic Intermediate Water.

2.7.1 Synopsis of the water mass.

Throughout the Southern Ocean, Antarctic Intermediate Water (AAIW) is identified as a salinity minimum layer, a ñtongueò, that descends across the SAF into the Subantarctic Zone (Sun and Watts, 2002; Santoso and England, 2004; Rusciano et al., 2012; Rimaud et al., 2012). The core of AAIW is closest to the surface just north of the APF, and deepens as the water mass subducts below the thermocline and flows northwards at intermediate depths, diving to approximately 1000dbar in the mid-latitudes (Piola and Georgi, 1982; Sloyan and Rintoul, 2001; Rusciano et al., 2012; Rimaud et al., 2012). In doing so, AAIW transfers heat and freshwater from the surface into the interior ocean (Banks et al., 2000). Based on all properties, the complete AAIW layer can be found within the isopycnal boundaries of 1027.0kg.m^{-3} to 1027.4kg.m^{-3} (Talley, 1996).

There is much debate regarding the various formation mechanisms of AAIW (Sun and Watts, 2002). The two dominant opposing formation theories are either thermohaline driven circulation, or wind driven convergence (Piola and Georgi, 1982). Sverdrup et al. (1942) stated that given the circumpolar presence of AAIW, it is likely formed via the subduction of surface water along the APF. However, Mc Cartney (1982) contrasted this theory by proposing that AAIW is a bi-product of Subantarctic Mode Water (SAMW), formed in a deep convective cell located in the southeast Pacific. Regardless of the formation mechanism, it is widely accepted that the properties of the AAIW layer are largely controlled by variability in circumpolar air-sea heat and freshwater fluxes, and sea ice melting rates (Santoso and England, 2004).

AAIW in the South Atlantic sector of the Southern Ocean forms part of the returning upper limb of the MOC to the North Atlantic, and is subsequently one of the major sources in the formation of North Atlantic Deep Water (NADW) (Sloyan and Rintoul, 2001). A study by Pahnke et al. (2008), which investigated isotopic variations in the middle depths of the tropical Atlantic Ocean, has suggested that the coupling between AAIW and NADW is so strong that AAIW could have had an important contribution, or even triggered, past abrupt

MOC reorganizations. Given the role AAIW plays in the MOC, the stability in properties of this water mass has global implications (Sloyan and Rintoul, 2001; Rimaud et al., 2012).

2.7.2 AAIW in the southeast Atlantic.

The southeast Atlantic is vital in facilitating major intermediate water mass exchanges (Peterson and Stramma, 1991; Rusciano et al., 2012). In this area, three regional varieties of Antarctic Intermediate Water (AAIW) converge and mix: Atlantic AAIW (A-AAIW), Indian AAIW (I-AAIW) and Indo-Atlantic AAIW (IA-AAIW) (Rusciano et al., 2012). I-AAIW flows southwestward along the east coast of Africa within the Agulhas current, and subsequently separates into two branches south of Africa at approximately 15^{o}E (Piola and Georgi, 1982, Rimaud et al., 2012). One branch retroflects back towards the Indian Ocean as part of the Agulhas Return Current, and the other flows into the Atlantic within mesoscale eddies (Biastoch et al., 2009; Rusciano et al., 2012). A-AAIW enters the African choke point from the west within a latitude band spanning from the STF to the SAF. A portion of the water mass proceeds directly eastward and into the Indian Ocean, while another component enters the Cape Basin and mixes with I-AAIW to form a new composite, IA-AAIW (Rusciano et al., 2012). Evidence that all these varieties of AAIW exist in the region is reflected in the large characteristic temperature and salinity ranges: 3.31^{o}C to 6.15^{o}C, and 34.15psu to 34.56psu (Jacobs and Georgi, 1977). One of the possible forces contributing to the erosion of the AAIW minimum in the region south of Africa could be the influence of highly saline Arabian Sea waters carried into the area by the Agulhas current, and mixed with other water masses via the elevated local mesoscale activity (Fine, 1993).

Large scale instabilities are thought to have a significant impact on the properties of AAIW. The strong eddy processes observed south of Africa are thought to play important roles in the stirring and mixing of the Atlantic and Indian AAIW varieties (Piola and Georgi, 1982). This is evident in strong modification of AAIW properties as it crosses from the South Atlantic to the South Indian Ocean (Rimaud et al., 2012). Passing through the African choke point from west to east, salinity of AAIW is found to increase by 0.1x10^{-3} psu, and temperature by 0.5 ^{o}C (Piola and Georgi, 1982). These changes and exchanges are highly complex and rely on many different factors, such as large-scale density gradients, wind, and meso- and sub-mesoscale processes (Rimaud et al., 2012).

AAIW is thought to contribute significantly in maintaining a stable ocean-climate system (Pahnke et al., 2008). Recent warming of AAIW has been identified, and results suggest that these changes are most likely a signal of anthropogenic climate change (Banks et al., 2000; Pahnke et al., 2008). However, due to the scarcity of data in the southern sector of the South Atlantic, the extent of intermediate water mass warming in this region is poorly understood. A warming of approximately 0.5 ^{o}C/100yr and salinity increase of 0.1/100yr was detected by Arbic and Owens (2001) for the southwestern Atlantic. Yet no such estimates are available for the southeast Atlantic as yet. AAIW is recently ventilated and thus is the appropriate water mass to study when endeavoring to observe the effects of a changing climate. ñRecent ventilationò means that atmospheric gasses are introduced to the deep ocean interior on a decadal time scale (Fine, 1992; Banks et al., 2000). However, after AAIW is formed, it is subducted below the thermocline and is thought to no longer come into contact with the atmosphere. The original properties are therefore largely retained, meaning that AAIW is a long distance supplier of heat, salt, and nutrients sourced from its formation region to the rest of the global ocean (Santoso and England, 2004). Despite the importance of this water mass to the Earthôs system, knowledge of its behavior in the Southern Ocean is limited due to insufficient hydrographic observations and poor representation in numerical models (Rimaud et al., 2012).

Southern Hemisphere intermediate waters are thought to be sensitive indicators of anthropogenic climate change and therefore present an important source of information for climate monitoring (Banks et al., 2000). Evaluations of the magnitude and dynamics of AAIW will greatly aid the detection and attribution of changes at intermediate levels in the Southern Ocean (Santoso and England, 2004). Quantifying the variability of AAIW is therefore essential in understanding the oceans response to a climate change.

3. Research Questions.

The Southern Ocean plays an integral role in the global ocean circulation, and in turn in climate regulation (Rintoul et al., 2012). It serves as a conduit for oceanic and atmospheric exchanges, drives important water mass transformation, and acts as a major sink for anthropogenic sourced CO_2 (Gille 2002; Boning et al., 2008; Rintoul et al., 2010). Despite the enormous importance of this region of the worldôs ocean, large gaps in knowledge and understanding exist, thereby leaving many important questions unanswered. The traditional method used to observe the Antarctic Circumpolar Current (ACC; dominant circulation feature of the Southern Ocean), has been via the acquisition of *in situ* hydrographic observations from research vessels. In more recent years, the increase of Argo float deployments within the region improved the resolution of *in situ* data (Gould et al., 2004). However, these data sources do not deliver continuous monitoring, which is what is needed in order to better understand and forecast the Southern Oceanôs role in a changing climate.

The ACC is ideal for the implementation of proxy methods due to the strong meridional density gradients and baroclinic nature of variability (Sun and Watts, 2001). This signifies that the potential temperature-salinity (ɗ-S) curve can be considered regular along streamlines (contours) of absolute sea surface height (Sokolov et al., 2004). It is consequently possible to obtain the thermohaline structure of the water column at a point with the knowledge of the dynamic height value at that location (Rintoul et al., 1997). This method is called the Gravest Empirical Mode (GEM), and was first implemented in the Southern Ocean by Sun and Watts (2001).

Of all the choke points associated with the ACC, the southeast Atlantic sector remains the least understood, despite its critical role in providing a link between the Indian, Atlantic and Southern Oceans (Ansorge et al., 2005; Speich and Arhan, 2007; Rimaud et al., 2012). The investigation undertaken by Baker-Yeboah et al. (2009) in the Agulhas leakage eddy corridor within the southeast South Atlantic decomposed the SSH variability into baroclinic and barotopic contributions using PIES data. However Swart et al. (2010) was the first, and currently the only existing study, to develop a GEM specifically for the region of the ACC south of Africa. The Swart et al. (2010) GEM relationships were built from hydrographic data sourced from seven research cruises spanning the time period from 1984 to 2005 (Swart et

al., 2010). Via the subsequent pairing with satellite altimetry data, Swart et al. (2010) created an Atlimetry GEM (AGEM), thereby generating 16 years of weekly T and S fields derived from the GEM proxy technique. This proxy-data is extraordinarily valuable as time series in the Southern Ocean, and particularly the African choke point, are rare.

This study proposes to develop an upgraded version of the GEM first developed by Swart et al. (2010) for the southeast Atlantic sector of the Southern Ocean. The hypothesis as to whether the performance of the GEM can be improved via the employment of updated cruise obtained hydrographic data, plus the inclusion of Argo float profiles, and the implementation of an alternative method of de-seasoning, is tested. The ensuing generation of an Altimetry GEM (AGEM) for the GoodHope (GH) track is proposed by uniting the GEM with the available 20 years of satellite altimetry measurements obtained in the region. Prior to drawing any conclusions from the results, it must be verified that both the GEM and AGEM adequately reproduce observations. This research focuses on the Antarctic Intermediate Water (AAIW) layer as this water mass plays a very important role in the transport of heat, freshwater, and biogeochemical tracers to the rest of the worldôs oceans. Obtaining a better understanding of the variability of AAIW in the region south of Africa is therefore of significant importance. Using the AGEM generated property fields, the temporal evolution of the water mass, along with the possible role eddies play in the water mass alteration, is investigated.

1) **Can a new and improved GEM be created that successfully represents the Atlantic sector of the Southern Ocean?**

   A GEM is created by projecting hydrographic data from 556 CTD stations and 2201 Argo float profiles into baroclinic stream function space parameterized by pressure and dynamic height. The use of a de-seasoning technique, the inclusion of a bathymetry data set, and the effects of marrying Argo data (limited to top 2000dbar) with full depth cruise data are investigated. The ability of this new GEM at reproducing *in situ* observations is assessed at each stage of development.

2) **How proficient is the developed AGEM at reproducing observed water properties along the GH line, especially within the AAIW layer?**

In order to assess the aptitude of the AGEM at reproducing the observed fields, extensive comparisons with cruise data are performed. The emphasis of these tests is on the AAIW layer as this water mass is the focus of this study, and assess the absolute T and S differences, the closeness of fit of the HC and SC budgets, and the RMS errors. In addition, the repercussions of an inexact absolute dynamic topography (ADT) are explored. In order to better understand the source of errors in the AGEM, an investigation into changing of the limits of Argo data used to set up the GEM is also undertaken.

3) **How variable is AAIW and what changes has this water mass undergone in the region south of Africa over the past 20 years?**

The AGEM generated T and S fields are used to investigate the temporal evolution and variability of AAIW in the Atlantic sector of the Southern Ocean over the last two decades. The heat and salt content (HC and SC) anomalies and trends over the whole region, and within each frontal zone, are examined. In addition, the changes in water mass thickness and isopycnal depth are inspected. So as to gain insight into one of the influences driving a portion of the observed AAIW alteration, a brief investigation of eddy behavior in the southeast Atlantic Southern Ocean from 1992-2010 is also carried out.

4. Data.

The oceanic domain south of Africa is a highly dynamic region (Rimaud et al., 2012). In addition, the African choke point of the Antarctic Circumpolar Current (ACC) is regarded as the section where the current experiences highest degree of variability (Swart et al., 2008). It is widely accepted that the upper branch of the Atlantic MOC (AMOC) originates in the southeast Atlantic (Rimaud et al., 2012). Yet, despite the recognized importance of this sector of the ocean for global circulation and consequential regulation of climate, it has been so far somewhat understudied due to limited *in situ* data and difficulties modeling such a dynamic system. This chapter describes the available data for the region upon which the GEM and AGEM relationships are built.

4.1 CTD data at the GH line.

The GoodHope (GH) line was established in 2004 as a repeat sampling track between the African and Antarctic continents, designed to address the deficiency in hydrographic data obtained south of Africa (Speich and Dehairs, 2008). The objectives of this initiative are to: improve understanding of the thermohaline exchanges through this choke point, gauge the impact of these exchanges on the MOC and in turn climate, and monitor the variability of particular features in the region (Ansorge et al., 2005; Speich and Arhan, 2007). The location of the GH track (magenta in Figure 4.1) was chosen to follow the Topex/Poseidon-Jason1 altimeter flight path, thereby allowing for satellite observations to compliment hydrographic sampling (Swart et al., 2008). The GH line also covers a set of PIES (Pressure Inverted Echo Sounders) deployed in the northern sector of the transect, and an array of German moorings located in the extreme south - both form part of the WECCON project. The Atlantic Oceanographic and Meteorological Laboratory (AOML) of NOAA have established a high density XBT transect that overlays the GH line, named AX25.

Pre-2004, transects of the region were undertaken within close proximity to the GH coordinates by a variety of institutions taking part in the World Ocean Circulation Experiment (WOCE). The data set produced by this initiative is the most comprehensive ever collected for the global ocean, with the timeline of the project spanning from 2000 to 2004 (WOCE International Project Office, 2003).

In total, eleven Conductivity Temperature and Depth (CTD) sections occupying the GH line contribute the cruise obtained hydrographic data used to set up the GEM (information available in Table 1; station positions shown in Figure 4.1). These sections span the time period from 1984 to 2009, 5 from WOCE up until 2002, and the rest GH transects from 2004 to 2009. All except the GH2005 section sampled the full depth of the water column. All hydrographic data is synthesized together in the GEM, irrespective of sampling date. In total 556 CTD stations are used in this study to contribute to creating a GEM projection for the GH line spanning from 38°S to 56°S. The measurements obtained from CTD profilers were interpolated onto a vertical grid of 5 dbar, starting at 5dbar depth ending at 2000dbar (resolution matches that of Argo floats), and only the downcast of the profile was used.

For further information regarding CTD calibration, sampling strategies and problems encountered, refer to the references provided in Table 1.

Section	**Date**	**Institute**	**Ship**	**Chief Scientist/Reference**
AJAX	Jan 1984	Scripps Institution of Oceanography	R/V Knorr	Reid/T. Whitworth (1985)
A21	Jan - March 1990	University of Hamburg	Meteor	W. Roether/Roether et al. (1990)
A12	May ï Aug 1992	Leibniz-*Institut für Meereswissenschaften, Kiel* (LfMK)	Polarstern	P. Lemke/Lemke (1992)
A1299	March 1999	*Alfred Wegener Institute*	Polarstern	E. Fahrbach
A1200	Dec 2000	*Alfred Wegener Institute*	Polarstern	E. Fahrbach/World Ocean Circulation Experiment (2002)
A1202	Dec 2002	*Alfred Wegener Institute*	Polarstern	Fütterer /World Ocean Circulation Experiment (2002)
GH2004	Nov 2004	*Shirshov Institude of Oceanology*	RV Akademik Sergey Vavilov	S. Gladyshev/Gladyshev et al. (2008)
GH2005	Oct 2005	*Shirshov Institude of Oceanology*	RV Akademik Sergey Vavilov	S. Gladyshev
GH2006	Oct ï Nov 2006	*Shirshov Institude of Oceanology*	RV Akademik Sergey Vavilov	S. Gladyshev

BGH2008	March ï April 2008	Laboratoire de Physique des Oceans	RV Marion Dufresne II	S. Speich/Speich and Dehairs (2008)
GH2009	Dec 2009	*Shirshov Institude of Oceanology*	RV Akademik Sergey Vavilov	S. Gladyshev

4.2 Argo data.

The Array for Real-time Geostrophic Oceanography (Argo) profiling float project was launched on a global scale in 2004, providing for the first time continuous global observations of temperature, salinity and velocity of the upper ocean in near real time (Gould et al., 2004). This initiative to collect high-quality data for the top 2000m of the world oceans is perhaps the most internationally collaborative effort in the history of oceanography (Roemmich et al., 2004). The data provided from Argo floats has delivered unprecedented insight into the evolving physical state of the ocean (Roemmich et al., 2003). Argo floats are battery powered and entirely autonomous. They drift mostly at depth where they are stabilized at a constant pressure level, rising to the surface to collect vertical profiles at approximately 10 day intervals. On surfacing, the data and float position information is transmitted via satellite to various Argo centres around the world (Gould et al., 2004). The project started with the launch of 869 floats, and grew rapidly to reach the active float target of 3000 in November 2007 (Roemmich et al., 2009). The Argo float program has been especially useful in providing data in remote and sparsely sampled regions, thereby transforming the scope for ocean research in these areas. Figure 4.1 shows the extent of float data available for the sector surrounding the GH track.

For use in this study, a total of 155 floats were found to be located in the study box around the GH line. The domain limits of the study box were discussed at length as the positives of including more data upon which to build the GEM relationships needed to be balanced by the negative effects of incorporating measurements of significantly different water masses obtained further away. It was decided that the study box would span 37°S to 56°S, and 5°W to 15°E, boundary positions can be seen in Figure 4.1. The temporal range of the Argo data is 2004 to 2012. The 155 floats located within the domain, rendered 2201 profiles that were used to set up the GEM projection. The profiles underwent various quality control procedures (for more details as to the processing please refer to http://www.argodatamgt.org/). In addition, further quality checks were performed under the auspices of the CLIVAR

international observing program. The Argo instruments themselves have a pressure accuracy of 3dbar, conductivity error within 0.03 $mS.cm^{-1}$, and temperature readings accurate to within ~0.03°C (Rusciano et al., 2012).

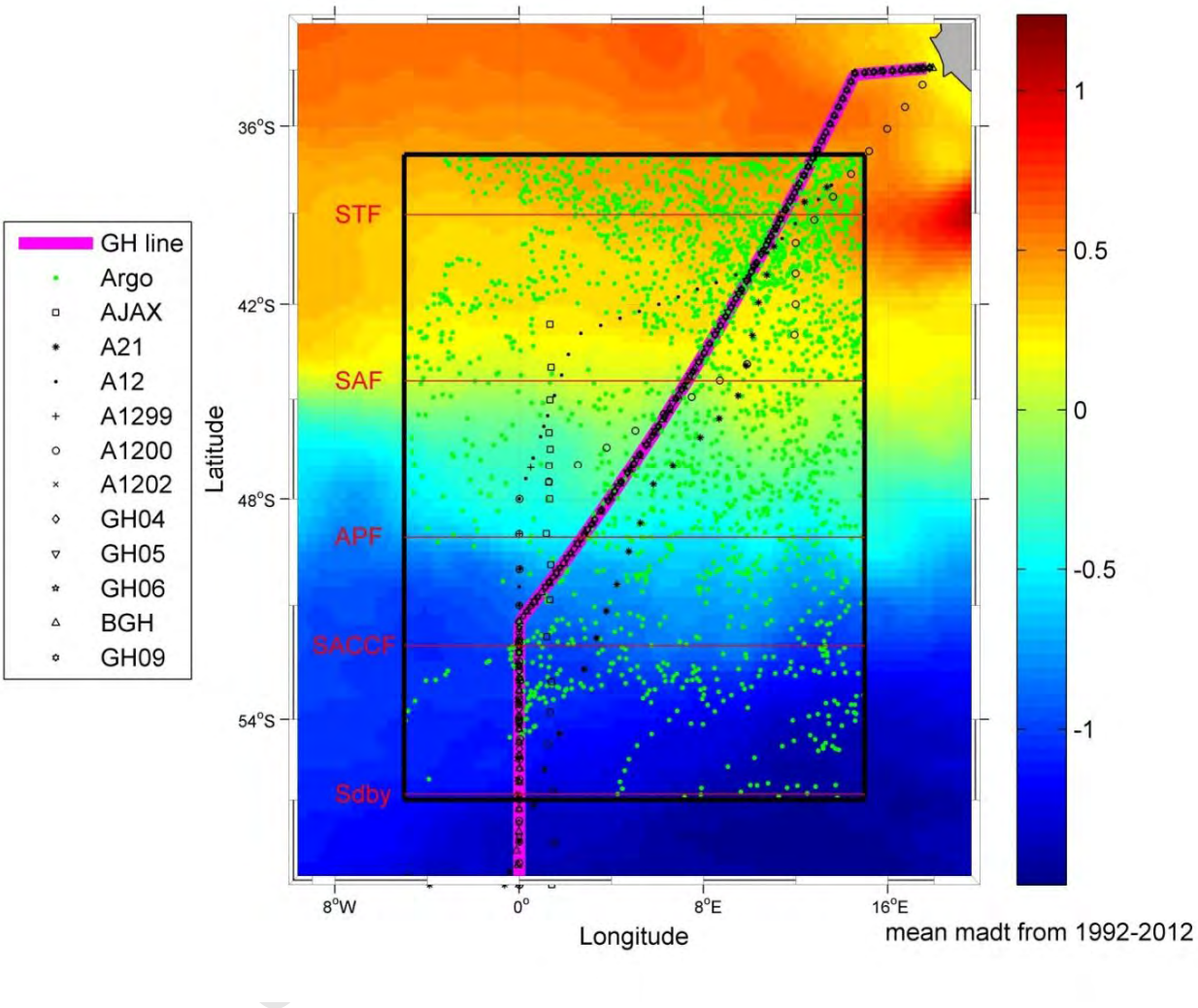

Figure 4.1 Map showing the positions of the hydrographic stations used in this study. Each cruise is marked with a different symbol, and all Argo data are shown as green dots. The position of the GH line is marked in magenta. The dimensions of the limits of the study box are shown, along with the average positions of the ACC fronts. The background shading is the mean dynamic height from AVISO MADT over the 20 year study period.

4.3 Satellite altimetry.

AVISO updated delayed weekly maps of the sea level anomaly (MSLA) are used at a 1/3º spatial resolution dating from October 1992 onwards. The MSLA incorporates data measured by multiple satellite platforms: the T/P, Jason-1, ERS-1/2, and Envisat altimeters. For details on the mapping methods and error corrections applied to these fields, refer to Le Traon et al. (1998), Le Traon and Ogor (1998), and Ducet et al. (2000). These maps give the circumpolar sea surface height (SSH) anomalies, and therefore the data must be subsequently interpolated onto the GH line coordinates. A mean dynamic topography (MDT) is then added to the satellite product to obtain an absolute dynamic topography (ADT) for the region. In this study, the MDT used was calculated from a synthesis of all available relevant hydrographic data. The decision to use an MDT calculated from the *in situ* data instead of the available AVISO MDT for the region was motivated by the fact that the AVISO MDT includes the barotropic and deep ocean components which are not relevant to the GEM. The ADT product of the MDT calculated from the hydrographic data plus the AVISO SLA measurements is referenced to 2000 dbar, thereby ensuring mostly baroclinic flow and exclusion of the deep ocean.

In total 1009 weeks of MSLA are utilized in this study. The MDT calculated specifically for the GH line is then added to these weekly MSLA to produce an ADT time series that begins on the 13 October 1992 and runs to 6 February 2012.

5. Methods

5.1 Developing a Gravest Empirical Mode for the southeast Atlantic sector of the Southern Ocean.

5.1.1 De-seasoning.

The CTD data is seasonally biased, as most cruises were performed in spring-summer due to the constraints of harsh sampling conditions in the Southern Ocean during the winter months. Argo float data, which is available year-round, was therefore used to build a seasonal model of temperature and salinity for the region. This seasonal model was computed according to

the process outlined in Faure et al. (2011). The longitudinal limits of float data used to create the seasonal model are 5ºW and 15ºE. The region is separated in the latitude dimension by 6 zones corresponding to the dynamic height (DH) signatures of the main Southern Ocean Fronts. Zone 1 is all DH greater than 1.55 dynm (Subtropical Zone - STZ), zone 2 corresponds to the DH range 1.290-1.550 dynm (Subantarctic Zone - SAZ), zone 3 ranges 0.90-1.29 dynm (Polar Frontal Zone - PFZ), zone 4 covers DH values from 0.62-0.90 dynm (Southern ACC Zone - SACCZ), zone 5 spans the DH interval 0.58-0.62 dynm (Southern Boundary Zone - SBZ), and zone 6 is all DH values less than 0.58 dynm (Antarctic Zone - AZ). The spatial location of the fronts, and resultant zone areas that were used for de-seasoning, can be seen in Figure 5.2.

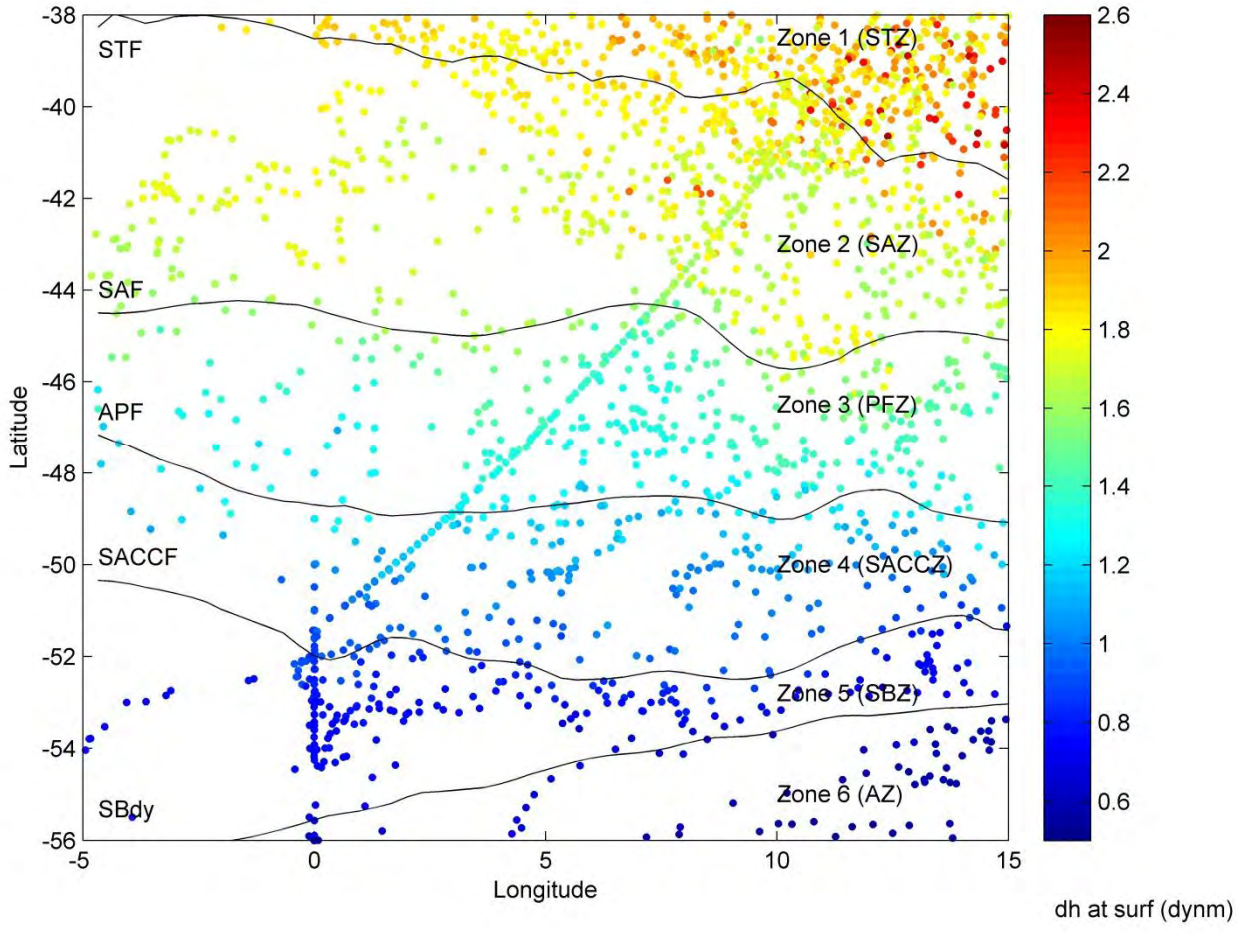

Figure 5.2 Dynamic height value at the surface relative to 2000 dbar for each hydrographic profile used to set up the GEM projection shaded in colour and plotted at the station location. Mean positions of fronts over a 20 year study period are overlaid.

For each zone, a yearly mean of temperature (T) and salinity (S) was computed. This mean essentially represents the ñmodalò, season-less state of the ocean. For each month of the year, for each zone, the difference between the hydrographic measurement and this mean was obtained. These differences are known as the residuals. For each zone and month, these residuals were averaged, and the process replicated three times, representing 36 months. This was undertaken in order to eliminate the effects of a running mean on the end points when obtaining a 3 month running mean. The middle 12 months were subsequently extracted from the final 3 year product to give the smoothed cycle of T and S for each depth, in each zone.

In order to de-season the hydrographic data, it too must be separated into the 6 zones delimited by the DH criterion. The DH value of each hydrographic station was calculated (for values see colour shading of dots in Figure 4.2), thus allowing for the appropriate separation of the data. The corresponding residuals were then subtracted from the top 300 dbar - the approximate layer affected by seasonal changes (Meijers et al., 2011a; Swart et al., 2010). In doing so the ñde-seasonedò T and S profiles are obtained.

Previous studies that have also developed GEMs for the Southern Ocean have approached the challenge of de-seasoning the data in a variety of ways. Watts et al. (2001) were the first to fit a seasonal model to the near-surface layers using historical data. This was done for a GEM parameterized by T, S, and acoustic travel time, located in region of the ACC south of Australia. Sun and Watts (2001) tackled the problem of de-seasoning by simply excluding the top 100dbar of data. Swart et al. (2010) used a similar method to that employed in this study where Argo float data was used to build a seasonal model, however the region was divided up into 10 zones based on fixed latitude positions. The zones of Swart et al. (2010) are separated by each 2 degrees of latitude for the region of the Southern Ocean south of Africa. Unlike zones delimited by DH, these do not allow for spatial dynamics. The residuals were removed from the top 500dbar of data in Swart et al. (2010), whereas this study removed residuals from the top 300bdar, as performed by Meijers et al. (2011a).

5.1.2 Projection onto baroclinic stream function space.

The baroclinic coordinate used in this study is dynamic height (DH), also known as geopotential thickness. Instead of using the spatial coordinates of latitude and longitude to delineate our region, the physical data is projected in streamline space of pressure and DH. In

doing so, advantage can be taken of the strong meridional gradients within the ACC, and thus its resultant equivalent barotropic form (Meijers et al., 2011b). The assumption is therefore that water properties and processes along a stream function have an almost identical vertical structure (Watts et al., 2001). The projection of the data this way allows for the acquisition of subsurface information from satellite SSH observations alone (Swart et al., 2010).

To project the hydrographic data into this stream function space, the surface DH is obtained for each station using the T and S profiles. The property values at each pressure level (between the surface and 2000dbar at 5dbar intervals) are then plotted against the DH calculated at the surface relative to 2000dbar. The scatter of the relationship displays a remarkable organization around a functional curve. A cubic smoothing spline can then be fitted to the scatter, thereby capturing the general trend of the data while ignoring the small scale geographical and instrumental noise. The choice of the spline coefficient is fairly subjective and depends on the desired sensitivity of the produced spline. In this study, a spline coefficient of 0.9997 for both T and S was decided upon, after much testing regarding the effect of different coefficients on the accuracy of the produced GEM. While generated fields using this established GEM relationship are not ñrealityò, they are built on empirical measurements, and due to the suitability of the ACC for the implementation of a GEM, are regarded as highly reliable.

A broader scatter about the smoothing spline of temperature and salinity values plotted against DH does however exist at higher DHs. The phenomena driving the deviation from the close fit of the lower DH values are likely the dynamic features prevalent in the northern sector of the region (e.g. eddies and associated Agulhas Retroflection turbulence; see Swart and Speich, 2010; Dencausse et al., 2010a). The close co-existence of diverse DHs over time for one area is typical of the highly variable mesoscale and submesoscale regimes prevalent in the region of the Southern Ocean south of Africa (Boebel et al., 2003; Swart and Speich, 2010; Rusciano et al., 2012). Here waters with different T and S properties but equal potential densities (same surface DH signature) converge as they are convected by jets, eddies and filaments. The presence of multiple options of T and S profiles along one streamline presents a challenge for the GEM, and thus the generated fields for the northern domain can be expected to be less accurate than those for the sector further south where thermohaline structure can be considered relatively stable over time along lines of equal DH.

5.1.3 Comparison of the GEM with observations.

In order to test the ability of the GEM to reproduce reality, the GEM thermohaline fields are compared with cruise observations. The DH value for each cruise station is obtained and used to generate a corresponding GEM property estimate. The GEM produced T and S data can then be compared with the cruise measurements in order to assess their proficiency. It is important to remove the cruise data (against which you are testing the GEM) from the synthesis of hydrographic profiles that are projected into stream function space before performing the test.

5.1.3.1 Statistical tests.

The most robust way to evaluate the closeness of match between the GEM fields and those of reality is to compute the Root Mean Square (RMS) error of the differences, and to assess the portion of the variance observed *in situ* that is captured by the GEM. Essentially the RMS is the square root of the mean of the squared differences between the cruise property and the GEM property. The usefulness of this RMS value is that it indicates how far the GEM error is, on average, from zero at each depth, for each station. The percentage of variance, on the other hand, indicates how much the CTD measurements are spread out about the GEM values (Meinen and Watts, 2000). Variance is calculated by first obtaining both the variance of the cruise measurements and the variance of the GEM values at each pressure level (Watts et al., 2001). Then the ratio of these indicates how much of the hydrographic variability is captured by the GEM field (Sun and Watts, 2001). This ratio can is subsequently converted into a percentage. The RMS and variance captured are the two parameters used in this study to indicate the reliability of the GEM fields. Visual comparison of the GEM versus CTD T and S sections is also useful to understand the capacity of the projection to reproduce certain features.

5.2 Generation of a satellite derived GEM for the southeast Atlantic Ocean.

A total of 1009 weeks of historic circumpolar SLA measurements, at a 1/3º latitude resolution, running from 14 October 1992 to 8 February 2012, are interpolated into the GH line. When the MDT derived from hydrography is added to these SSH anomalies (to render

an ADT), 20 years of DH values are obtained. It is important to note that this ADT is representative of the entire water column, as the AVISO maps of SLA represent baroclinic changes occurring throughout the full water column as well as a deep ocean barotropic component. To generate the MDT used as input DH for the GEM, however, the SLA values are paired with an ADT referenced to 2000dbar. Mostly baroclinc changes are therefore represented and the associated errors comparatively small. Additional errors emerge in the GEM simply via the use of satellite data, which has its own inherent problems. These supplementary offsets are introduced by temporal and spatial sampling discrepancies and interpolation, mapping errors, and tides that are not wholly removed from the altimeter signal (Swart et al., 2010). In spite of these factors, the ADT data is found to be very similar to the cruise obtained estimates of DH. Swart et al. (2008) verified this for the region, and this is further confirmed in this study by comparing the cruise DH and the ADT for the dates of a specific cruise. A robust match indicates that the ADT largely reflects the baroclinic changes in the upper layer, and is therefore appropriate for use as input for a GEM projection in the region.

By utilizing the GEM relationship developed according to the methodology described in Section 5.1, a time series of T and S can be produced from the available 20 years of ADT DH data. The name given to these time evolving fields is the Altimetry GEM (AGEM). This AGEM has the potential to provide unprecedented insight into the baroclinic evolution and variability of the ACC south of Africa over the last two decades at eddy permitting spatial and temporal scales.

5.3 Using the AGEM generated fields to investigate AAIW.

The Atlantic sector of the Southern Ocean is an important region for the mixing and transformation of Antarctic Intermediate Water (AAIW), as in this area the Indian and Atlantic varieties meet and mix, thereby forming a new variety ï Indo-Atlantic AAIW (Rusciano et al., 2012). Due to the turbulent nature of the ocean domain south of Africa, the region is thought to play an important role in water mass alteration (Garzoli and Matano, 2011). The dynamic behaviour of AAIW itself in the southeast Atlantic renders it essential in facilitating intermediate property exchanges (Peterson and Stramma, 1991). The variability and property changes of AAIW in the southeast Atlantic sector of the Southern Ocean are

therefore of global importance. Despite its significance, however, knowledge of the temporal behaviour in this region is limited (Rimaud et al., 2012).

AAIW is located largely within a layer of the GEM where the errors are at a minimum, and therefore the T and S fields for this area can be considered highly reliable. The AGEM thus allows for observation of this water mass at unprecedented temporal and spatial scales. For this reason, a large focus of this study is an investigation into the evolution of AAIW in the region. As AAIW is recently ventilated, changes observed in this water mass can be linked to climatic forcing, thereby exposing the value in the results presented here.

5.3.1 Defining AAIW and computation of its heat and salt content.

The isopycnal boundaries chosen to delineate the limits of AAIW were chosen as 1027.0 $kg.m^{-3}$ and 1027.4 $kg.m^{-3}$ (Talley, 1996). As it is somewhat impossible to locate the exact position of the potential density limits, an interval of within 0.01 $kg.m^{-3}$ was used to search for the isopycnals. The depths of the parameters were noted and the T and S values located within the layer bounded by the two limits extracted as belonging to AAIW.

The heat content (HC) and salt content (SC) of the AAIW layer were then calculated as follows:

$$HC = \int_{z\text{-lower}}^{z\text{-upper}} \rho \, C_p \, T \, dz$$

$$SC = \int_{z\text{-lower}}^{z\text{-upper}} \rho \, 0.001 \, S \, dz$$

Where z-upper and z-lower are the depths of the upper and lower isopycnal limits of AAIW, ρ is the density of seawater (1027 $kg.m^{-3}$), Cp is the heat capacity of seawater at a constant pressure (4000 $J\ kg^{-1}K^{-1}$), dz is the thickness of the water mass layer, T is the temperature (ºC), and S is the salinity.

5.3.2 Division into frontal zones.

Within the region of the Southern Ocean, south of Africa, five established fronts are found: the Subtropical Front (STF), Subantarctic Front (SAF), Antarctic Polar Front (APF), Southern ACC Front (SACCF), and the Southern Boundary (SBdy) of the ACC (Orsi et al.,

1995). An oceanic front marks the horizontal interface between two regions of significantly different water characteristics and properties. The fronts are useful in identifying the behaviour of AAIW within appropriate spatial sections over the meridional extent of the region.

The weekly locations of the Southern Ocean fronts along the GH line were identified using the dynamic height signatures from Rusciano et al. (2012) applied to the AVISO rio09 MADT time series. The HC and SC for the AAIW layer for each frontal zone were plotted over time, along with the location of the isopycnal limits and the vertical thickness of the water mass. The HC and SC anomalies from the 20-year mean were also examined. Trends were fitted to these temporal fluctuations in order to gauge the general change over the study period.

5.3.3 Validation of the AGEM.

The most effective way of gauging the proficiency of the AGEM at reproducing reality is to compare the generated fields with *in situ* cruise observations. It is essential to note that the CTD section against which the AGEM was tested was removed from the hydrographic data used to set up the projection. The SLA satellite data was obtained for the relevant week for each station of the cruise. As a station was often located mid-week, and the dates for each week of SLA data correspond to the day at the start of the week, the SLA altimetry Julian day closest to the station date were used. The DH product of the SLA for the date of the cruise plus the MDT calculated from the hydrography was subsequently interpolated onto the coordinates of the cruise. GEM fields were consequently rendered at the location of each CTD station and the results compared with the *in situ* observations.

The focus of this study is AAIW, and therefore the errors within the water mass layer were examined in detail. Identification of the position of the isopycnal boundaries of AAIW was carried out separately for the GEM profiles and the cruise measurements. Subsequently a comparison of average HC and SC for AAIW layer was undertaken and the differences in estimates per station reported. The differences in temperature and salinity for AAIW were obtained at each pressure level, along with the RMS error, and the percentage of variance captured.

6. Development of an upgraded Gravest Empirical Mode for the southeast Atlantic Ocean.

The available high-density hydrographic observations of the Southern Ocean are mostly confined to the three ACC choke points: the regions south of Australia, south of Africa, and the Drake Passage. Compared to the other choke points, the passage south of Africa has been relatively understudied despite the important role it is thought to play in regulating the MOC and in turn global climate (Swart et al., 2008; Speich et al., 2011). The water mass exchanges and transformations that take place in the southeast Atlantic render this area of much interest when endeavoring to better understand ocean circulation, with local variability having global implications (Rimaud et al., 2002). The in situ hydrographic observations are mostly centered about the GoodHope (GH) line, with precise tracking of the GH line available post 2004 (Gladyshev et al., 2008), and historic CTD data dating back as far as 1984. Argo float profiles are available for the upper 2000m of the water column for region from 2004 (Roemmich et al., 2009).

In order to improve the temporal and spatial resolution of temperature and salinity data for the area, a Gravest Empirical Mode (GEM) can be developed by projecting the hydrographic data into baroclinic stream function space parameterised by pressure and dynamic height. Swart et al. (2010) was the first to develop a GEM specifically for the region of the ACC south of Africa based on hydrographic cruise observations obtained during transects along the GoodHope line from the early 1980ôs up until 2006. This study will build on the work undertaken by Swart et al. (2010) via the inclusion of more *in situ* data, and improvement of various methods. The main enhancements of the dataset come from including Argo hydrographic profiles, which became significantly available in the region from 2004 onwards. In order to validate deviations from the existing method, and to ensure that the GEM created in this study is in fact an improved product, extensive testing is performed at each step. In this section the results from the changes and developments implemented for the creation of a new ñupgradedò GEM for the south Atlantic region of the Southern Ocean are presented, and a summary and discussion offered.

6.1 Using additional cruise data and a new seasonal model.

The increase in number of cruises occupying the GoodHope line (see Table 1, Section 4) compared to Swart et al. (2010) has enabled the inclusion of more in situ data upon which to build the GEM relationships between temperature (T) and salinity (S), and dynamic height (DH). In order to de-season the T and S fields so as to obtain the modal state of the ACC, a seasonal model delimited by DH (as described in Section 6.1.1) was implemented.

a) Temperature

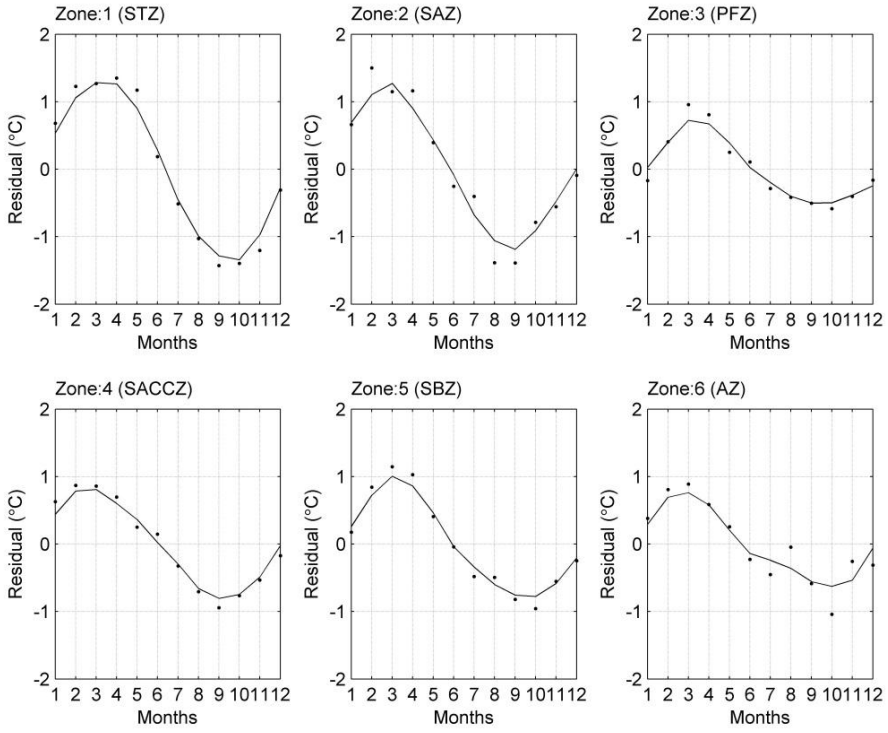

b) Salinity

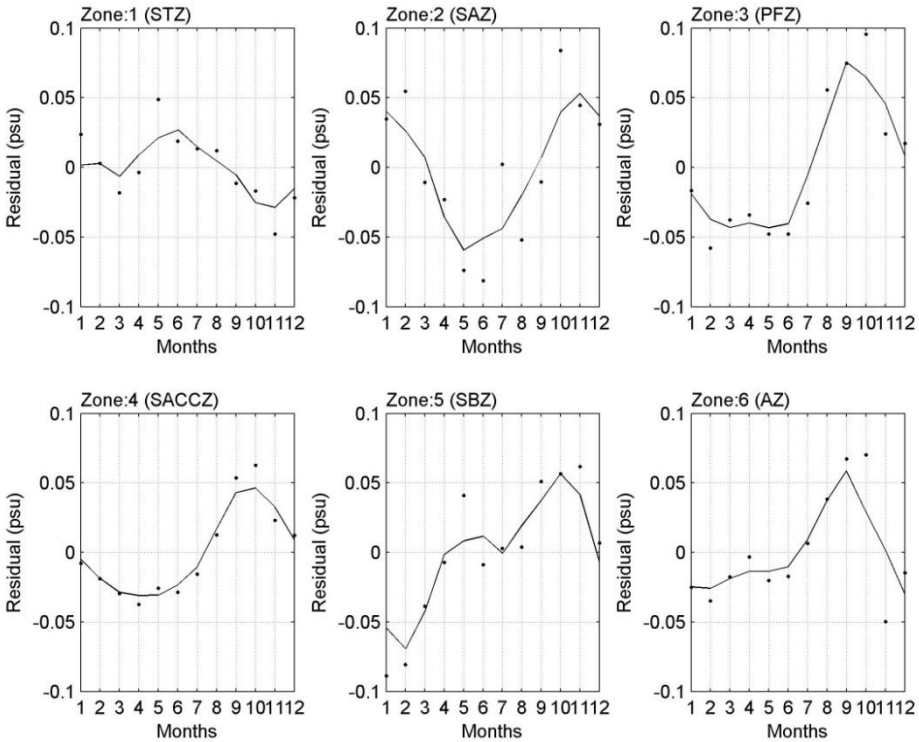

Figure 6.1 Annual march of the (a) temperature and (b) salinity anomalies from the mean for each zone. The residuals for the upper 100dbar for each zone are marked as dots, and a three month running mean is overlaid as a solid line.

A prominent seasonal cycle is evident in all zones for the T residuals, with the S annual cycle somewhat less distinct (Figure 6.1). Zones 1 and 2 (STZ and SAZ respectively), experience the highest amplitude of variation in T residuals, the magnitude of fluctuation thereafter decreases progressively pole-ward with the smallest fluctuations seen in zone 6. There does not seem to be a clear pattern in the change of S residuals with each zone, and unlike the T residuals the maxima and minima do not exhibit similar amplitudes. This is due to the highly variable influences on the salt budget such as precipitation, evaporation and sea ice formation and melting; while heat budget variance in driven principally by seasonal variability of intensity of solar radiation.

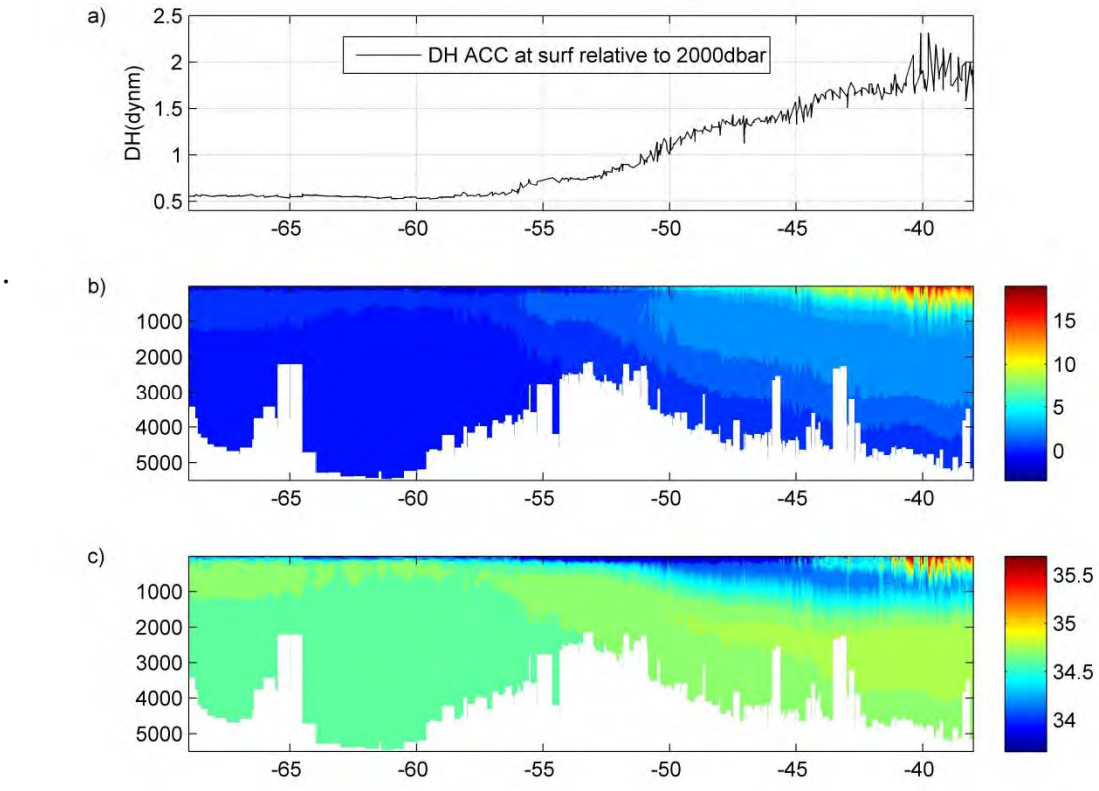

6.2 a) Dynamic height at the surface of the ACC, relative to 2000dbar, from a synthesis of all available cruise data. b) Section of de-seasoned temperature for the ACC from synthesized full depth cruise data. c) Same as (b) but for salinity.

The resultant T and S fields, following the removal of the seasonal cycle, can be seen in Figure 6.2 b and c. The DH increases northwards in response to elevated temperatures and decreasing thermocline densities (Figure 6.2a) and north of 40ºS the variability of the DH increases significantly, which is synonymous with the location of warmer and saltier anomalies seen in Figure 6.2 b and c. The white areas at the bottom of Figure 6.2 b and c represent the maximum depth that the CTD sampled to, note that this does not correlate with the location of the ocean floor.

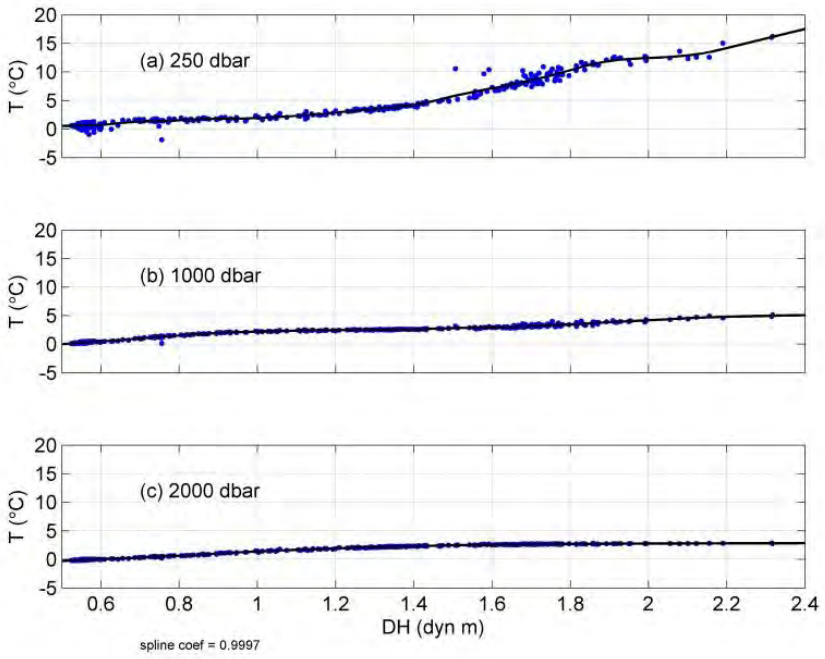

Figure 6.3 All available cruise obtained temperature data plotted as a function of surface dynamic height, relative to 2000dbar, for three pressure levels: (a) 250dbar (b) 1000dbar and (c) 2000dbar.

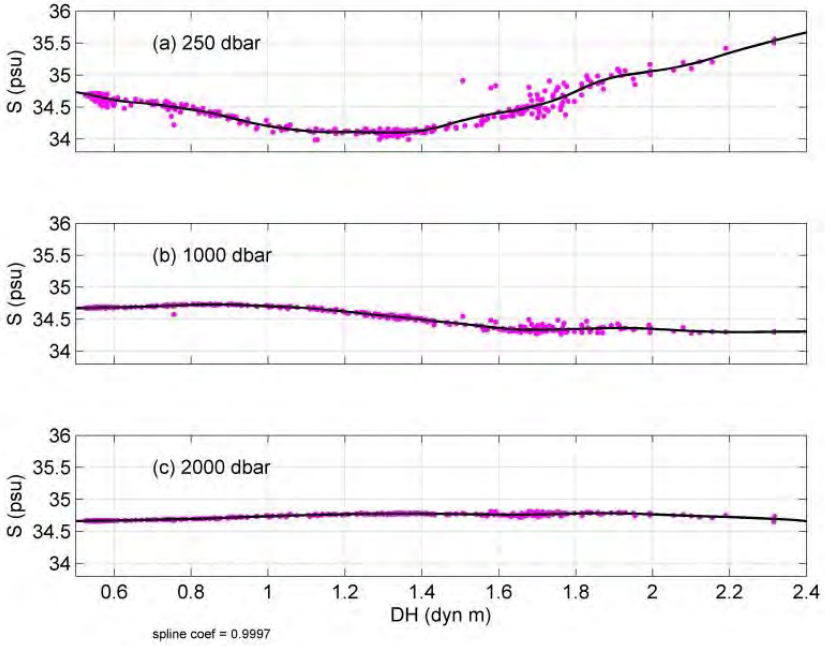

Figure 6.4 Same as Figure 6.3 but for salinity

The relationships between T, S, and surface DH show a strong tendency of the data to cluster around a common curve (Figures 6.3 and 6.4). The scatter is widest for higher DH values in the upper water column and gets progressively tighter with decreasing DH and increasing pressure. Cubic smoothing splines have been fit to the relationships with a sensitivity coefficient of 0.9997. These splines are effectively used as look-up tables for the T and S value at each depth that corresponds to a given DH measurement.

6.1.1 Testing the GEM against observations

In order to validate and assess the reliability of the updated and alternatively de-seasoned GEM, the resultant fields are tested against in-situ observations of T and S obtained from CTD data. GoodHope 2004 (GH2004) was selected as an appropriate transect against which to compare the GEM due to the numerous number of stations and even spatial coverage of the ACC. As stated in Section 5.1.4, the most effective way to test the GEM is via the calculation of variance captured and RMS error. The results from these statistical analyses are presented here along with a comparison of the T and S sections and the subsequent heat and salt content (HC and SC) estimates.

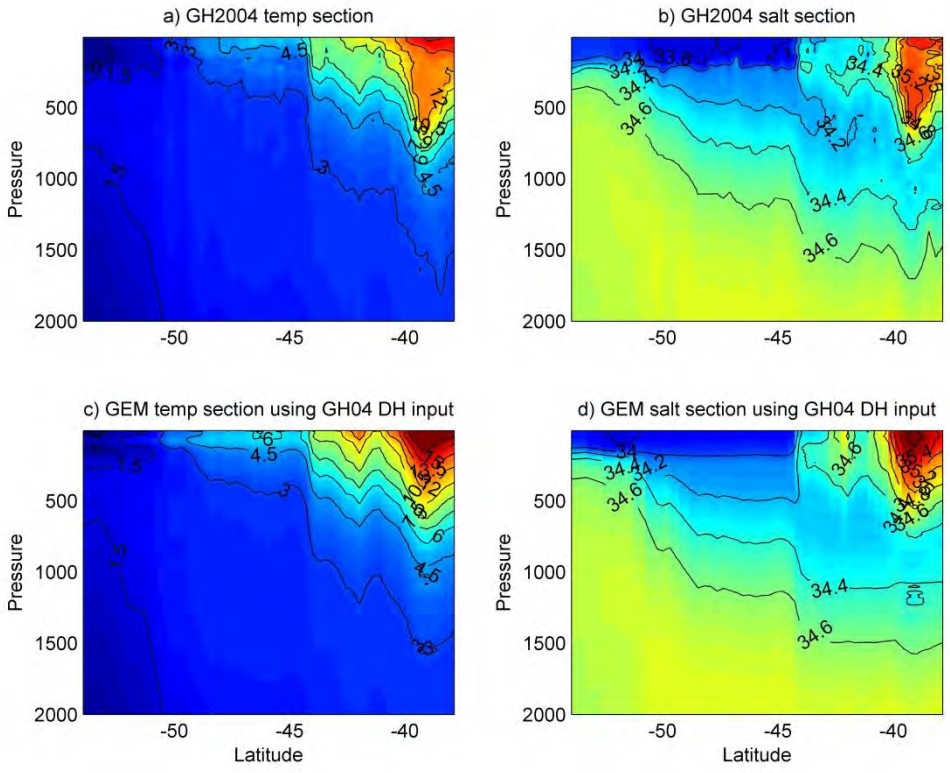

Figure 6.5 a) Cruise temperature section with depth and latitude for the upper 2000dbar. b) Same as (a) but for salinity. c) GEM produced temperature section using DH station values from GH2004. d) Same as (c) but for salinity.

The GEM T and S sections produced using GH2004 DH input compare well with the original cruise plots, adequately capturing the thermohaline structure with both depth and latitude (Figure 6.5). A slight over estimation of GEM estimates for T and S is evident in the upper 500dbar for the region north of 40ºS. At ~42ºS, a feature of elevated temperatures and salinities is portrayed in the GEM produced fields (Figure 6.5 c and d), however this warm core eddy feature is far less pronounced in the cruise observations (Figure 6.5 a and b).

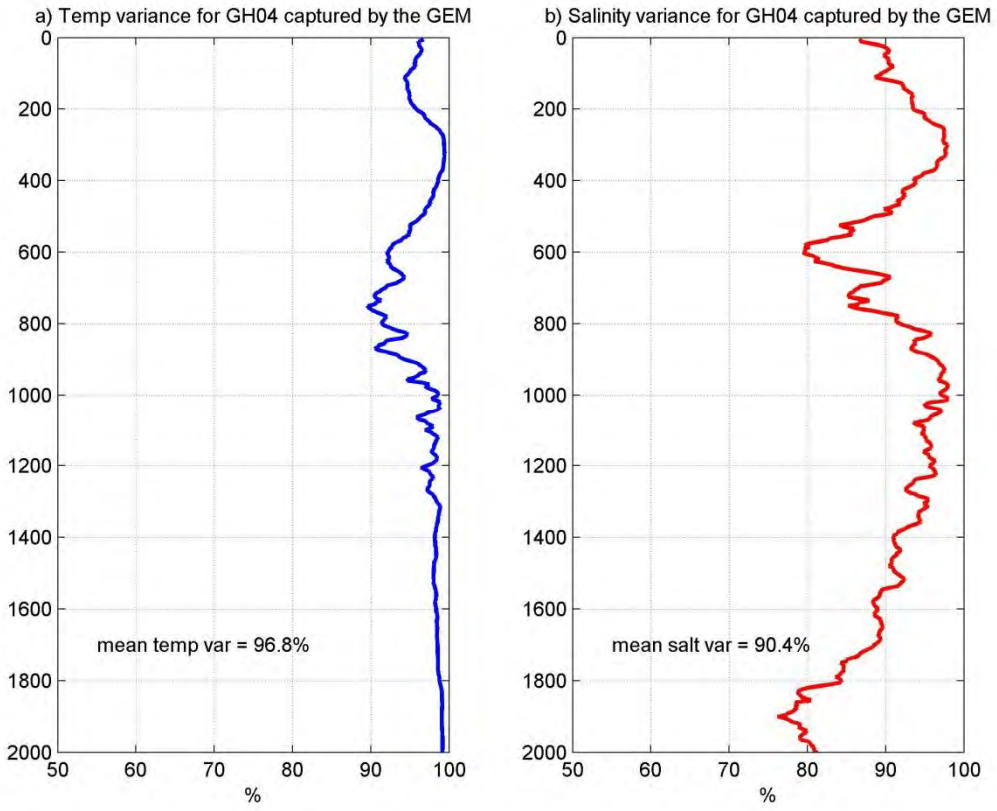

Figure 6.6 Percentage of observed (a) temperature and (b) salinity variance captured by the GEM.

The GEM at this stage of development is found to capture on average 96.8% of the T variance, and 90.4% of the S variance observed in the upper 2000dbar of the *in situ* cruise data. The distribution of the magnitude of variance captured with depth can be seen in Figure 6.6. For both T and S curves a drop in variance captured is evident between 600 and 800dbar, likely driven by the difficulties the GEM encounters in reproducing properties in the northern

domain. Below 1000dbar the T curve then recovers to represent over 95% variance at all depths, while the S curve consistently drops in values of variance captured deeper than this depth.

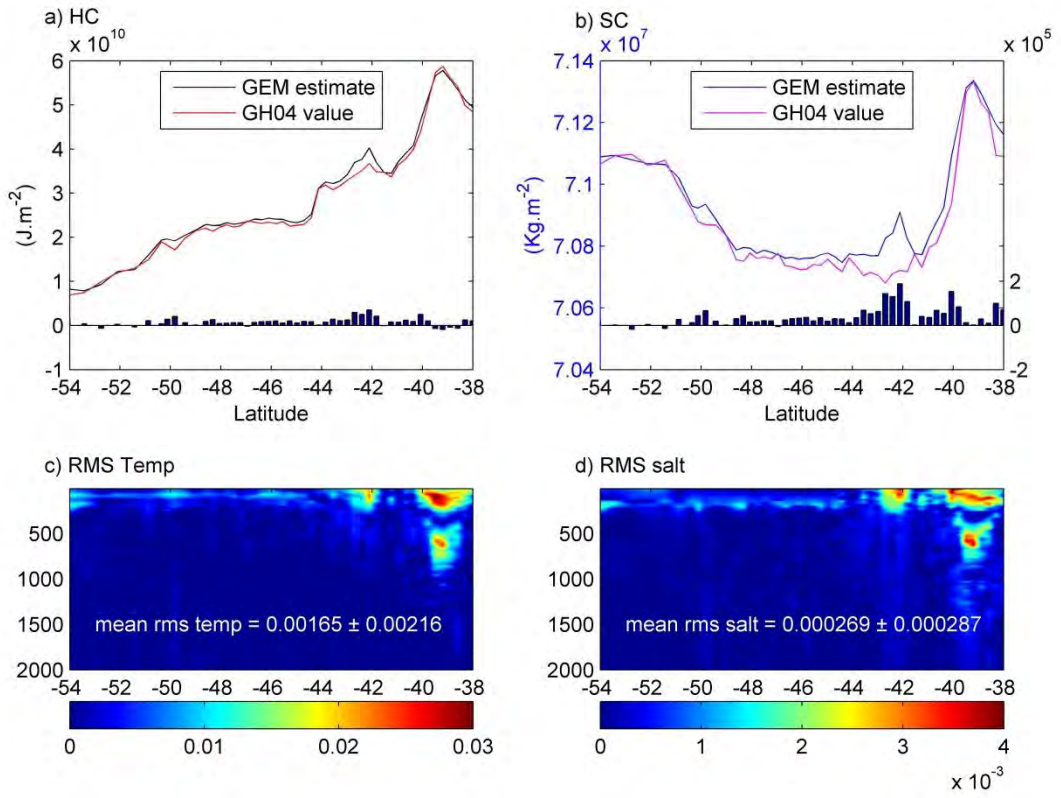

Figure 6.7 a) Heat content for the upper 2000dbar of the water column plotted with latitude. The cruise and GEM calculated values are depicted as lines, and the differences between the two estimates (GEM-GH04) are presented as bars. b) Same as (a) but for salt content. c) Root Mean Square (RMS) error in the difference between the GEM temperature field and the observed cruise measurements (GEM-GH04). d) Same as (c) but for salinity.

The GEM estimated heat content agrees well with observations at all latitudes, with only a minimal offset observed at ~42ºS where the GEM overestimates the heat budget (see Figure 6.7a). This overestimation corresponds to the position of the warm and salty eddy visible in Figure 6.5 c and d, yet the feature is less prominent in the observations. The GEM deduced salt content (Figure 6.7b) shows a similar decent agreement at this location with the cruise estimates, except for the anomalous spike where the GEM overestimated salt - evident as larger barred differences at ~42ºS. The location of the deviations seen in Figures 6.7 a and b

correlate with the exaggerated reproduction of T and S values in the upper 500dbar noticed in Figure 6.6. The RMS errors in T and S observed in Figures 6.7 c and d are two orders of magnitude smaller than those reported by Swart et al. (2010). Two patches of elevated RMS differences in both T and S are noticeable, one at ~42ºS and the other a deeper reaching deviation north of 40ºS.

6.2 Inclusion of bathymetry.

Up until this point, the maximum depth of the T and S fields used to set up the GEM projection correlated with the deepest pressure that the CTD was deployed to. In order to better represent reality, Etopo2 Bathymetry obtained for the GoodHope line coordinates is now employed as the bottom limit of the hydrographic data used to create the GEM. The use of this bathymetry allows for a smoother and less erratic bottom limit of the property fields, compared to the maximum depth that the CTD sampled to which often changes substantially between stations.

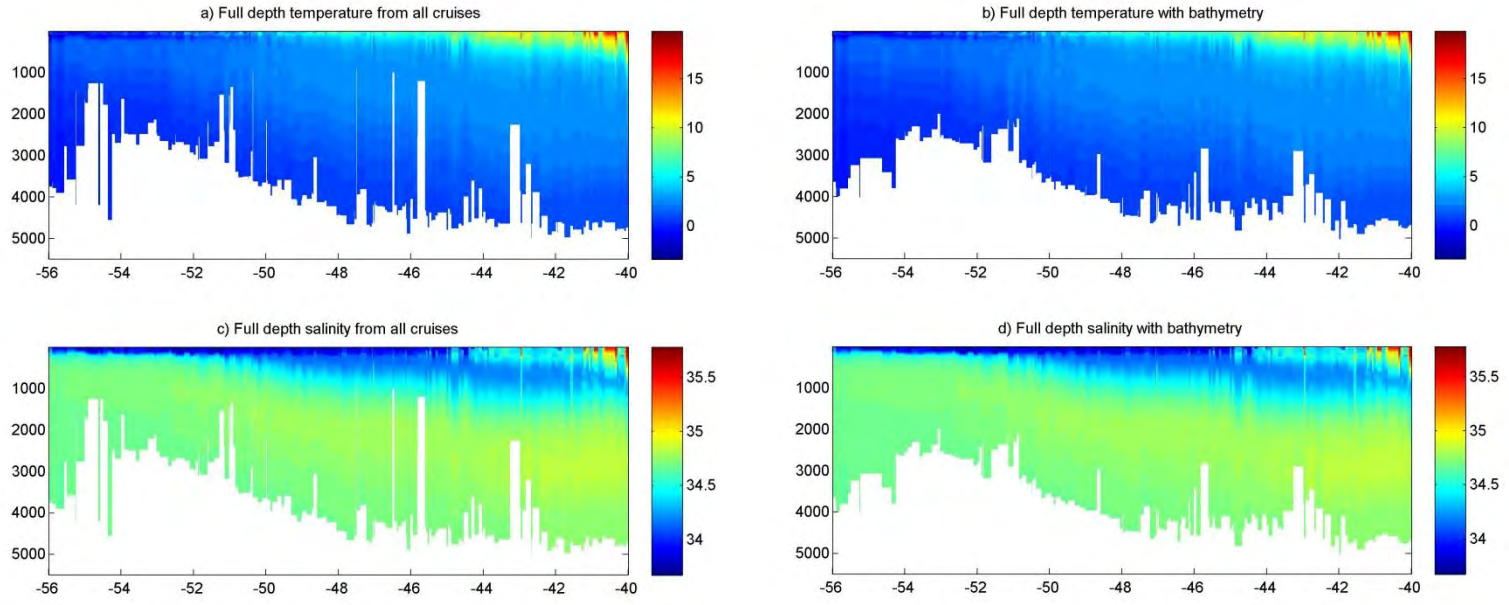

Figure 6.8 a) Temperature section from all synthesized de-seasoned cruise data with maximum depth of property field being that of the CTD cast. b) Temperature section from all synthesized de-seasoned cruise data with the maximum vertical limit set by the depth of the bathymetry. c) Same as (a) but for salinity. d) Same as (b) but for salinity.

The inclusion of bathymetry allows for a smoother bottom limit for the T and S sections, as can be seen in Figure 6.8 b and d compared to the spikes in the white shading of Figure 6.8 a and c due absence of values as the CTD stopped measuring at inconsistent depths. The use of realistic bottom topography allows for a more accurate depiction of the vertical water column structure and property distribution along the GoodHope line.

6.2.1 Testing GEM including topography against observations.

In order to verify that the use of Etopo2 Bathymetry, as the bottom vertical limit of the property fields used to set up the GEM projection, has not introduced errors, the full depth GEM produced fields (using the cruise DH input of GH2004) are compared with the in-situ observations.

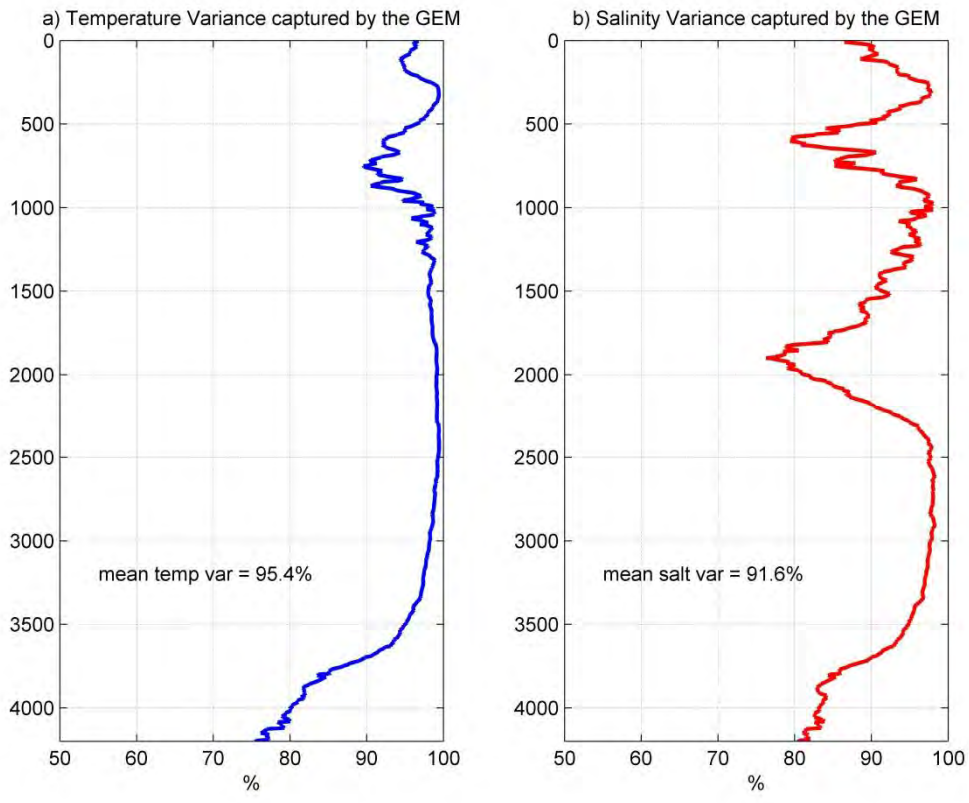

Figure 6.9 Percentage of full depth (a) temperature and (b) salinity GEM-captured variance observed in GH2004.

On average, over the entire water column, the GEM is able to capture over 95% of the total T variance and 92.4% of the total S variance. The percentage of T variance captured remains

high for most of the profile, only dropping to just less than 80% below 3500bdar. The GEM is in general less successful at capturing the S variance, with minima in variance captured located at ~600dbar, ~1900dbar, and ~4200dbar. The full depth error fields shown in Figure 6.10 exhibit small errors in the upper 1000dbar at ~42ºS and north of 40ºS, but in general the RMS differences are small.

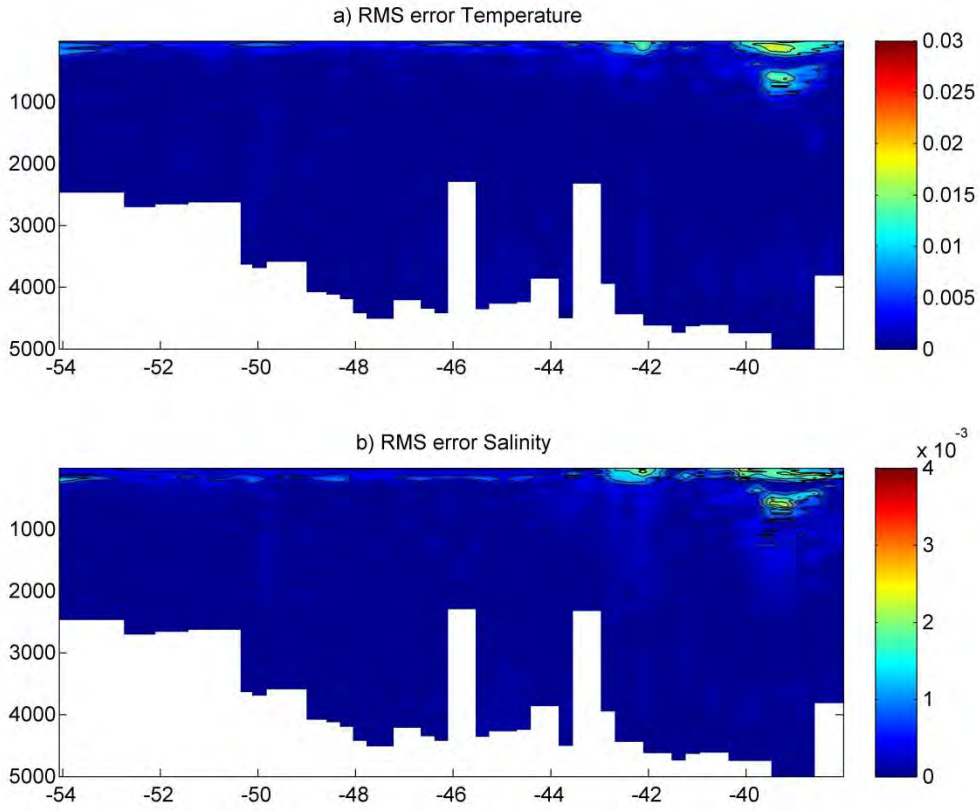

Figure 6.10 Full depth RMS error in (a) temperature and (b) salinity between the GEM fields and observed data (GEM-GH004). Note: the maximum depth of the error fields is that of the in-situ cruise CTD measurements, not the depth of the topography.

6.3 Inclusion of Argo data.

Argo data is available for the region since 2004, providing improved spatial and temporal resolution of the upper 2000dbar of the water column. All float measurements located within the study box (refer to Section 4.2) were synthesized with the cruise data to render an updated GEM product. The upper 2000dbar of the T and S fields used to set up the GEM are therefore

a compilation of both cruise and Argo profiles, while all measurements below 2000dbar up until the bathymetry belong to the cruise sampled values.

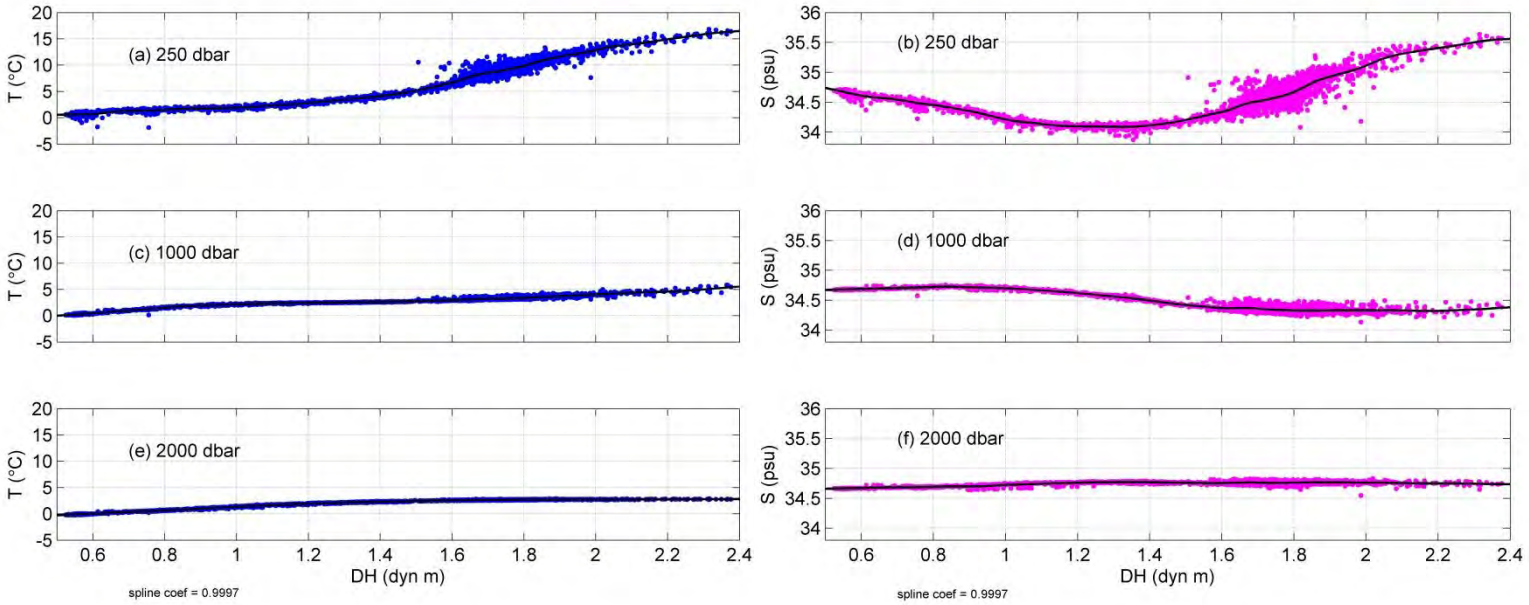

Figure 6.11 Relationship of temperature vs DH at (a) 250dbar, (c) 1000dbar and (e) 2000dbar for all available hydrographic data in study box limits fitted with a smoothing spline. (b), (d), and (f) same as (a), (c), and (e) respectively but for salinity.

Figure 6.11 shows the effect of the inclusion of Argo data via the substantial increase in reference points for the splines when compared to Figures 6.3 and 6.4. Both T and S are observed to have a strong tendency to cluster around a smoothing spline (Figure 6.11). The magnitude of scatter distance of properties about the splines is largest at 250dbar at dynamic heights higher than 1.6 dyn m, with salinity showing the widest distribution. The proximity of values to the splines gets tighter with increasing depth indicating a higher level of accurate predictability of T and S values corresponding to a DH measurement.

The Argo stations are not located exactly on the GoodHope line (as this would render very few profiles), but instead are within the geographical limits of the study box. For reference, the study domain and the location of each station can be seen in Figure 4.1. The challenge that is presented when including Argo data into the GEM is that the float maximum sampling depth is limited to 2000dbar. Therefore all data deeper than this is restricted to that obtained from CTD deployments only. In order to merge the top layer (above 2000dbar; cruise and

Argo) with the bottom layer (below 2000dbar; just cruise), the bottom layer must be interpolated onto the station coordinates of the top layer profiles. In this process the bathymetry is distorted and therefore a trade-off presents itself between the massive increase in magnitude of reference points upon which to build the GEM relationships, and the loss of real usefulness of the data below 2000dbar. It was therefore decided for the purposes of this study that the GEM will be limited to the upper 2000dbar, and for now will not be full depth.

6.4 Focus on the AAIW layer.

Antarctic Intermediate Water (AAIW) was selected as the water mass upon which to focus the bulk of the investigation due to the import role it plays in ocean circulation and climate regulation. Despite the global significance, little is known about the variation in the heat and freshwater budgets of this water mass within the southeast Atlantic Southern Ocean. The AAIW layer is consistently located above 2000dbar and therefore within the vertical limits of the Argo and cruise based GEM. In order to assess the ability of the GEM to reproduce the properties of this water mass, the GEM is tested against GH2004. The location of the AAIW layer was determined using the method and criterion described in Section 5.3.1.

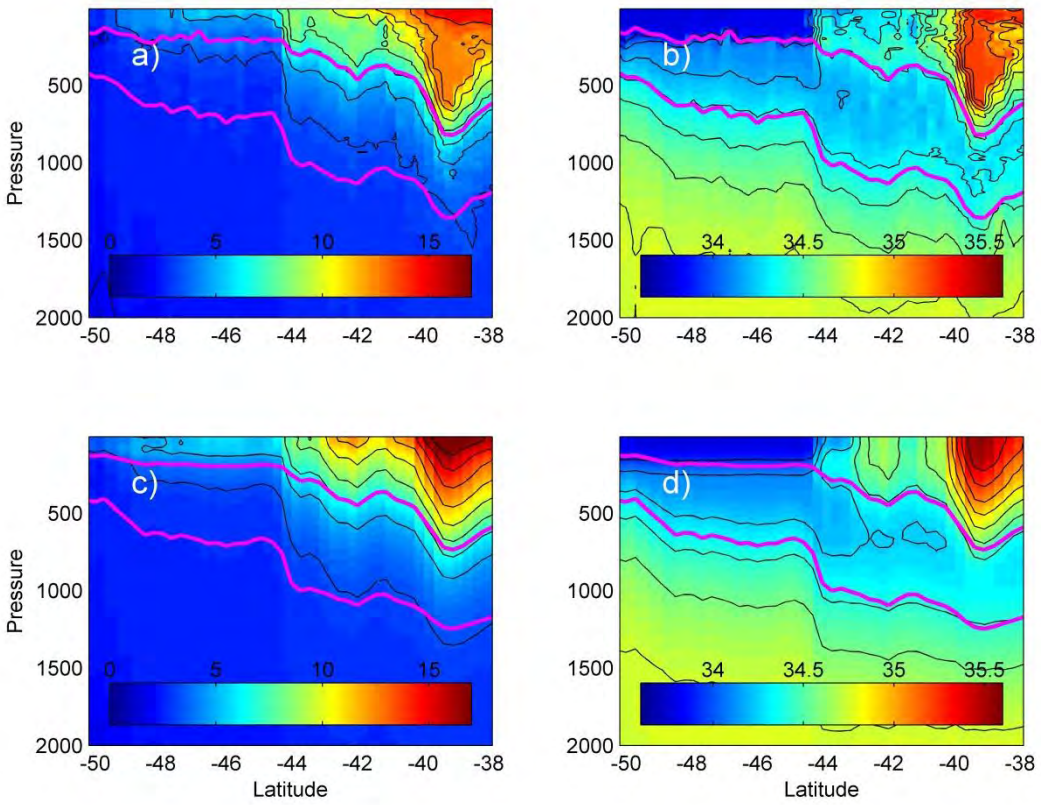

Figure 6.13 (a) Temperature and (b) salinity section from cruise measurements showing the upper and lower limits of AAIW (magenta lines). Panels (c) and (d) show the same but for the GEM produced temperature and salinity fields using GH2004 DH data as input.

Upon observation of Figure 6.13, it is evident that AAIW is located within a depth range of the GEM where the deviation from observations is minimal. For the whole upper 2000dbar, the GEM successfully represents the T and S fields observed in reality; showing even further robustness at doing so within the AAIW layer outlined in Figure 6.13 c and d.

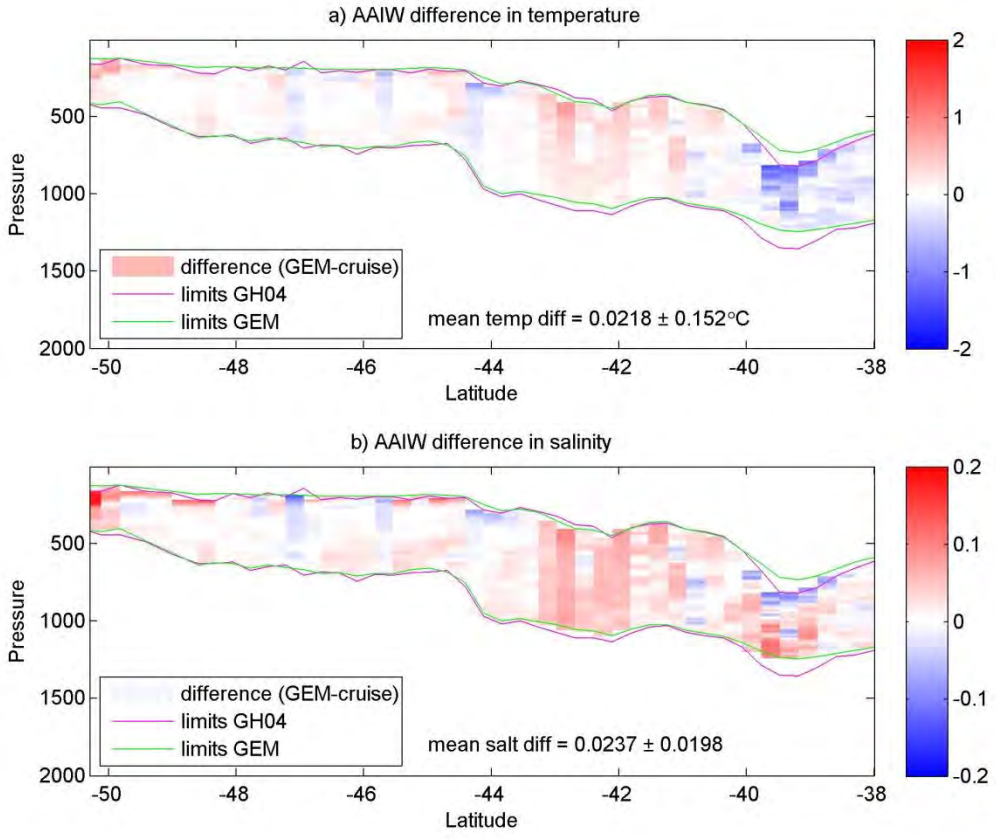

Figure 6.14 a) Temperature difference between GEM and original cruise measurements at all latitudes within the depth range of the AAIW layer. The total mean offset is reported, and the water mass limits calculated from the GEM and GH2004 potential density fields are overlaid. b) Same as (a) but for salinity.

The actual difference in T and S values at each depth within the AAIW limits common to both cruise and GEM is presented in Figure 6.14. There does not appear to be an overall

sizeable under- or over-estimation of temperature, with small positive differences located between 41ºS and 43ºS, and south of 50ºS, and a localised negative temperature difference present at ~39ºS. The salinity differences, on the other hand, show that the GEM is rendering slightly elevated salinities with this phenomenon being more pronounced at the same location of the anomalies in temperature. The average offsets for AAIW layer are small with comparatively large uncertainties, namely a mean temperature difference of 0.0218 ± 0.152 ºC and mean salinity difference of 0.0237 ± 0.0198. In general, the limits defined using potential density signatures in the GEM fields also correlate well with the positions of those limits identified in the cruise data.

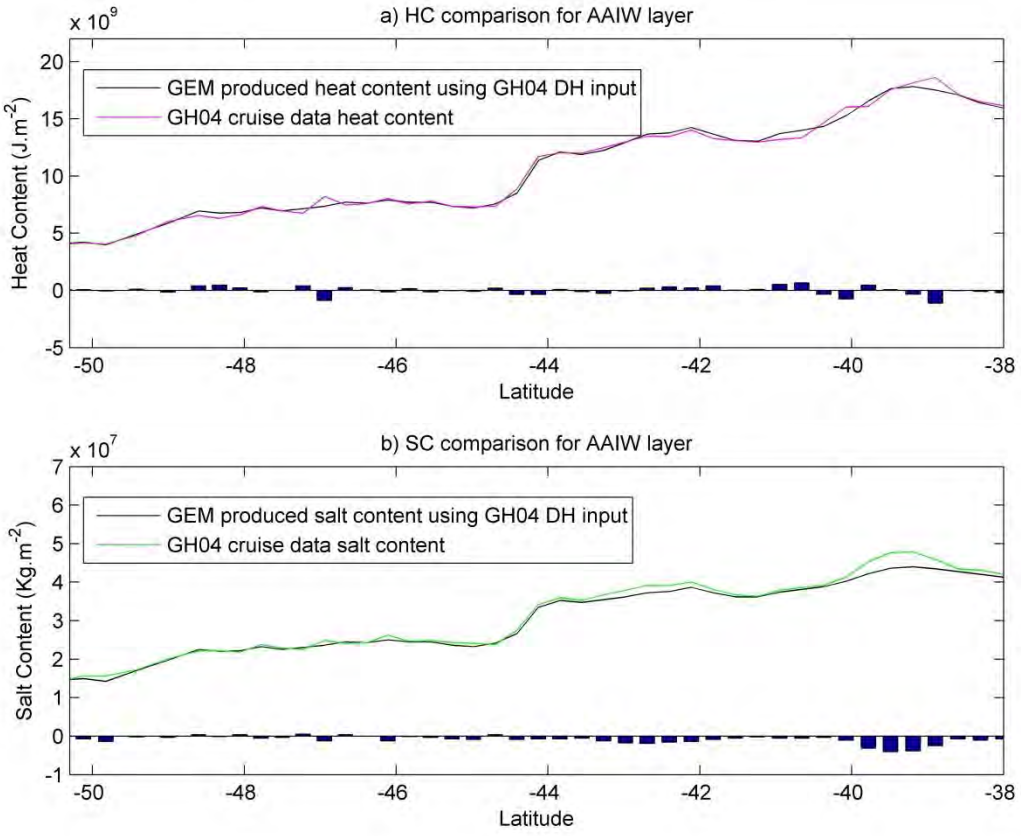

Figure 6.15 a) Heat content estimates calculated at each latitude for the AAIW layer for both GEM and cruise data. The difference between the two estimates (GEM-GH04) is presented as bars on the x-axis. b) Same as (a) but for salinity.

The estimates of heat and salt calculated from the GEM fields for the AAIW layer agree very well with reality (see Figure 6.15). South of 44ºS the offsets are almost negligible with the GEM HC and SC budgets overlaying the cruise calculated values almost exactly. North of 40ºS, a region of elevated mesoscale activity, the GEM estimates deviate more significantly from observations, underestimating both heat and salt (see Figure 6.15).

6.5 Discussion of results.

6.5.1 Addition of updated cruise data and implementation of new de-seasoning method.

The first step towards improvement of the existing GEM developed for the GH monitoring line (Swart et al., 2010), south of Africa, was to augment the hydrographic data used to establish the GEM relationships, and use an alternative de-seasoning process. On observation of the temperature residuals used to create the seasonal cycle, a cyclic pattern was evident, with the magnitude of the maxima and minima in residuals decreasing with zones progressively closer to the pole. As the oceans response to heat changes follows a relatively robust progression, it is expected that the seasonal cycle of temperature is equally regular. However, as factors driving salt variations in the Southern Ocean are far less distinct (e.g. precipitation, evaporation, and upwelling), the seasonal cycle of salinity residuals is less clear. When investigating the resultant de-seasoned T and S sections, both temperature and salinity increase steadily northwards, with anomalous highs in the northern limits representing the influence of Agulhas Rings. The influence of these mesoscale features and the presence of multiple water masses mixing at the same location in the northern limits of the study domain can be seen in the wider scatter of T and S values around the smoothing splines at higher DH values. It is this scatter that illustrates the difficulty in using the GEM proxy relationships to obtain thermohaline profiles from DH values north of 42ºS in the Southern Ocean.

Upon comparison with cruise data, the GEM is found to reproduce the observed thermohaline structure remarkably well. A slight overestimation of both T and S values is, however,

noticed in the northern limits of the study section. This exaggeration of properties is an artifact of the GEM process, whereby the T and S profiles of an entire column are laterally shifted to the location of the DH input measurement. In doing so T and S can be overstated in response to an elevated DH reading, as the GEM is unable to identify and replicate density compensating features at various depths. Some of these shortcomings of the GEM are exposed in the profiles of variance captured with depth. As even though the GEM does an outstanding job of reproducing the overall variability of the region, drops in both T and S between 600 and 800dbar, and a consistent drop in percentage of S variance captured below 1000dbar is noticed. Mixing of water masses resulting in different thermohaline values and vertical property structures corresponding to one DH signal is the likely culprit impeding the GEM from being highly accurate in reproducing the observed variability at these depths.

The heat and salt content estimated from the GEM for the upper 2000dbar is observed to follow a robust latitudinal agreement with that calculated from the cruise data. Small deviations are observed, but the magnitudes of these differences are minor. The same is true for the surprisingly small RMS error of the GEM. The errors presented in Figure 6.7 are two orders of magnitude smaller than those obtained by Swart et al. (2010) for the same region, as well as those observed by Meijers et al. (2011a) using a circumpolar GEM for the Southern Ocean. The largest RMS error values are located north of 40ºS, which is to be expected as this region presents an especially large challenge when using the GEM technique due to the elevated levels of mesoscale variability and water mass interaction. Overall, at this stage of development where the number of profiles used to set up the GEM has been augmented and updated, and a new and improved seasonal cycle has been implemented, the GEM is observed to perform with impressive aptitude. The GEM rendered T and S fields agree well with observations, capturing a large percentage of the variability and experiencing minimal errors.

6.5.2 Use of Etopo2 bathymetry.

The bottom vertical limit of the property fields obtained from CTD measurements was originally the maximum depth of the cast. In order to better represent reality, it was decided

that Etopo2 topography values along the GH line be used instead to delimit the depth of the ocean floor. The use of bathymetry allows for a smoother bottom boundary, avoiding the anomalous spikes where the CTD cast did not reach full depth. Upon comparison with in-situ observations, on the whole the variance captured is high, with over 95.4% and 91.6% of the observed respective T and S variability reproduced by the GEM. Drops in variability are observed, with minima located at the approximate depth of water mass interaction leading to mixing and transformation. At these depths the GEM is unable to adequately reproduce the variability observed in reality and thus the percentage of variance captured drops. It is important to keep in mind however, that these interactions are highly complex and even the most sophisticated high-resolution models have trouble reproducing these phenomenon.

Upon investigation of the full depth RMS error of the GEM generated property fields it is evident that the GEM projection is highly proficient at representing reality. Even the largest of the observed RMS values remain two orders of magnitude smaller than those observed by both Swart et al (2010) and Meijers et al (2011a). Larger errors are observed in the surface layer due to the presence of ocean-air exchanges, and in the northern limits of the domain as a result of the presence of eddy features. Both the mixed layer, and turbulent features such as eddies, present an obstacle for GEM success due to the presence of multiple options of water column structure along a single streamline (value of DH). This phenomenon is clearly visible in Figure 6.11 where T and S properties display a wide scatter about the smoothing spline at shallow depths and high DHs. Figure 6.12 exposes the source of this deviation from the spline, wherein it is shown that significantly different DH values exist within close proximity to one another north of the STF. The co-existence of multiple DH values for the same location over time is typical of the highly variable mesoscale and submesoscale regimes that dominate the northern limits of the Southern Ocean south of Africa.

6.5.3 Inclusion of Argo data.

In order to improve the spatial and temporal resolution of the hydrographic data used to set up the GEM relationships and establish the splines, all Argo float measurements available for the study box region were synthesised with the ship-based observations. The positive effect

of the inclusion of Argo data is evident in Figure 6.11 as a significant increase in reference points upon which to base the construction of the splines and thereby increasing the data pool from which the GEM statistical relationships are based upon. The benefits of the increased data resolution, however, come at the cost of the complete distortion of bathymetry. A possible solution would be to interpolate both the upper layer and lower layer data onto the common coordinates of the GoodHope line and then include the Etopo2 topography for the transect, however this would significantly decrease the number of data points upon which to build the splines, and in turn render the GEM less robust. It is critical that the ñoutliersò in the relationship of T and S with DH remain, as these provide important reference points for the anomalous events that occur in the region. It is at this point that the decision was made to concentrate on the upper 2000dbar, as AAIW ï the focus water mass of this study - is located in this depth range. However, for an alternative investigation where observation of the bottom layers is desired, the data can be interpolated onto the GH coordinates and the full depth property fields utilised.

For the purposes of this study even though the loss of the bottom layer data is unfortunate, the disadvantage of this is outweighed by the advantage of the massive improvement in resolution of the upper 2000dbar. With cruise and Argo combined, the de-seasoned modal sections are far more representative of the ACC than when previously using ship based observations alone. Further confirmation, regarding the benefit of increasing the quantity of hydrographic data, is shown in Figure 6.13 where the outstanding ability of the GEM to reproduce observations over the entire upper 2000dbar, and especially within the AAIW layer, is revealed. The AAIW water mass is located within an area of the GEM fields where the results are most accurate. This notion is supported by the very low RMS error within the entire AAIW layer. In general, the actual differences in T and S values show very small offsets throughout. The largest dissimilarities are located in the northern domains, and south of 50ºS. Elevated offsets equator-ward of 42ºS is to be expected due to the influence of the Agulhas Current region and associated variability, whereas the positive anomalies in the southernmost reaches are unexpected and are believed to be artefacts of the subsurface temperature minimum of Winter Water. As the characteristics of winter water change during its life time from formation, to interaction with the atmosphere, and then subduction, so would the T and S characteristics in this layer vary with season thus presenting a challenge to the GEM. Overall, the evidence presented confirms the robustness and suitability of using the GEM to further investigate the characteristics and variability of AAIW in the region.

6.5.4 Focus on AAIW layer.

To validate the proficiency of the GEM at reproducing the property fields of AAIW, the results are tested against cruise observations. The blue shading in the anomaly plots (Figure 6.14), and the negative offset bars in Figure 6.15 of heat and salt content, show that the GEM underestimates both temperature and salinity north of 40ºS within the AAIW layer. This may be an indication of the GEMôs incapacity to accurately replicate the deep reaching influence of mesoscale features in the region. For example, anomalously warm and salty water flowing within the Agulhas Current is injected into the GEM study box region via eddy shedding. While the GEM is able to represent these warm saline features in the upper 500dbar (as seen in Figure 6.13 c and d), it does not register the extent of elevated T and S reaching the AAIW layer. As a result the GEM slightly overestimates the thermohaline properties within the surface layer, and underestimates them within the AAIW layer.

On the whole the GEM appears to do an outstanding job at reproducing the thermohaline properties of the water mass layer, showing minor absolute T and S differences, and a very good agreement to heat and salt budgets, when compared to observations. AAIW is located within a depth range where the larger errors associated with the GEM produced fields are mostly avoided. The water mass is found deeper than the surface layer where ocean-atmosphere exchange presents a challenge for the GEM, at depths greater than the sizeable deviations present in the northern reaches of the domain, yet always residing above 2000dbar where the combination of Argo float and ship-based observations provide high resolution coverage of the region and a sizeable data pool from which to base the new GEM. The upgraded GEM can therefore be used with confidence to generate T and S fields relevant for the AAIW layer along the GH line.

7. The Altimetry GEM.

Values of DH obtained from cruise CTD measurements have, up until this point, been used as input to derive thermohaline fields for the southeast Atlantic sector of the Southern Ocean using the GEM. However, AVISO updated delayed weekly maps of sea level anomaly (MSLA) are available for the region starting from 1992 and running to the present. By interpolating the SLA fields onto the GH line, and combining them with a mean dynamic topography (MDT) specifically relevant to the study region (calculated from all the available hydrography), an absolute dynamic topography (ADT) is attained (Swart et al., 2008). This ADT offers DH values relevant to the GH line at weekly time steps from October 1992 to February 2012. By uniting this satellite measured dataset with the GEM, an altimetry GEM (AGEM) is obtained.

Satellite altimetry data itself has its own errors. It is therefore essential that the AGEM is rigorously tested before any robust conclusions can be drawn from the resultant proxy fields. The fields generated using DH values for the exact dates of a certain cruise are compared to the *in situ* measures (note the cruise data is removed from the hydrographic fields used to set up the GEM during this testing process). To ensure a thorough assessment of the AGEMôs proficiency within the AAIW layer this test is not only executed for GH2004, which has been the traditional cruise against which to assess the GEMôs performance, but also for the GH2006 and GH2009 cruises.

7.1 Testing the AGEM against cruise based observations.

The AGEM created fields are generated using an input DH value produced by adding the satellite measured SLA for a certain date to the MDT corresponding to the location of the altimetry measurement. The GEM established relationships are then used to attain the T and S value at each depth interval that corresponds to this surface ADT value of DH.

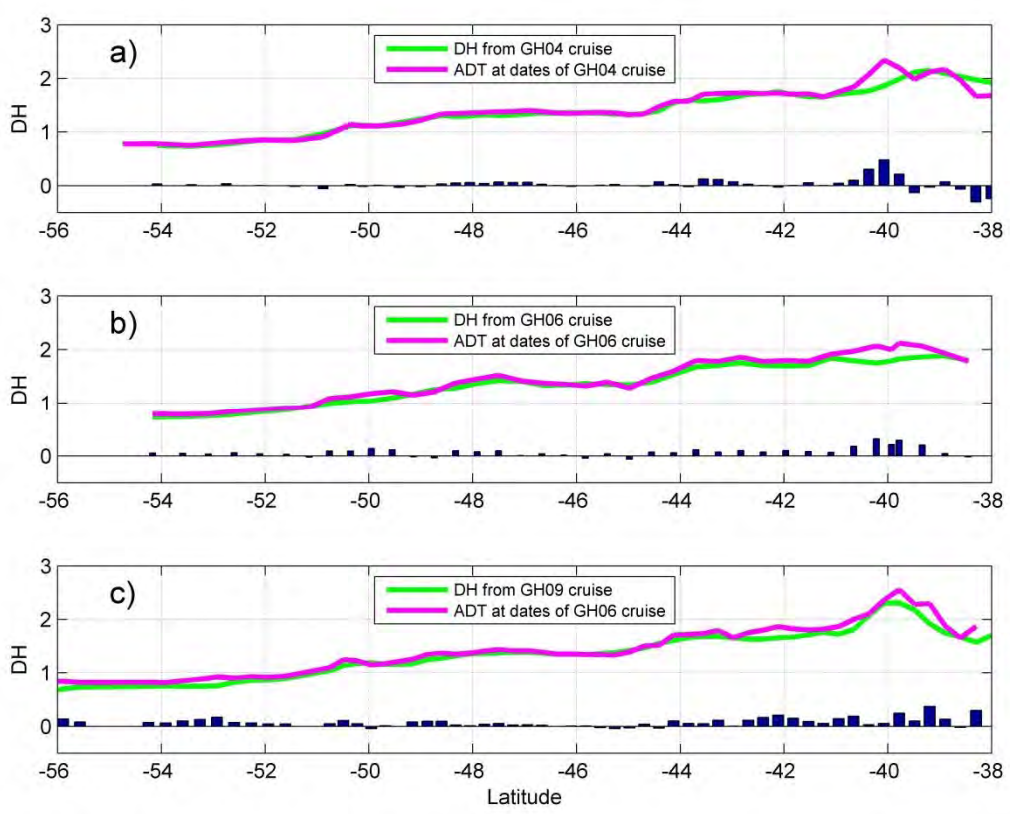

Figure 7.1 Dynamic heights at the surface relative to 2000dbar (calculated from cruise T and S fields) plotted with latitude in green, and ADT (aviso SLA plus Mean Dynamic Topography (MDT) product) plotted in magenta for (a) GH2004, (b) GH2006, and (c) GH2009 comparisons. Difference between ADT and cruise DH presented as bars.

The ADT product for the region in general matches well with DHs calculated from cruise measurements capturing the general change in sea surface height with latitude (Figure 7.1). The largest deviations are evident in the northern sector of the transect where the ADT consistently exaggerates DH with the higher magnitudes of offset located between 39ºS and

41ºS. The deviation of the ADT product from the DHôs observed in the cruise data is larger in general over all latitudes for the GH2009 comparison (Figure 7.1c). What is somewhat unusual, compared to the GH2004 and GH2006 comparisons, is the larger deviation between ADT and cruise DH south of 52ºS. In this sector, the altimeter reported higher SSH anomalies than those observed in reality. For both the GH2004 and GH2006 tests (Figure 7.1 a and b respectively), the largest and most significant deviations are centred about 40 ºS. The ADT appears to be frequently overestimating the DH in this area with, for example, either a complete exaggeration of a spike or dual spikes represented in the ADT fields when only a single peak of reduced magnitude is observed in reality.

The MDT is constant with time and it is therefore the SLA measured by altimetry that is the likely source of the error in the DH estimates. The SLA fields are constructed based on a weekly composite of the satellite transects, which are then subsequently interpolated onto the GH coordinates. It therefore appears from Figure 7.1 that the altimeter product frequently measured positive SSH anomalies relevant to the region during the times that the various cruise profiles were obtained, but evidently these elevated DHôs were not present on the exact date of the *in situ* stations.

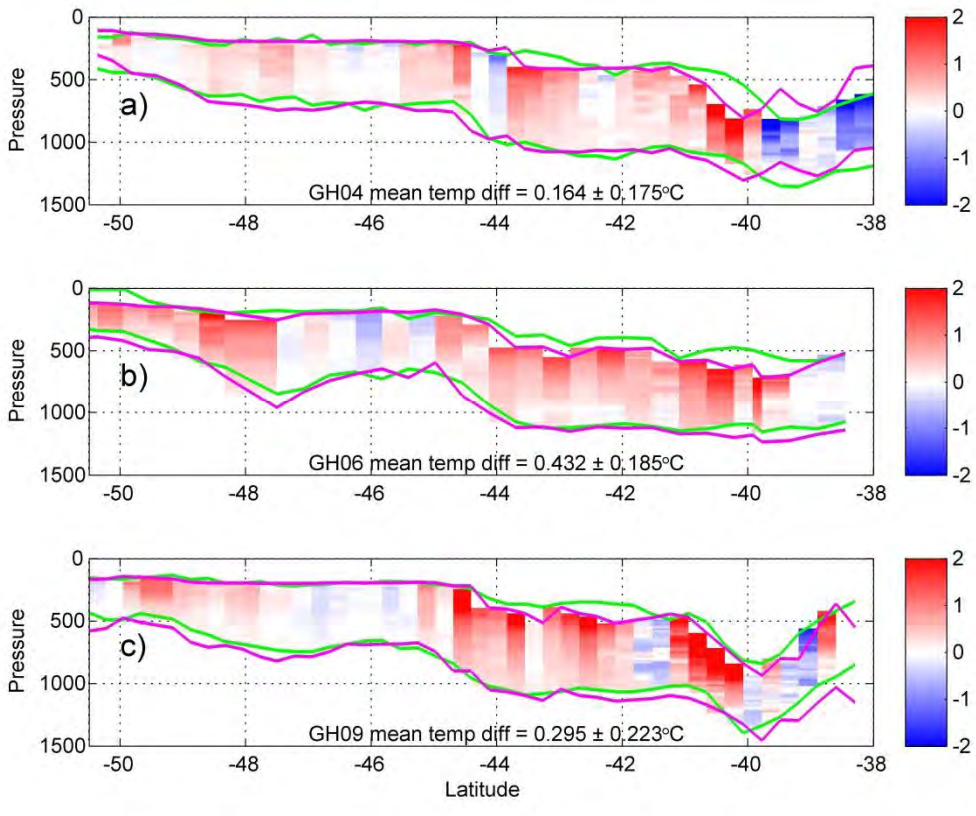

Figure 7.2 Temperature difference between AGEM and original cruise measurements at all latitudes within the depth range of the AAIW layer for (a) GH2004, (b) GH2006 and (c) GH2009 tests. The green contours represent the cruise calculated isopycnal limits of AAIW and the magenta contours indicate the AGEM calculated limits of the water mass.

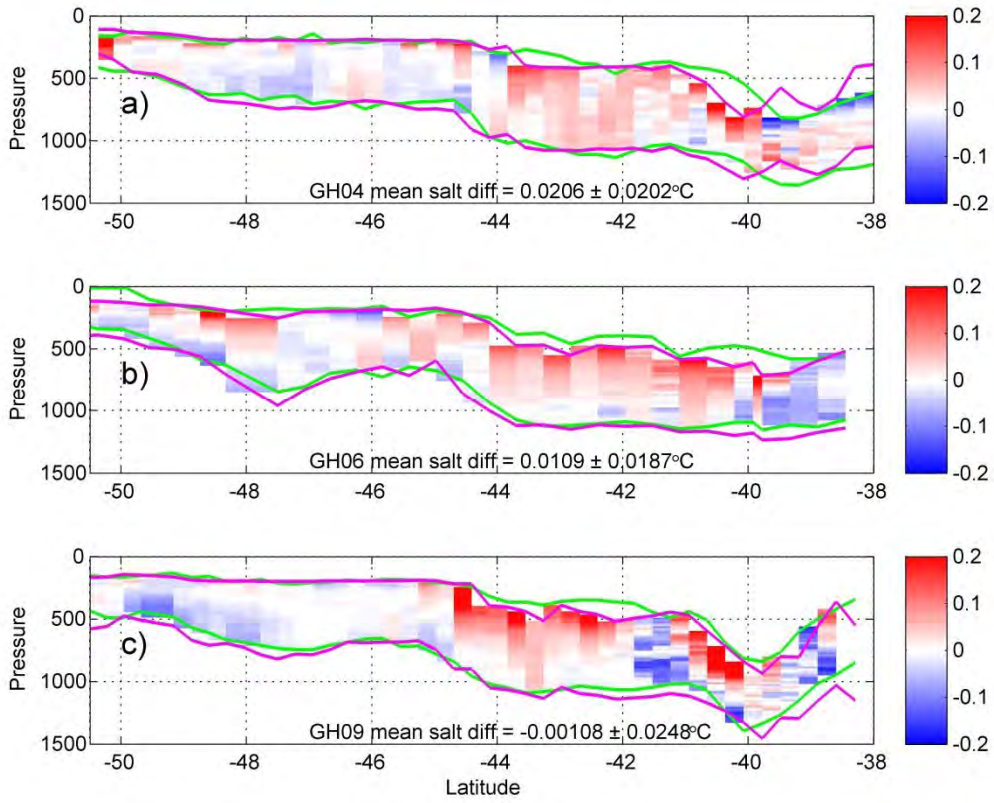

Figure 7.3 Salinity difference between AGEM and original cruise measurements at all latitudes within the depth range of the AAIW layer for (a) GH2004, (b) GH2006 and (c) GH2009 tests. The green contours represent the cruise calculated isopycnal limits of AAIW and the magenta contours indicate the AGEM calculated limits of the water mass.

The absolute differences in T and S presented in Figures 7.2 and 7.3 are larger than those observed in Figure 6.14 for the GEM before it was coupled with satellite data. The T differences are overall positive at most latitudes, with the GH2006 cruise (Figure 7.2b) showing the largest mean offset. Negative AGEM T anomalies are noticeable north of 39ºS for all three tests, yet are most prominent for the GH2004 comparison (Figure 7.2a). No clear dominance of positive or negative values is visible for the AGEM offset in S, as the

anomalies vary both with cruise comparison and latitude. The GH2004 and GH2006 tests (Figure 7.3 a and b respectively), present positive mean S anomalies. The GH2009 comparison exposes the largest magnitudes of positive S difference at a single depth and location (shown by strong red shading in Figure 7.3 c), yet the mean reported offset averaged for all latitudes within the AAIW layer is negative. The results for the anomalies in AGEM calculated T values compared to those of the cruise are plainly seen to be overall positive, while the S offset results are somewhat less clear.

The differences presented in Figures 7.2 and 7.3 are calculated by subtracting the cruise property measurement from the AGEM value. Therefore a positive anomaly signifies an overestimation by the AGEM. The bar differences between the DH of the ADT and that calculated from cruise measurements are mostly positive at all latitudes shown in Figure 7.1. This higher DH estimate used as AGEM input thus appears to effect more so the AGEMôs ability to accurately reproduce T fields than S fields, resulting in elevated T values compared to those observed in reality.

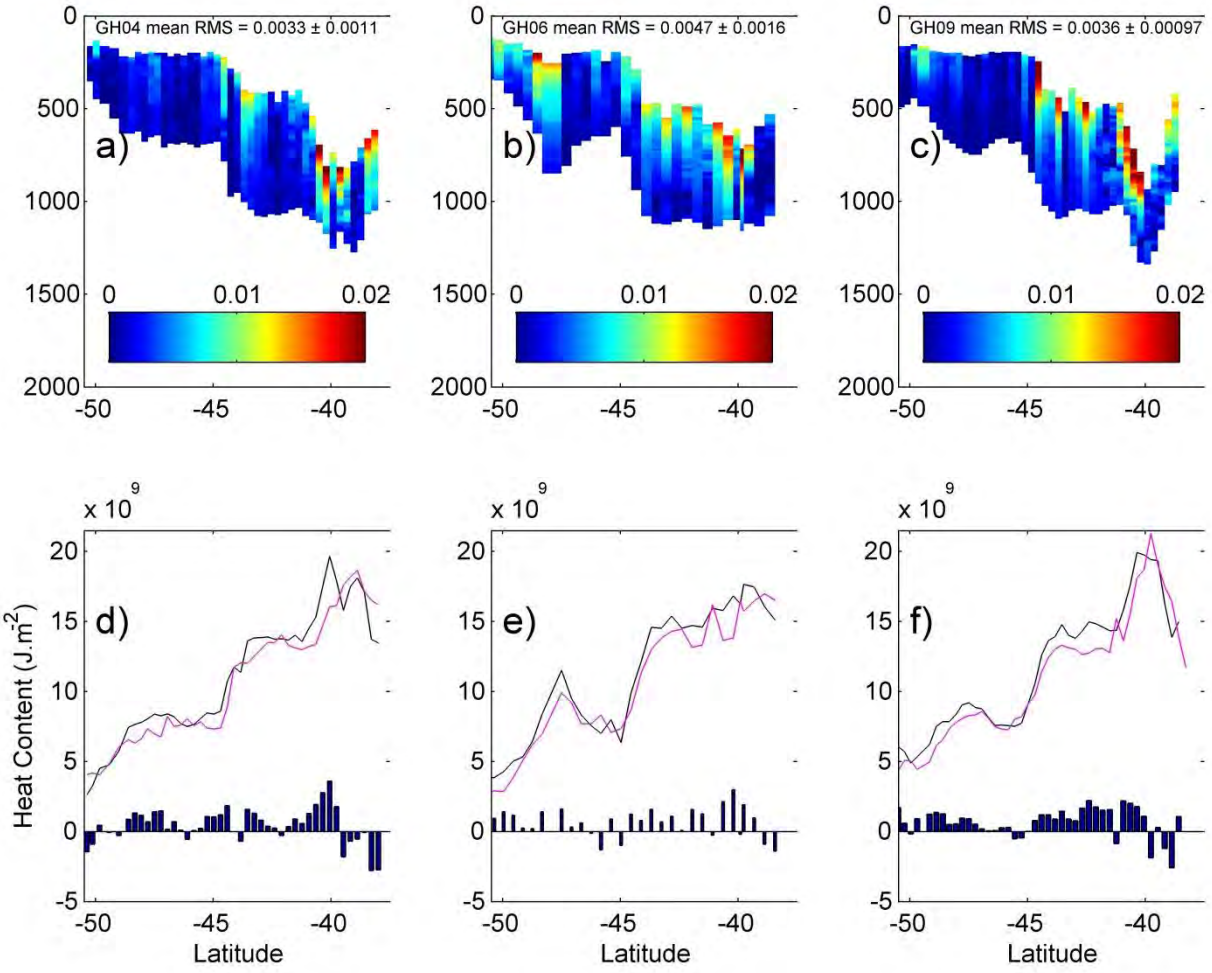

Figure 7.4 Temperature RMS error at all depths within the AAIW layer for the AGEM compared with (a) GH2004, (b) GH2006 and (c) GH2009 fields. The average error for the entire AAIW segment is also reported. Heat content (HC) comparison for the AAIW layer for the (e) GH2004, (f) GH2006, and (g) GH2009 tests. Black line represents the AGEM calculated HC, and magenta the estimate from cruise obtained data. The differences in estimates are presented as bars (AGEM-cruise).

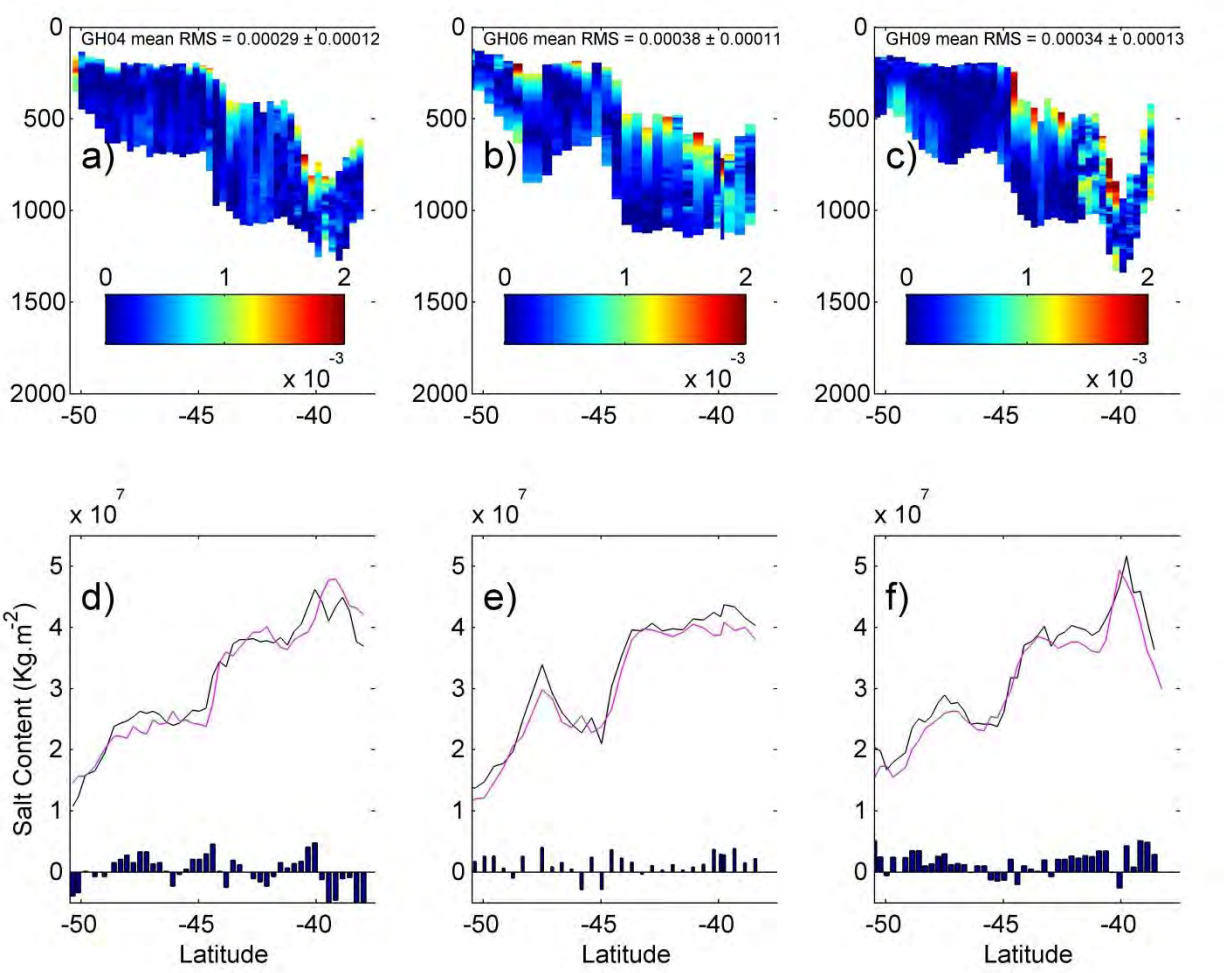

Figure 7.5 Salinity RMS error at all depths within the AAIW layer for the AGEM compared with (a) GH2004, (b) GH2006 and (c) GH2009 fields. The average error for the entire AAIW segment is also reported. Salt content (SC) comparison for the AAIW layer for the (d) GH2004, (e) GH2006, and (f) GH2009 tests. Black line represents the AGEM calculated SC, and magenta the estimate from cruise obtained data. The differences in estimates are presented as bars (AGEM-cruise).

The AGEM RMS T and S errors associated with the depth range belonging to AAIW are relatively small (Figures 7.4 a-c and 7.5 a-c), remaining two orders of magnitude less than those reported by Swart et al. (2010). The mean T RMS error reported for the GH2004 comparison of $3.3 \pm 1.1 \times 10^{-3}$ (Figure 7.4a), is just over double the value estimated for AAIW when the GEM (before altimetry) was compared with these same cruise measurements. The mean S RMS error for GH2004 (Figure 7.5a) of $2.9 \pm 1.2 \times 10^{4}$ is, however, only slightly larger than the original GEM salt error. The errors following the inclusion of satellite data therefore appear to manifest themselves in the AGEM generated T values more than in the S fields, as was previously noticed by comparing the anomalies of Figure 7.2 with those of Figure 7.3. Taking a more detailed look into the RMS differences, larger errors are observed to reside in the upper portion of the AAIW layer. This is most pronounced in the GH2009 comparison presented in Figures 7.4c and 7.5c. The GH2004 test exhibits the smallest RMS errors; the most sizeable being located around 40ºS (Figures 7.4a and 7.5a).

The AGEM heat content (HC) and salt content (SC) budgets for the AAIW layer presented in Figure 7.4d-f and Figure 7.5d-f respectively, agree very well with cruise estimates, tracking the general trend almost exactly. The differences in HC and SC (plotted as bars), are shown to be in general positive, indicating an overestimation of heat and salt by the AGEM (Figures 7.4d-f and 7.5d-f). Even though these differences are evident, their magnitudes are very small. Overall the AGEM appears to be highly successful at replicating the AAIW properties sampled during the all three cruises.

7.2 Effect of changing the study box domains.

One of the aims of this study is to obtain an AGEM possessing the smallest error possible. Therefore in order to investigate the source of the rise in offsets detected for the AGEM presented in Section 7.1, compared the GEM before the fusion with satellite data, an exploration into the limits of Argo data is undertaken. The fact that the ADT product is relevant to the GH line, yet the Argo data used to set up the GEM relationships is limited to a larger boxed domain, may possibly introduce some deviations in AGEM results compared to

observations. Much thought was applied to the choice of location of the boundaries of the data box, as a trade-off exists between the advantages of having more numerous reference points for the smoothing splines, and the disadvantages introduced via profiles that may loosen the GEM relationships due to their increased distance from the GH track. To investigate whether the performance of the AGEM can be improved via an alternative delimitation of Argo data, three smaller study boxes that closely fit about the GH line are proposed (see Figure 7.6), and the test results from the subsequent AGEM are compared with the current test relevant for the GH2004 cruise.

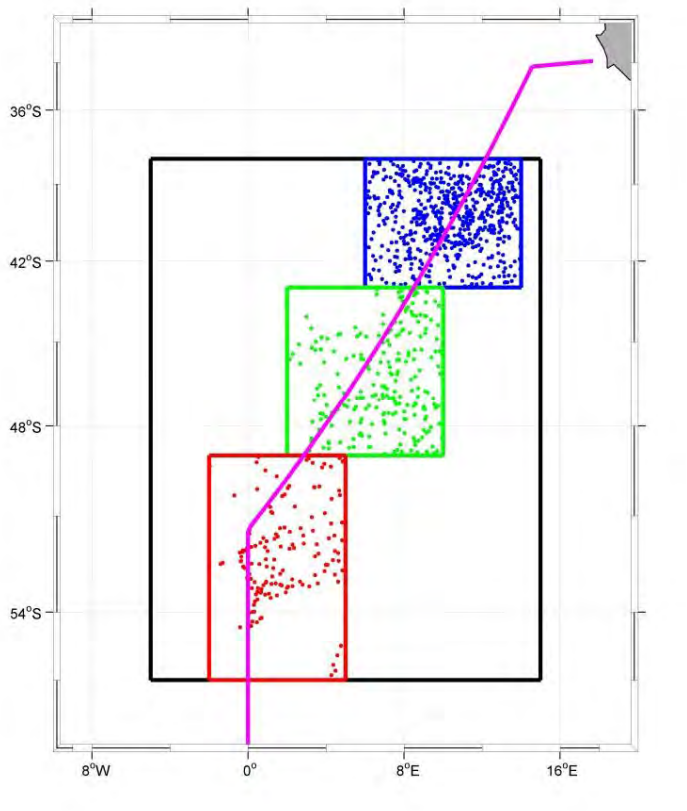

Figure 7.6 Map showing the southeast Atlantic Southern Ocean with the GoodHope line overlaid in magenta. The boundaries of the original study box are marked in black and the alternative three smaller study boxes are marked in colour, with the location of Argo float profiles within each box represented as a dot.

The Argo data used to set up the alternative AGEM is sourced from the three smaller coloured boxes shown in Figure 7.6. The float profiles are less numerous than previously but

are more representative of the water properties relevant to the GH line, due to the proximity of stations to the cruise track.

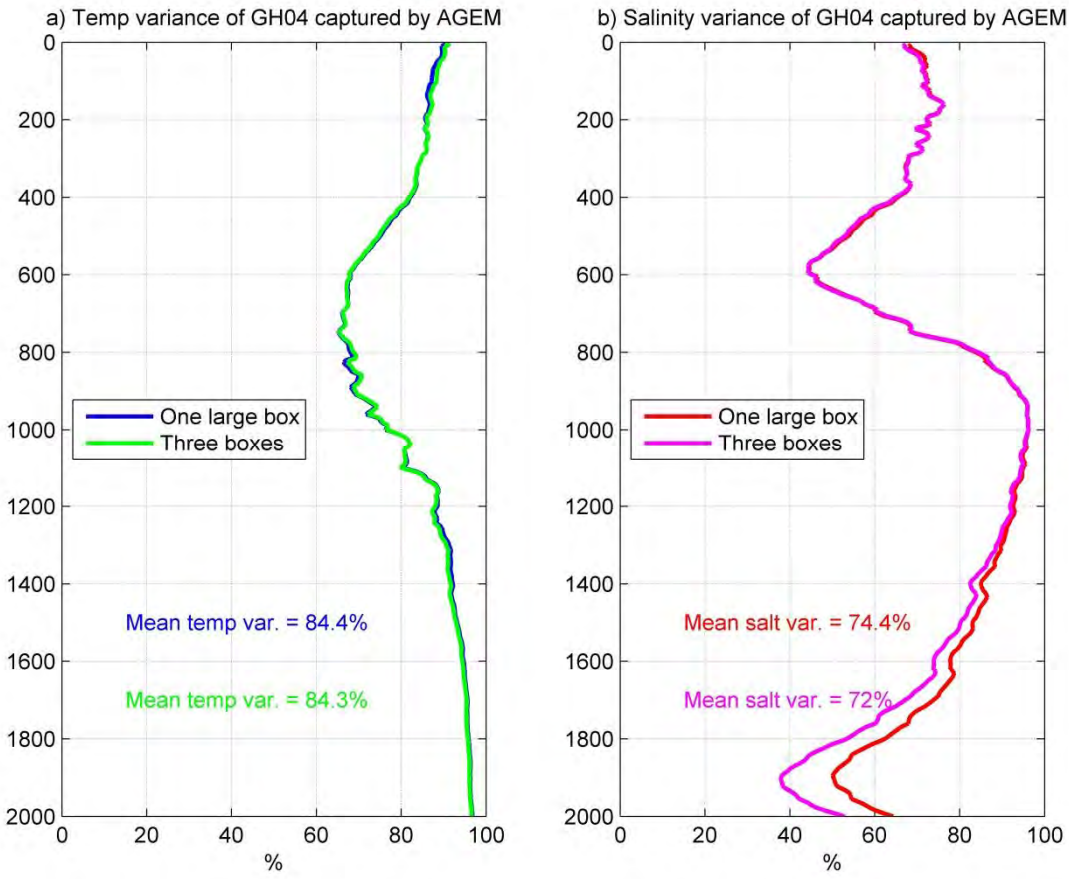

Figure 7.7 Percentage of (a) temperature and (b) salinity variance observed in the GH2004 cruise captured by the AGEM for the original Argo box limits and for the alternative Argo boundaries delimited by three smaller boxes.

It is evident from Figure 7.7 that limiting Argo to tight fitting boxes about the GH track does not increase the T and S variance captured. The variance plots for T practically overlay one another with a difference in mean variance of 0.01%. The profiles of percentage of S variance captured match tightly for the upper 1000dbar, but deviate at depth as the variance of the alternative Argo three box boundaries drops more extremely than that of the one large box limit.

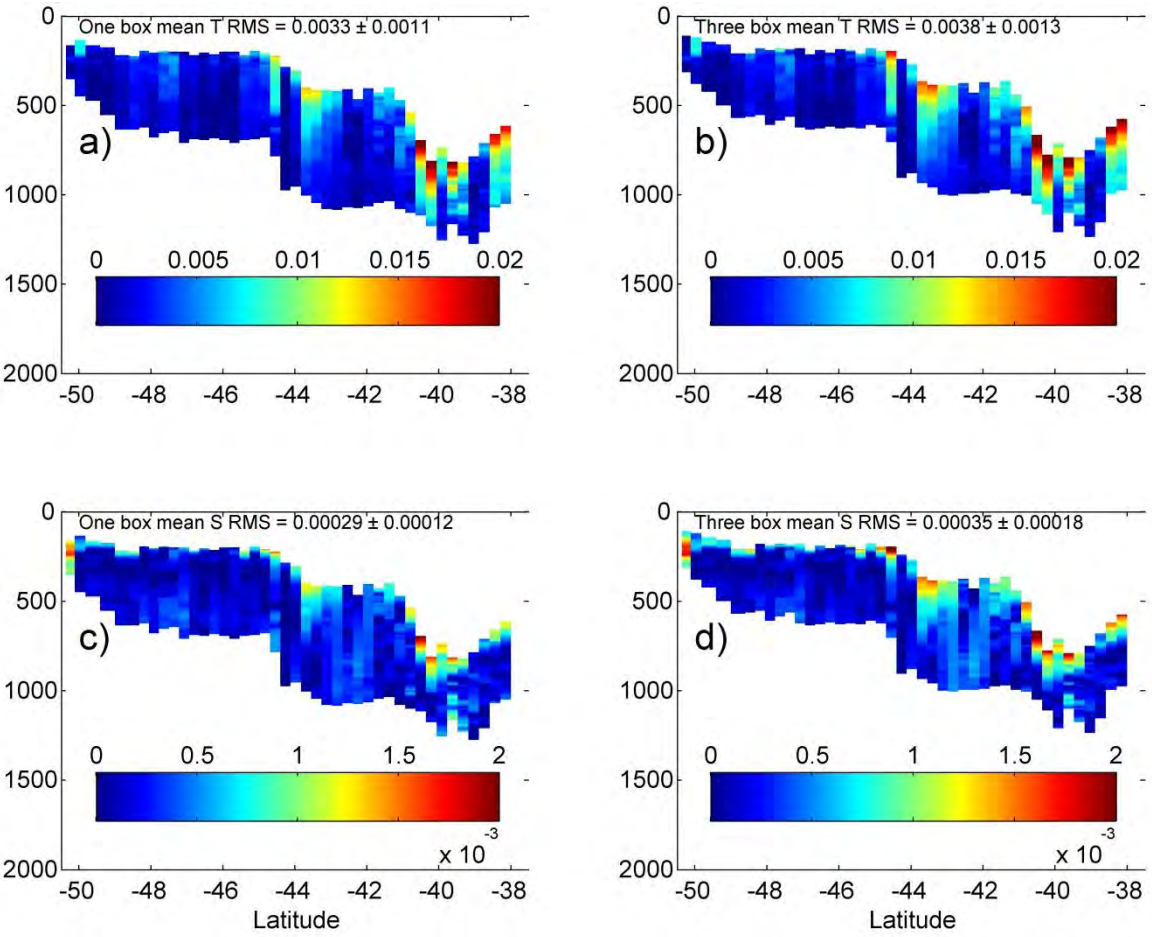

Figure 7.8 RMS temperature error of the AAIW layer for AGEM associated with (a) three box Argo delimitation and (b) one large Argo box limits. AAIW layer RMS salinity error for AGEM associated with (c) three box Argo delimitation and (d) one large Argo box limits.

The differences in RMS errors associated with the original Argo box limits and the alternative suggested three boxes are almost visually undetectable over all latitudes (see Figure 7.8). Nevertheless, what is evident from the mean errors reported in Figure 7.8 is that the average error associated with the three smaller box delimitation is slightly larger than the original box mean errors for both T and S. The differences are minor; however it is clear from this comparison that the alternative Argo data boundaries do not reduce the errors.

As neither an improvement in variance captured, nor a reduction in RMS, is provided by employing the alternative three box limits, the Argo data used to set up the GEM will remain bounded by the larger box shown in black of Figure 7.6. In doing so more Argo profiles are available, thereby providing more T and S data points upon which to build the spline fit, resulting in more robust GEM relationships.

7.3 Discussion.

The AGEM is created via the pairing of the GEM with satellite SLA measurements. In order to create a DH product to be used as input for the GEM developed in Section 6, SLA values interpolated onto the GH line are added to an MDT calculated from all available hydrographic observations (cruise and Argo) of the region. The MDT is calculated relative to 2000dbar (likely excludes much of the barotropic influences), yet the SLA measurements reflect changes below 2000dbar and include a barotropic component. The GEM fields are projected into baroclinic stream function space and do not represent any barotropic variations. This property of the GEM technique, combined with the fact that the SLA measurements are interpolated onto the GH track, and along with additional inherent altimetry errors, are likely responsible for much of the observed deviation in ADT from cruise DH calculations (Figure 7.1). Subsequent AGEM detected deviations from reality appear to be born largely from the errors in the DH used as input to generate the T and S fields. Here the AGEM results are summarised and discussed.

7.3.1 AGEM performance.

Upon reflection on the actual minor magnitude of the AGEM errors, it is evident that the generated T and S fields actually agree very satisfactorily with cruise measurements. It is to be expected that the inexact match of the ADT with cruise DH would generate some offset. The effects of this are seen in an increase the absolute thermohaline differences within the AAIW layer going from GEM to AGEM. An interesting phenomenon is visible north of 40ºS in the T and S anomaly plots (Figures 7.2 and 7.3), where the AGEM underestimates

property values. This indicates a lack of ability of the AGEM to translate an elevated DH reading to deep enough depths within the water column. Eddies found in this region of the ocean are deep reaching, with some features observed to trap water to up to 1600m depth (Dencausse et al., 2010b). The AGEM however cannot exactly capture the extreme ocean conditions associated with these features, hence resulting in the observed negative T and (less so) S offsets.

The RMS errors are minor within the AAIW depth range, with mean errors remaining two orders of magnitude smaller than those presented in previous Southern Ocean GEM studies. A similar outstanding agreement of HC and SC budgets is observed. These observations validate that even though errors are introduced through the deviation of the ADT DH from that observed in reality; these errors are not translated to greatly affect the AGEMôs ability to adequately reproduce the AAIW layer. The advantage of being able to generate thermohaline fields for at a weekly temporal resolution far outweighs the disadvantages of the errors introduced via the use of altimetry.

7.3.2 Alternative Argo delimitation.

An inexact ADT is identified as driving an increase in error comparing the AGEM to the GEM alone. In order to verify that these errors are soured from the altimetry SLA component of the ADT, and not the MDT calculated from hydrographic profiles, an investigation into the effects of changing the Argo boundaries is undertaken. It was hypothesised that possibly a wide spread of Argo data about the GH line (for which the MDT is relevant) may be the source of deviation. Upon examination as to whether the errors associated with the AGEM can be reduced via a tighter delimitation or Argo profiles, it was however found that having fewer data points upon which to build the GEM relationships reduced the variance captured and increased the RMS error. The changes are slight, but it is clear that no improvement is provided via the alternative 3 box Argo division. It thus appears that the source of AGEM errors is not the spatially wide distribution of hydrographic profiles used to create an MDT relevant for the GH line, but rather problems associated with the use of satellite data.

7.3.3 An inexact ADT.

Estimates of ADT deviate from the DH calculated from cruise obtained measurements largely due to sampling differences in time and space. This ñinexactò ADT is used as input for the AGEM, thereby creating property fields that deviate from observations. For the GH2006 cruise, for example, the ADT DH values were almost consistently higher than those calculated from cruise observations, subsequently creating overall positive absolute T and S differences and RMS errors. As the MDT remains temporally constant and the SLA evolves with time, it is likely that the weekly SSH anomaly fields at the time of the cruise dates are the source of this larger bias. The weekly SLA represents the mean conditions for a 7 day period and thus there is sure to be some deviation of this average from the daily conditions. In addition, the SLA is interpolated onto the GH track and therefore the measurements are not necessarily entirely accurate for this line. It was decided that the gridded maps of SLA data should be used in place of the along-track measurements as even though the northern sector of the GH line is directly overlaid by an altimetry track. This decision was based in the fact that once the AGEM is extended to be four dimensions (4D) and relevant to the entire ACC domain south of Africa, the along-track data is of no use. Therefore in order to cater for the future planned expansion of this work into a 4D GEM, the gridded and subsequently interpolated SLA fields were chosen. The error introduced via the interpolation of the gridded ADT data onto the GH coordinates is thought to be minor due to the overall proximity of the GH line to the Topex/Poseidon Jason 1 flight path, with the northern sector being directly overlaid by the altimeter track. Another source of possible bias lies within the inherent errors associated with the use of satellite data itself.

It is important to maintain perspective that even though errors are introduced via pairing the GEM with satellite altimetry, not only are these errors minor, but also that the advantages of obtaining time evolving T and S fields far outweigh the challenges associated with the use of altimetry. The actual size of the errors presented in this study are two orders of magnitude smaller than those reported by Swart et al. (2010), whose AGEM this research is designed to build and improve on. The results here presented are highly satisfactory, showing a comparatively outstanding agreement of the AGEM with observations relevant for AAIW.

The tests provided in this section thus foster confidence in the AGEMôs ability to accurately reproduce the thermohaline properties belonging to the AAIW layer.

8. Temporal evolution of AAIW.

AAIW can be identified throughout the Southern Ocean as a salinity minimum tongue and oxygen maximum (McCartney 1982; Sun and Watts, 2002). The core of this layer is closest to the surface just north of the Southern ACC Front (SACCF), and deepens as the water mass travels northwards, subducting below subtropical Central Waters layer to reside mostly at intermediate depths, composing the lower thermocline throughout the worldôs ocean (Piola and Georgi, 1982; Sloyan and Rintoul, 2001). As a product of this process, AAIW transports heat, freshwater and biogeochemical tracers from the surface to the interior ocean (Banks et al., 2000).

In the region of the ocean south of Africa, AAIW itself experiences high levels of mixing and consequent property transformation (Rusciano et al., 2012). Changes experienced by AAIW in the Atlantic sector of the Southern Ocean have a significant impact on global circulation, due to the important role the water mass plays in the Atlantic Meridional Overturning Circulation (AMOC) (Sloyan and Rintoul, 2001; Speich et al., 2001; 2007; Rimaud et al., 2012). However, as time series are largely absent for the southeast Atlantic Southern Ocean, little is known regarding variability and long term temporal evolution of the water mass, leaving many questions unanswered with regards to changes in thermohaline properties. It is thought that the Southern Ocean is warming at a rate faster than the global average, and that this warming is largely localized to the ACC (Gille, 2002; Gille, 2008). So as to gain some insight into the response of AAIW to a changing climate, the 20 years of AGEM generated fields are used to investigate the changes in heat content and salt content (HC and SC), variations in positioning within the water column, and alterations in thickness of the water mass. It is hypothesised that eddies may be influencing some of the observed changes occurring within the AAIW layer. So as to explore the validity of this notion, an eddy atlas for the southeast Atlantic Southern Ocean is employed to investigate the variation in frequency of respective cyclonic and anticyclonic activity and the change in the featuresô absolute dynamic topography (ADT) from 1992 to 2010.

8.1 AAIW behaviour at the GH transect.

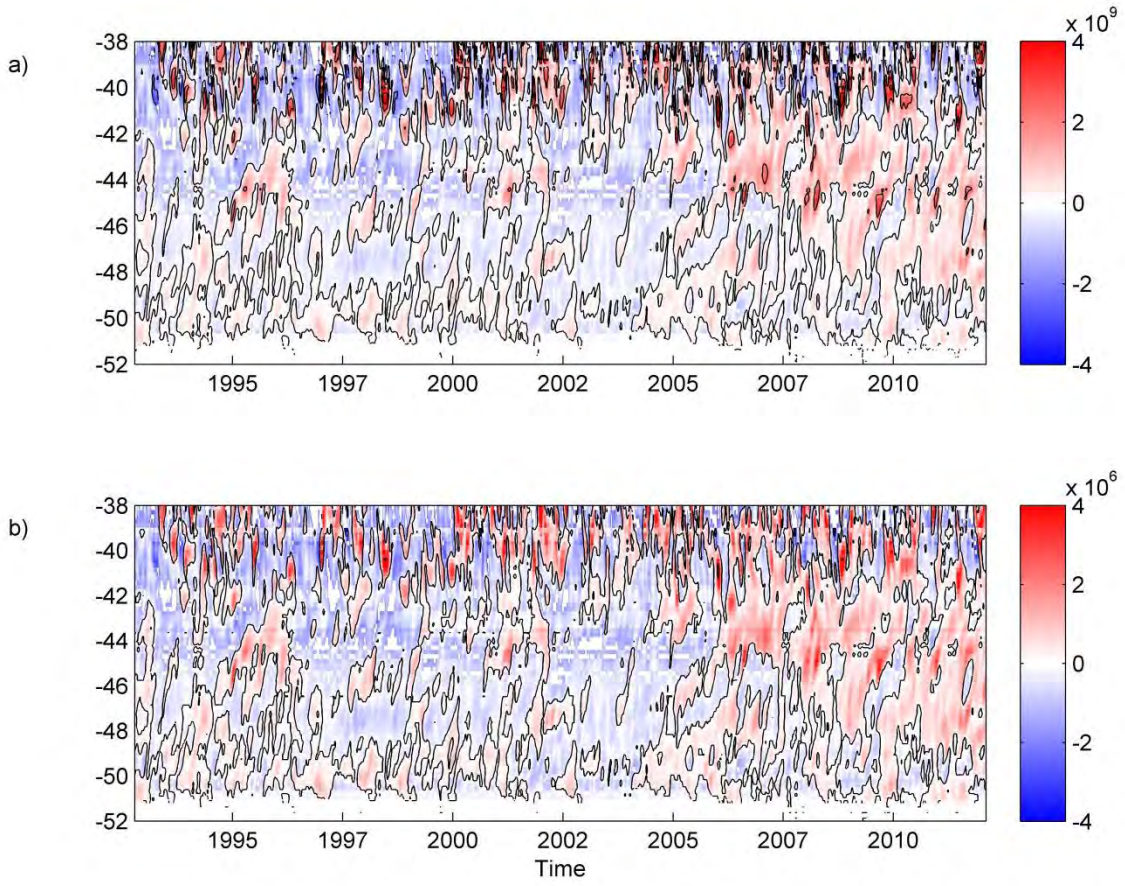

Figure 8.1 Anomalies in (a) heat content and (b) salt content, from a 20 year mean for the AAIW layer shown with latitude along the GH line from 1992 to 2012. Red shading represents a positive difference from the mean, while blue represents negative. Contours have been overlaid for clarity.

The magnitudes of the anomalies in HC and SC of the AAIW layer are seen to increase over the last two decades. This augmentation is shown by the change from blue to red anomaly shading with time in Figure 8.1 a and b. Post-2005 both HC and SC exhibit a relatively extreme change from negative to positive anomaly with respect to the 20 year mean. Before this year there seems to be a co-existence of anomalies of different signs, with a dominance of the negative ones (Figure 8.1). However, after 2005, positive changes dominate, with few blue patches visible. The increase in heat and salt over time appears to be relevant for all latitudes investigated here, with the increase more extreme north of 46ºS.

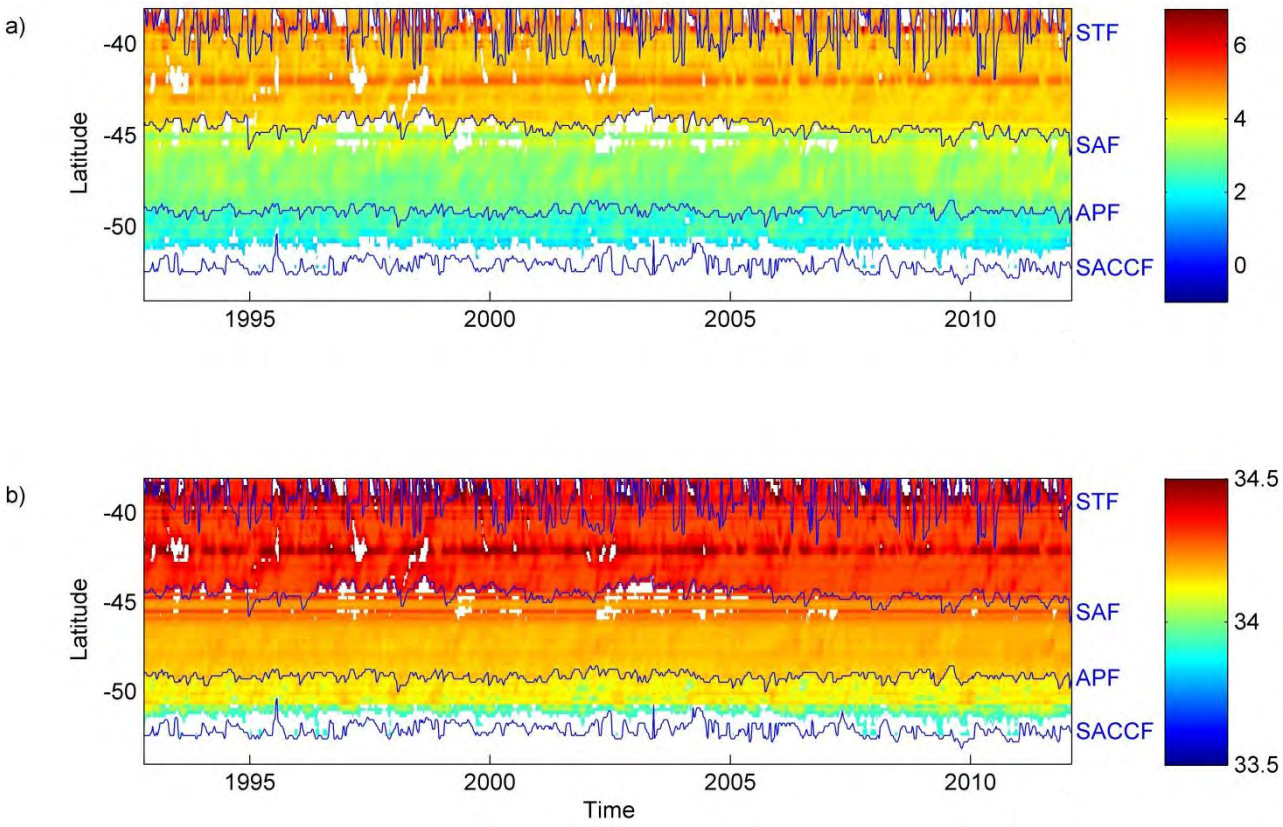

Figure 8.2 Mean values of (a) temperature, and (b) salinity for the AAIW layer shown with latitude along the GH line from 1992 to 2012. The positions of the Southern Ocean fronts with time defined using DH signatures explained in Rusciano et al. (2012) from AVISO Rio09 MADT are marked and labelled in blue

The spatial separation of AAIW thermohaline properties experienced with a change in latitude along the GH line is illustrated in Figure 8.2. The mean T and S values of AAIW are observed to vary quite drastically over frontal barriers. While the general trend in T and S with time is not clear in these plots, they do provide much insight into the water mass characteristics. It is likely that the maxima in both properties visible throughout the time series at 42ºS are artefacts of an elevated MDT value at this location, which subsequently influences the AGEM generated fields. Upon inspection of the frontal locations themselves, the STF clearly experiences the largest variability with time. This is likely due to the influence of mesoscale features in the northern domains of the GH line. The SACCF also exposes sizeable variability, likely due to sea ice cover. The large absence of data south of 52ºS is due to the absence of a detection of the AAIW isopcynal signatures this far south. The data gaps in the rest of the region are a result of occasional outcrops at the sea surface of the upper isopycnal limit of AAIW.

8.2 Division of AGEM results into frontal zones.

In order to obtain improved insight into the spatial and temporal changes that AAIW has undergone from 1992 to 2012 along the GH line, the region is split up into latitudinal zones delimited by the position of the Southern Ocean fronts shown in Figure 8.2. The weekly locations of the fronts were determined using the DH signatures from Rusciano et al. (2010) applied to the AVISO Rio09 MADT time series (see Figure 8.2 for positions). The region spanning from the STF to the SAF is called the Subantarctic Zone (SAZ), the area from the SAF to APF is named the Polar Frontal Zone (PFZ), and the section from the APF to the SACCF is the Southern ACC Zone (SACCZ). As the AGEM fields are limited to south of 38ºS, the location of the STF is bounded in the north by this latitude. The southernmost limit of data availability depends on sea ice cover and so often the southern limit of the SACCZ data is not the SACCF, but the position of maximum sea ice extent.

8.2.1 Subantarctic Zone.

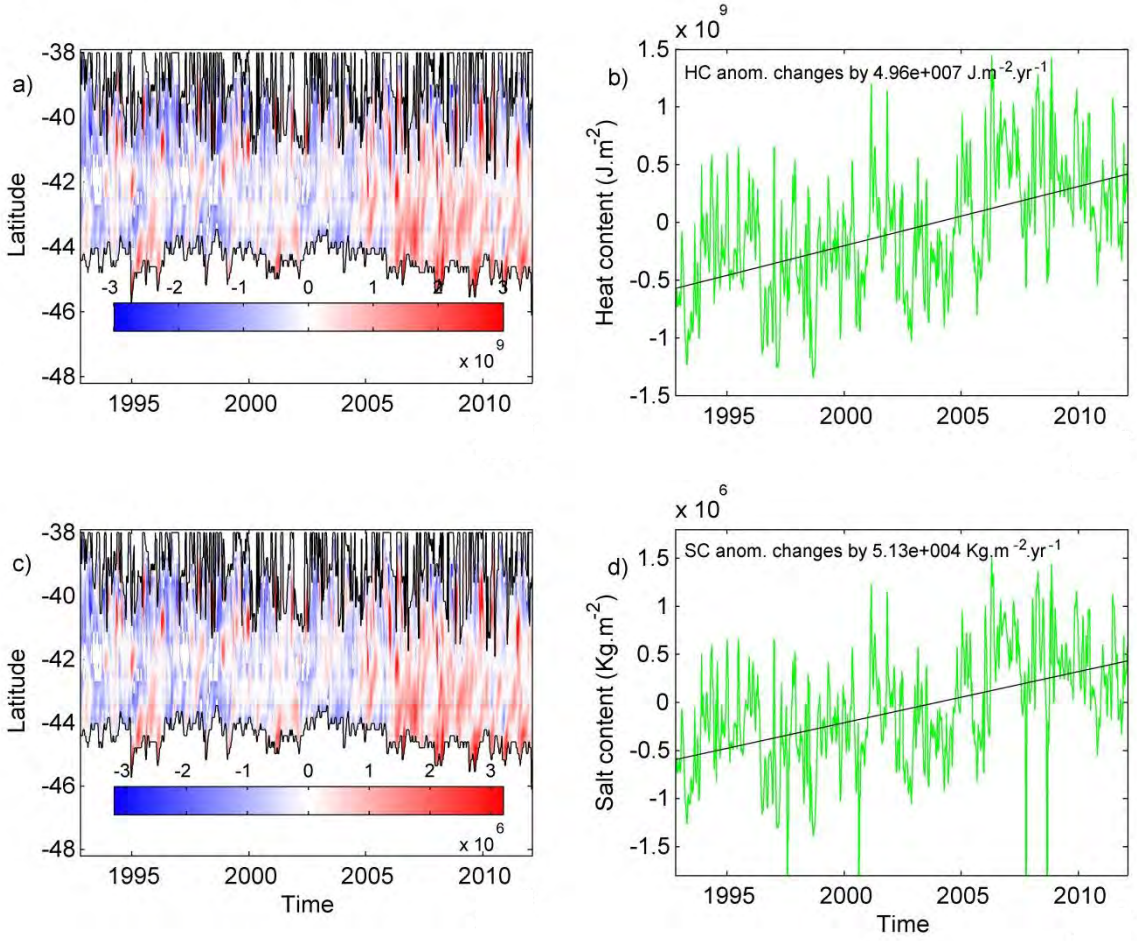

Figure 8.3 Hovmöller plot of spatial distribution of anomalies of (a) HC in $J.m^{-2}.yr^{-1}$and (c) SC in $kg.m^{-2}.yr^{-1}$ from a 20 year mean for the AAIW layer over the Subantarctic Zone (SAZ) from 1992 to 2012. Mean anomaly in (b) heat and (d) salt for the entire region of the SAZ with time. A trend line is fitted to data and the gradient is reported.

When investigating the changes in HC and SC detected within the SAZ, a substantial change from a dominance of negative anomalies pre-2005, to strong positive anomalies after this year is evident. This is visible as a move to deeper red shading in the Hovmöller plots (Figure 8.3 a and c), and the positive trend lines transiting from below to above zero just before 2005 (Figure 8.3 b and d). The drastic alteration of the STF with time creates a highly variable northern limit of the SAZ, while the southern boundary of the zone (SAF) remains relatively stable. In the northern sector of the area, maxima in anomalies can be seen (Figure 8.3 a and c), an artefact of eddies penetrating into the SAZ.

Budgets of anomalies averaged over the entire SAZ are clearly shown to increase over the 20 year period (Figure 8.3 b and d). Between 1992 and 2005 no drastic increase in anomalies is noticeable, as even though the HC and SC anomaly plots are highly variable. A large increase is then evident from 2005 to approximately 2009, after which the magnitude of anomalies appears to decrease slightly. The SC anomalies depicted in Figure 8.3d exhibit dramatic negative spikes indicating a significant drop in SC value. This likely due to the influence of eddies in this zone, not directly decreasing the salt budget so drastically, but rather creating a doming of the isopycnal limits towards the surface, thereby squeezing the vertical extent of the water mass. In general the HC and SC anomalies are highly variable, changing rapidly from positive to negative in response to the elevated levels mesoscale activity that are typical in this area.

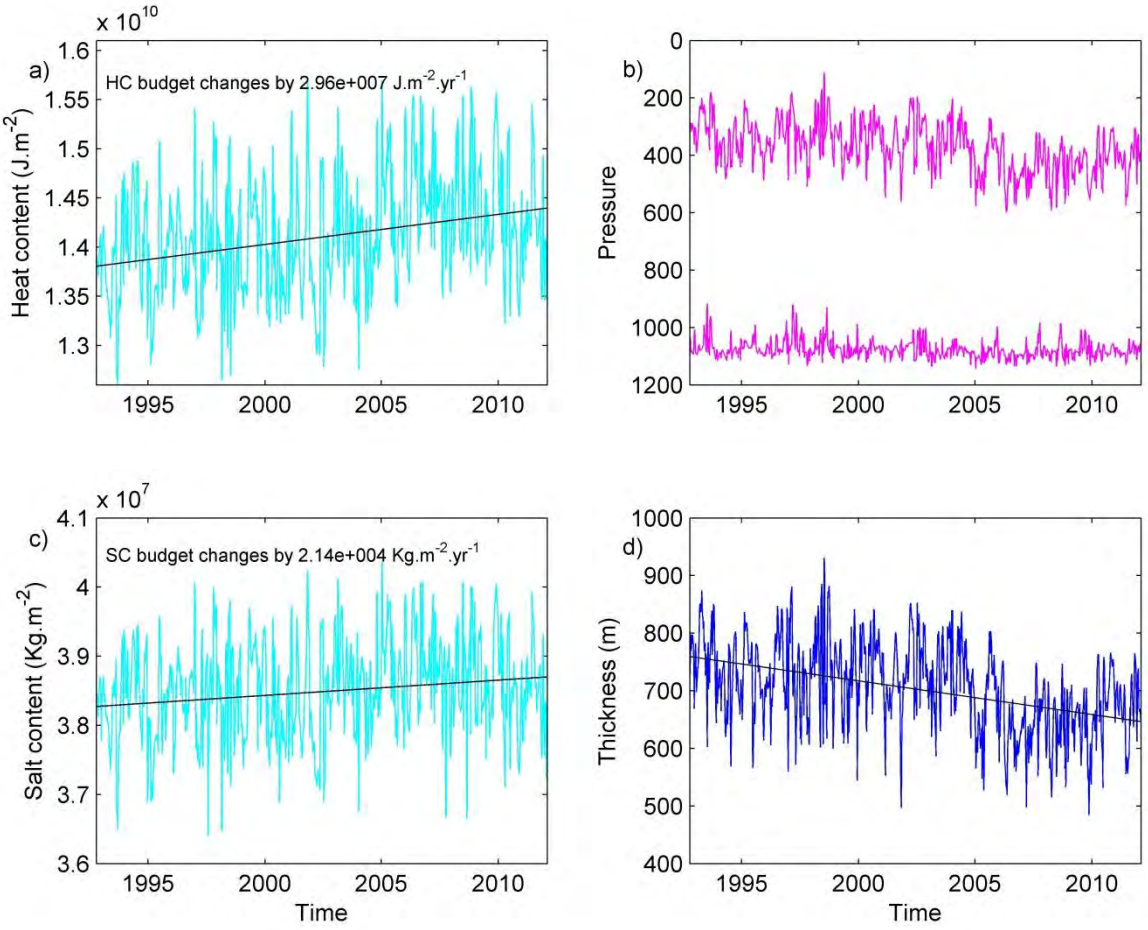

Figure 8.4 Budgets of (a) heat and (c) salt for the entire AAIW layer located within the SAZ plotted from 1992 to 2012. A trend line is fitted to the data and the gradient of change reported. b) Depth of isopcynals that delimit the boundaries of the AAIW layer within the SAZ. d) Vertical extent in meters of the water mass over time. Trend lines are fitted for clarity.

Both heat and salt budgets are observed to increase over the 20 year period within the SAZ (Figure 8.4 a and c). Much variation is evident on an intra-annual and inter-annual basis, with large spikes and troughs apparent. It is harder to decipher the changes from the raw HC and SC plots (Figure 8.4 a and c) compared to the anomaly plots (Figures 8.3), however what remains clear are the general positive trends over the time series, possessing sizeable rates of change. Upon observation of the position of the AAIW isopycnal boundaries with time (Figure 8.4b), it is evident that the lower limit remains at an approximately constant depth, while the upper limit can be seen to deepen during the last decade. The upper isopycnal of AAIW (1027.0 $kg.m^{-3}$) also exhibits more variability, changing depth by as much as 400m within the short period of a few months. The resultant effect of a deepening of the upper limit

of AAIW, while the lower limit resides within the same approximate depth range, is a general decrease in thickness of the water mass with time (Figure 8.4d). The vertical extent of AAIW in the SAZ is therefore detected to drop by ~100m over the 20 year study period. The fact that the HC and SC anomalies are seen to increase over time, despite a decrease in the thickness of the water mass, further highlights the actual magnitude of the change experienced.

8.2.2 The Polar Frontal Zone.

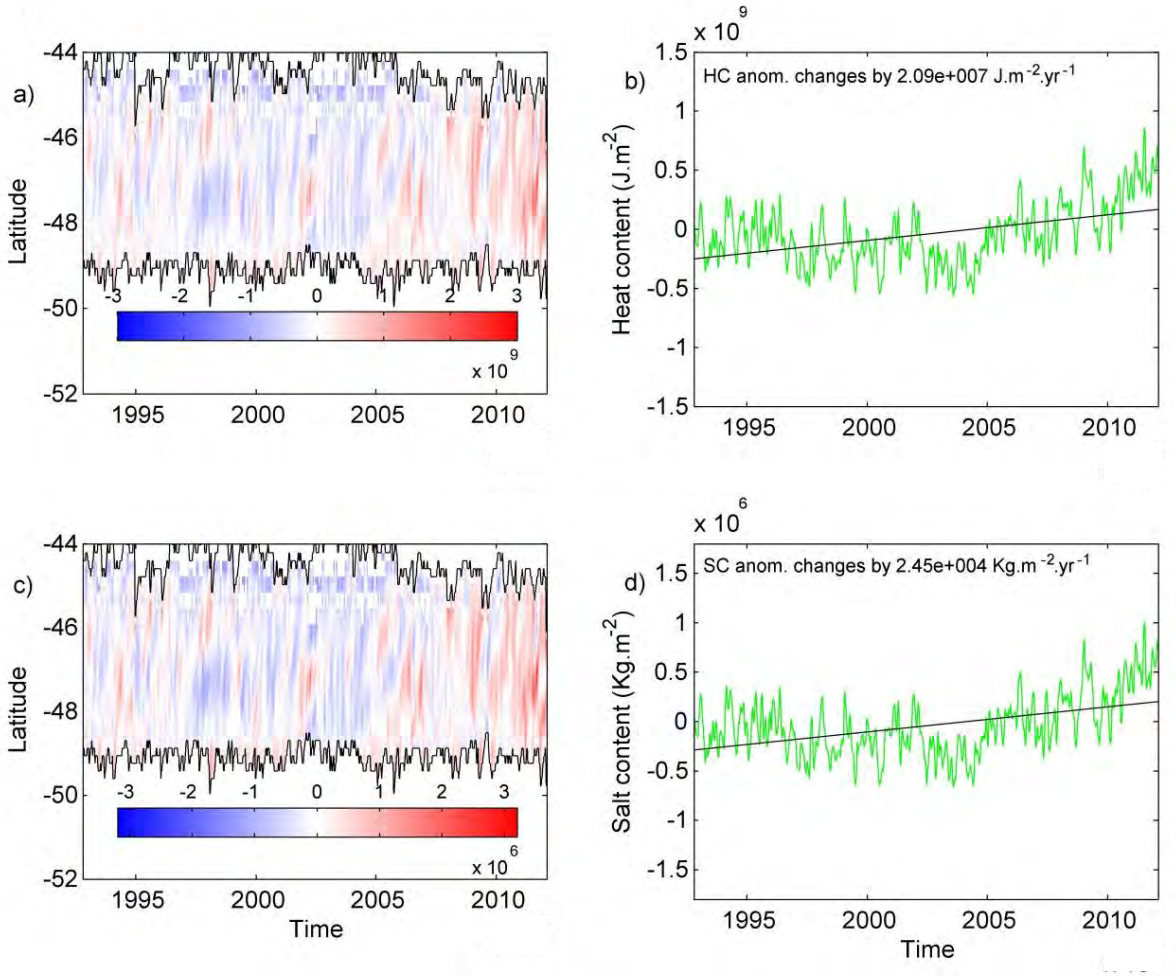

Figure 8.5 Hovmöller plot of spatial distribution of anomalies of (a) HC and (c) SC from a 20 year mean for the AAIW layer over the Polar Frontal Zone (PFZ) from 1992 to 2012. Mean anomaly in (b) heat and (d) salt for the entire region of the SAZ with time. A trend line is fitted to data and the gradient is reported.

The scales of the colour axis for the Hovmöller plots presented in Figure 8.5 a and c are the same as those of Figure 8.3, thereby enabling a zone comparison of the magnitudes of change in HC and SC anomalies. The anomalies belonging to the SAZ are certainly more extreme than those observed for the PFZ; however the general trend in data is concurrent. Both HC and SC anomalies are observed to increase over all latitudes belonging to the frontal region during the time span of the study period. In Figure 8.5, this increase in HC and SC appears to occur more drastically after 2008/2009, versus post-2005 as seen in Figure 8.3. Blue shading dominates most of the time series, with the red anomalies most concentrated in the last 2 years. The position of the frontal boundaries of the PFZ seen in Figure 8.5 a and c, the SAF in the north and the APF in the south, do not experience high levels of variability with time. That said, the SAF is observed to migrate southwards slightly post 2005 thereby decreasing the horizontal extent of the water mass.

While the magnitude of change in HC and SC anomalies is smaller for the PFZ compared to the SAZ, a general positive trend is once again observed. By utilizing the trend lines provided, patches of larger deviation from the general increase in both mean HC and SC anomaly with time can be identified. Between 2002 and 2004, large negative anomalies are apparent, and post-2009 large sizeable positive anomalies are evident. Therefore, while the trend lines do aid in clarifying the general changes in the region, the variation in size and sign of anomalies themselves are more useful in providing a detailed account of changes experienced by AAIW within the PFZ.

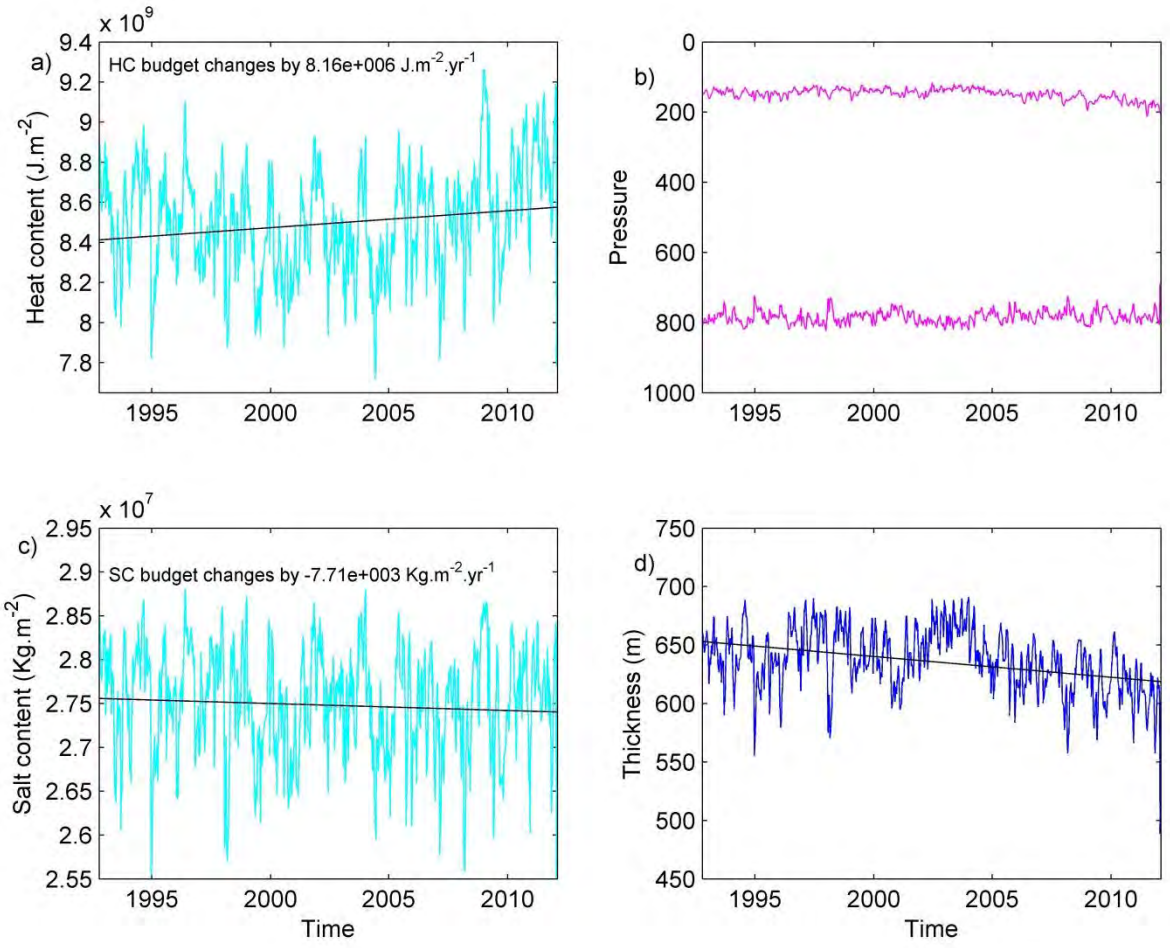

Figure 8.6 Budgets of (a) heat and (c) salt for the entire AAIW layer located within the PFZ plotted from 1992 to 2012. A trend line is fitted to the data and the gradient of change reported. b) Depth of isopcynals that delimit the boundaries of the AAIW layer within the PFZ. d) Vertical extent in meters of the water mass over time. Trend lines are fitted for clarity.

Figure 8.6 a and c provide improved insight into the actual heat and salt changes detected for the AAIW layer over the past 20 years. The trends represented show a net increase in HC with time, but a net decrease in SC. The general positive trends in anomalies evident in Figures 8.5 fail to expose that even though positive anomalies are becoming more dominant with time, the nature of change is such that only a small increase in heat budget, and in fact a slight decrease in the salt budget, is observed when comparing 1992 to 2012. Upon examination of the positions of the isopycnal limits belonging to AAIW within the PFZ (Figure 8.6b), there appears to be a small diving of the upper limit and a rising of the lower limit post approximately 2005. The general trend in thickness subsequently exposes a decrease in vertical extent of the water mass. The changes are slight yet significant and relevant in putting the observed changes in heat and salt into context. A decrease of the

thickness of AAIW over time implies a decrease in the HC and SC budgets if the T and S profiles were to remain constant, however this is not the case, thereby implying non-negligible changes.

8.2.3 Southern ACC Zone.

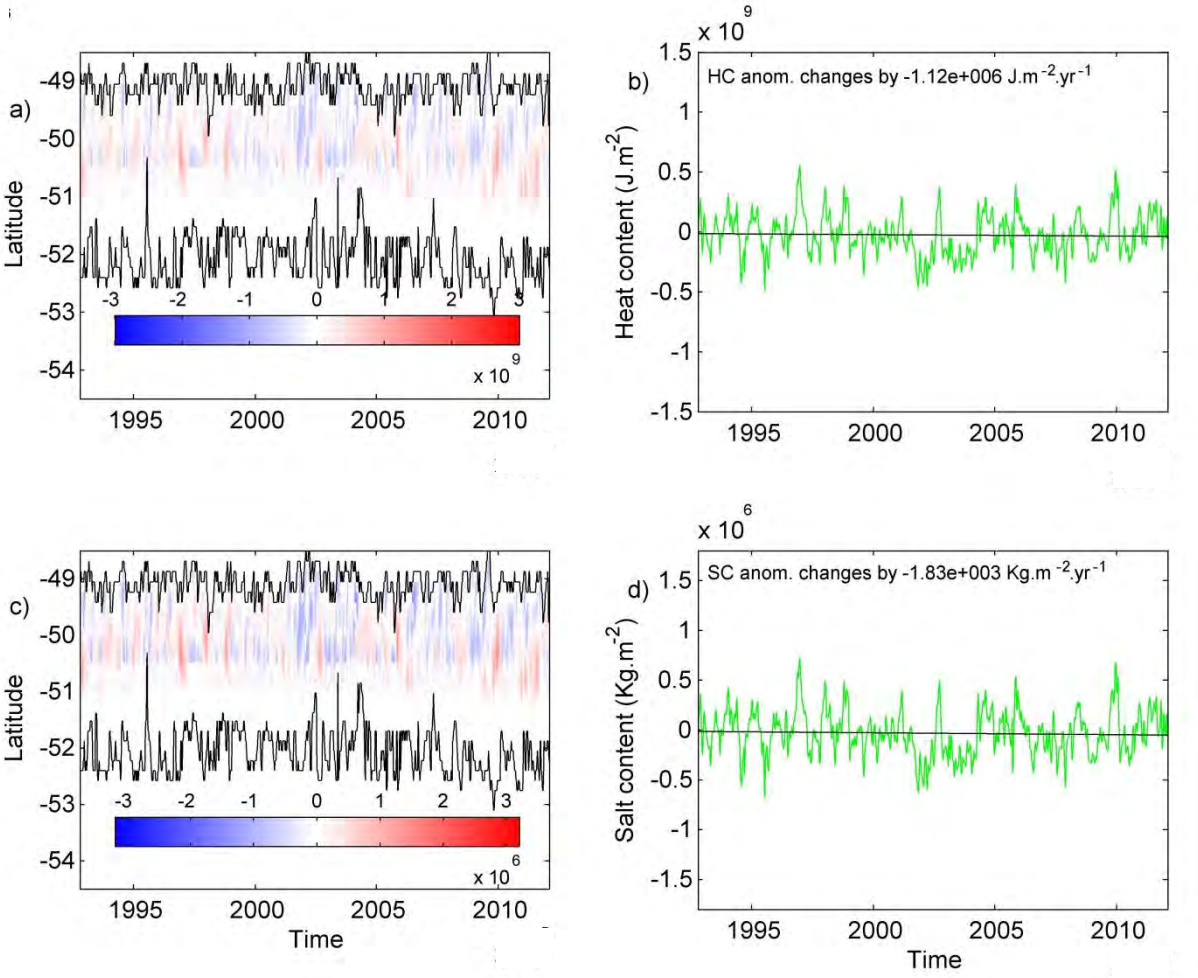

Figure 8.7 Hovmöller plot of spatial distribution of anomalies of (a) HC and (c) SC from a 20 year mean for the AAIW layer over the Southern ACC Zone (SACCZ) from 1992 to 2012. Mean anomaly in (b) heat and (d) salt for the entire region of the SACCZ with time. A trend line is fitted to data and the gradient is reported.

Via inspection of Figure 8.7, there does not appear to be a clear change in dominance of either positive or negative HC or SC anomalies with time. The magnitudes of anomalies presented here are much smaller than those observed for the SAZ (Figure 8.3) and PFZ (Figure 8.5). The SACCZ is bounded by the APF in the north and the SACCF in the south, thereby residing in the southern sector of the ACC where little variability is observed. The southernmost sector of the SACCZ is often covered in ice, as is evident in Figure 8.7 a and c by the absence of data south of 51ºS. In response to the influence of sea ice, the position of the SACCF appears relatively erratic compared to the APF. The trend lines of mean AAIW HC and SC anomaly for the entire zone shown in Figure 8.7 b and d expose a decrease in magnitude of anomalies with time. This trend gradient towards negative values is very slight, with the general impression being that of no significant change.

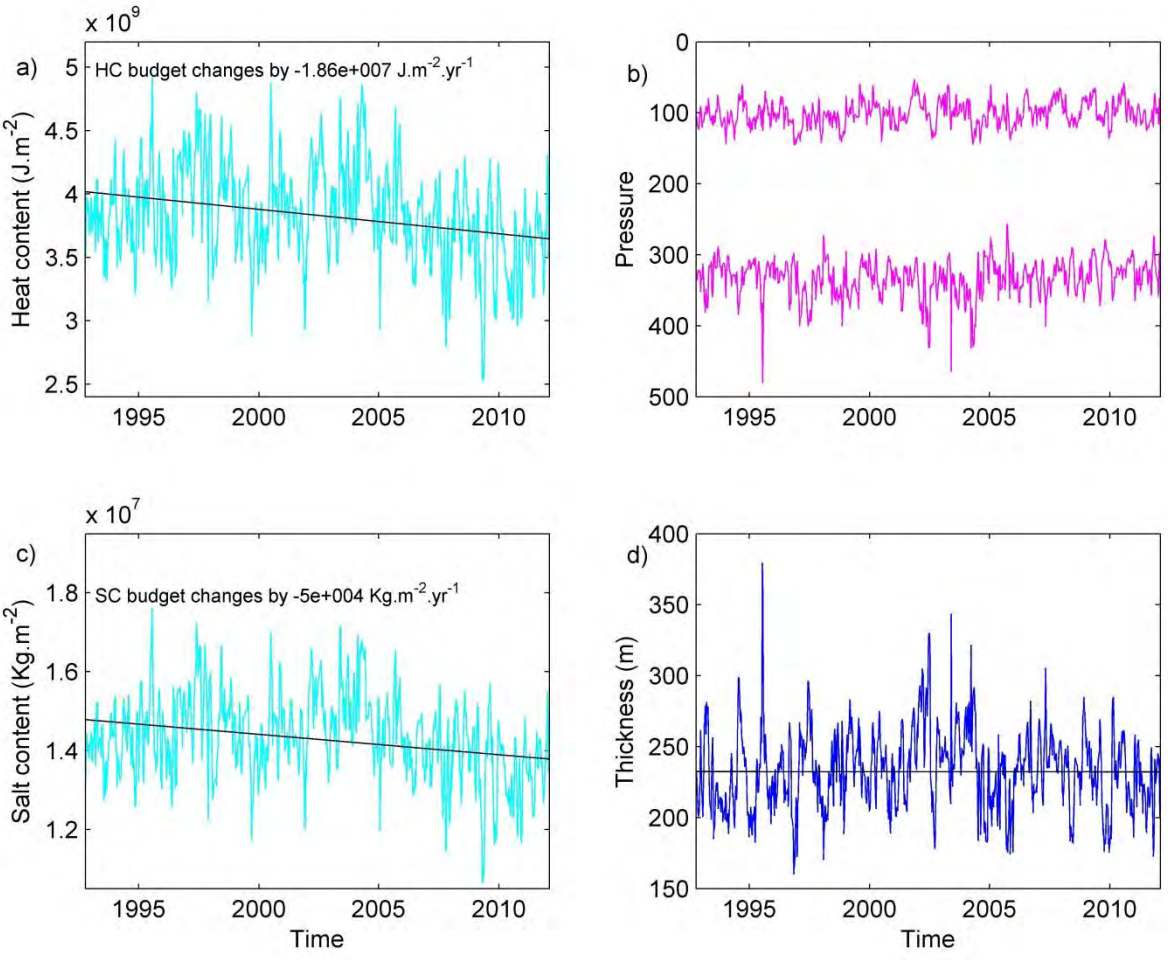

Figure 8.8 Budgets of (a) heat and (c) salt for the entire AAIW layer located within the SACCZ plotted from 1992 to 2012. A trend line is fitted to the data and the gradient of change reported. b) Depth of

isopcynals that delimit the boundaries of the AAIW layer within the SACCZ. d) Vertical extent in meters of the water mass over time. Trend lines are fitted for clarity.

The actual HC and SC budgets for the AAIW layer within the SACCZ are both observed to decrease with time over the 20 year study period (Figure 8.8 a and c). The drops in HC and SC represent a drop in value of the T and S profiles for the SACCZ area from 1992 to 2012. The rates of change reported for trends in HC and SC within the SACCZ are of the same order of magnitude (yet different signs) to those calculated for the SAZ, therefore exposing the significance of the changes experienced in this zone.

No evident change in water mass boundaries or resultant thickness estimates is detected for AAIW within the SACCZ (Figure 8.8 b and d). In this region AAIW is located shallower within the water column compared to the SAZ and PFZ, with a mean thickness of about 230 meters, versus 600m for the PFZ and 700m in the SAZ. Spikes in thickness presented in Figure 8.8d line up with the date of a significant drop in the position of the lower isopcynal shown in Figure 8.8b (e.g. see event during 1995). This massive change in depth of the isopycnal is somewhat unrealistic and therefore is likely an artefact of the identification of a potential density signature that meets the criteria for AAIW, yet due do to the density compensating nature of features, does not actually belong to the salinity minimum layer of AAIW. The long term stability of the thickness and limits exposed in Figure 8.8 b and d enforces the significance of the negative trends in HC and SC seen previously for the SACCZ.

8.3 Temporal changes in eddy properties.

An eddy atlas relevant for the southeast Atlantic developed by David (2012) was used to isolate all turbulent features detected in the study box domain delimited by 5ºW to 15ºE, and 38ºS to 56ºS. The temporal range of this data spans from 15 October 1992 to 1 January 2011, producing a daily output in the dataset. The region was spatially divided according to the average latitude over the 20 year time period of the fronts identified using the criteria of Rusciano et al. (2012) from the satellite SSH data (effectively the temporal average of frontal boundaries depicted in Figure 8.2). Within each frontal zone, the features were subsequently identified as being either cyclones or anticyclones, and the temporal change in properties of these two eddy types investigated. Each eddy possesses an eddy number within the atlas, and thus by noting the number of different eddies detected in a region within a month, the frequency of occurrence is attained. The monthly mean ADT of each eddy type within each frontal zone was also obtained, and is presented along with the occurrence frequency.

8.3.1 Subantarctic Zone.

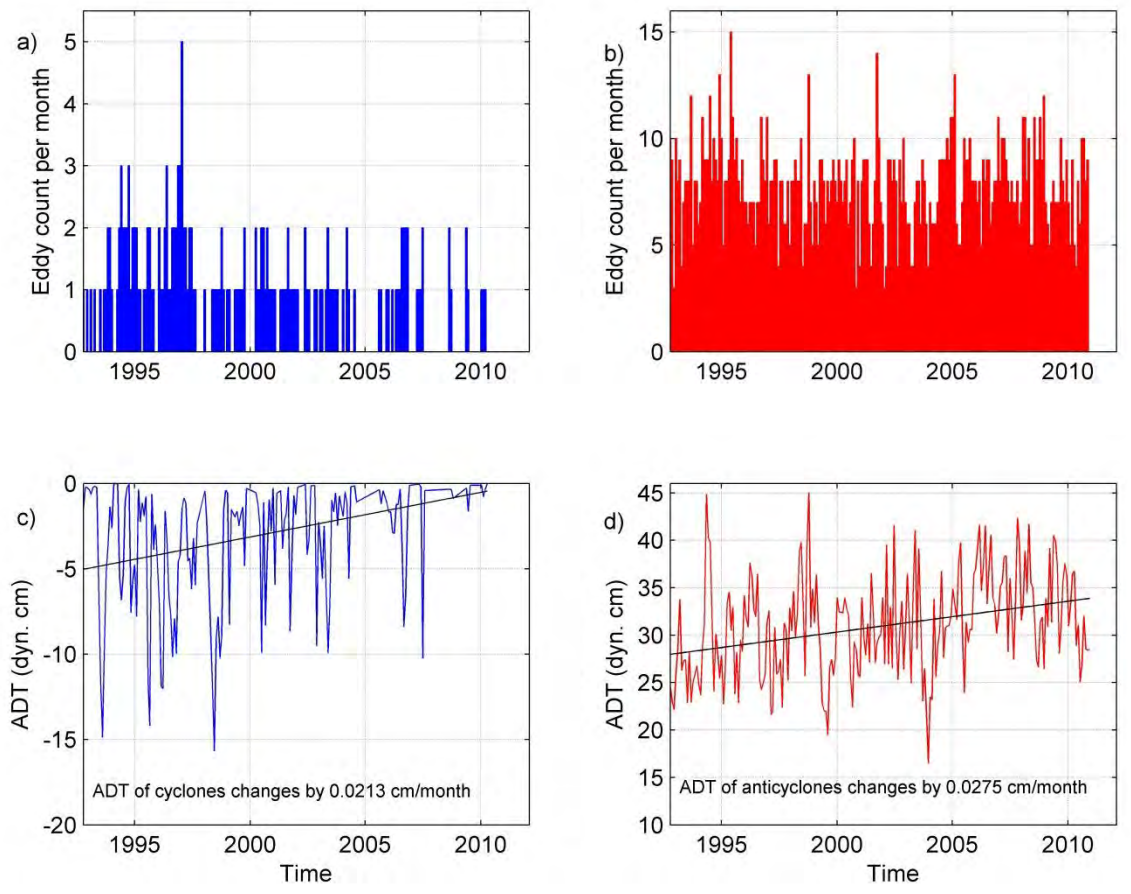

Figure 8.9 Number of (a) cyclones and (b) anticyclones detected within the SAZ each month from 1992 to the start of 2011. The monthly mean ADT of (c) cyclones, and (d) anticyclones residing within the SAZ. A trend line is fitted to the ADT curve and the monthly rate of change reported.

The frequency of cyclones appears to decrease over the time series (Figure 8.9a), with a peak in 1997 of five features detected per month, dropping to eventually only one feature identified on a monthly basis for 2010. Anticyclones are also observed to occur less often dropping from a maxima of 15 detected per month during 1995 to 10 during December 2010 (Figure 8.9b). This change is however relatively far less pronounced than that of the cyclone frequency, and could be attributed to natural variability. Anticyclones, also known as Agulhas Rings within the SAZ, are by far the dominant turbulent feature in this area. This is shown by both the elevated frequencies and the magnitude of the ADTôs belonging to these features. Over the time period, the measurements of cyclonic ADTôs are clearly seen to increase towards the positive on average by 0.0213m/month, signifying shallower and thus less extreme turbulent features (Figure 8.9c). The magnitudes of the cyclonic ADT values drop rather drastically from up to 15 dynamic cm measured in the early 1990s to near zero during 2010. This coupled with the drop in frequency shows a general decrease in dominance of cyclones in the SAZ over time. The rate at which cyclones are observed to decrease in magnitude is comparable with the rate of change of an increase in size of anticyclone ADT (Figure 8.9d). Anticyclones are detected to grow in magnitude and extremity during the time period. This signifies that the features are becoming significantly less dense and thus possess higher sea surface heights.

8.3.2 Polar Frontal Zone.

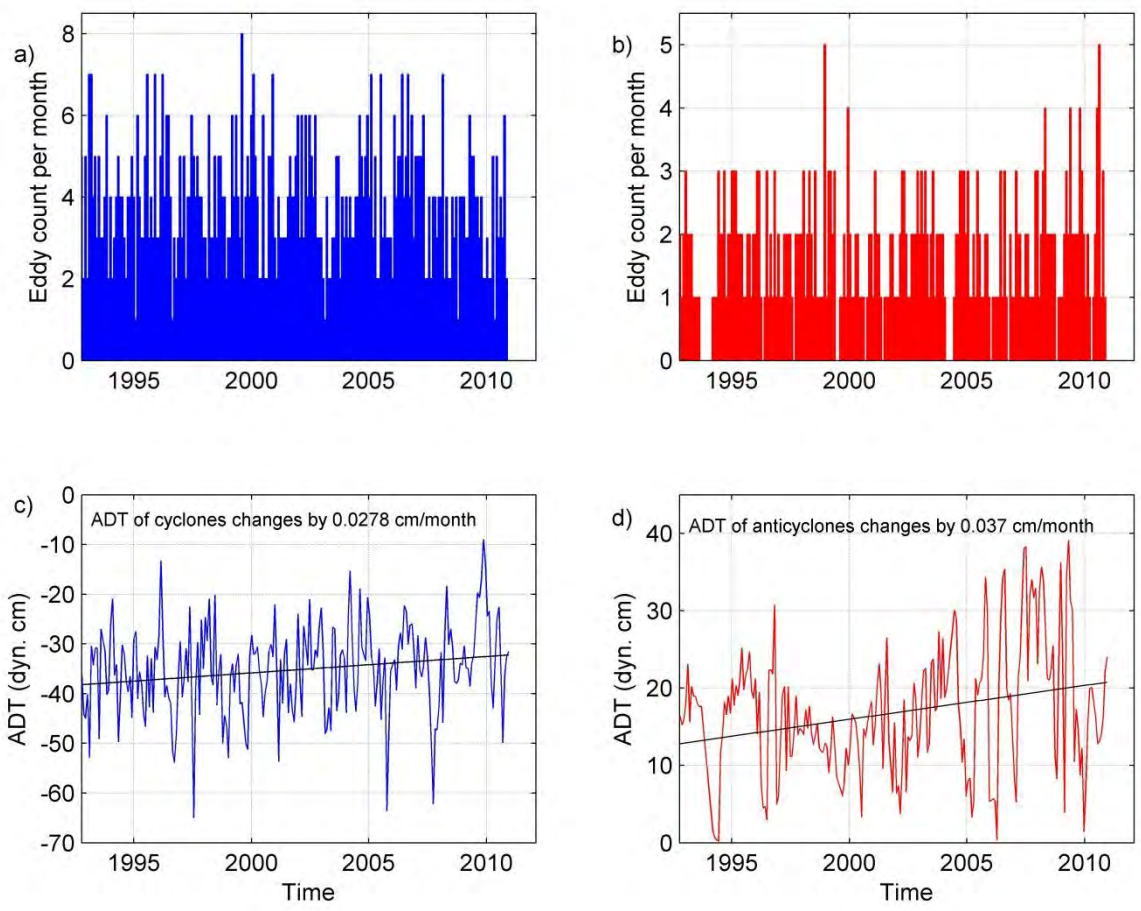

Figure 8.10 Number of (a) cyclones and (b) anticyclones detected within the PFZ each month from 1992 to the start of 2011. The monthly mean ADT of (c) cyclones, and (d) anticyclones residing within the PFZ. A trend line is fitted to the ADT curve and the monthly rate of change reported.

Upon observation of the changes in frequency of cyclones and anticylones detected for the PFZ (Figure 8.10 a and b), there appears to be a slight decrease in cold core features and an increase in count of warm core features. The alteration of ADT magnitude for turbulent systems within the area, however, is sizeable. Cyclones are found to become less extreme with an average trend towards positive values of 0.0278 cm/month, a rate of change slightly larger than that detected for the SAZ. The amplification of anticyclonic ADT magnitude is also more extreme than that reported for the SAZ, with features growing by on average 0.037 cm/month (Figure 8.10 d). The amplitude of variation of anticyclone ADT is large, exposing

significant inter-seasonal and inter-annual variability. Between 2005 and 2010 the magnitude of ADT oscillates dramatically about the trend line varying by as much as 30 dynamic cm within a year (Figure 8.10 d). Overall, a decrease in frequency and magnitude of cyclones, along with an increase in dominance and extremity of anticyclones, indicates elevated levels of turbulent activity of warm core features in the region.

8.3.3 Southern ACC Zone.

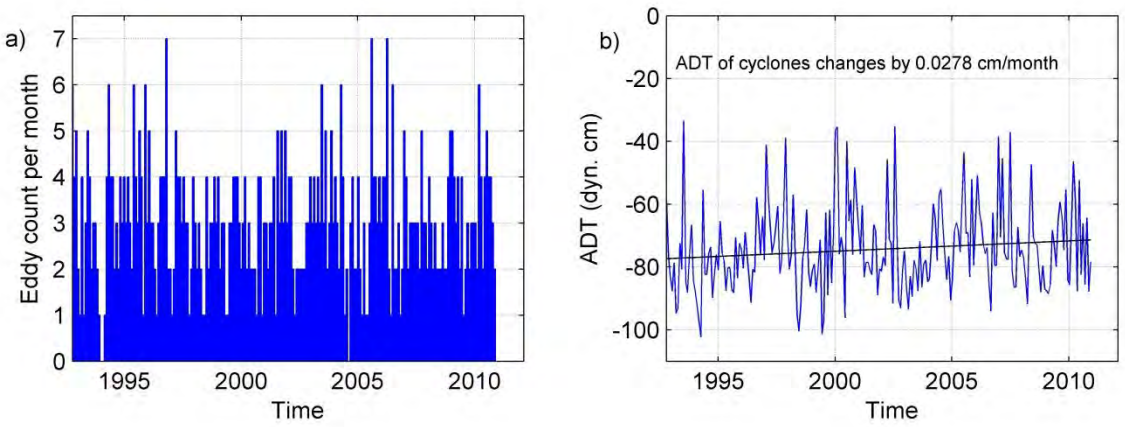

Figure 8.11 (a) Number of cyclones detected within the SACCZ each month from 1992 to the start of 2011. (b) The monthly mean ADT of cyclones within the SACCZ. A trend line is fitted to the ADT curve and the monthly rate of change reported.

Anticyclonic (warm core) features are not found within the SACCZ, therefore only an analysis of cyclonic activity is reported in Figure 8.11. Within this zone, no immense changes are evident, with a natural variation in eddy frequency visible along with a slight augmentation in ADT magnitude. This small increase towards the positive of cyclonic ADT size, however, may carry some important messages as shallower features signify less dense waters. With no warm core features entering the region to provide an injection of heat and salt, a decrease in cyclone extremity indicates some important local changes in thermohaline properties experienced.

8.4 Discussion.

Over the entire GH line for the period 1992 to 2002, the magnitude of anomalies in HC and SC are observed to on the whole increase with time. The year 2005 is identified as the point where the anomalies change from negative positive in the time series. Post-2005, few negative anomalies are visible, and at almost all locations a strong positive increase in both heat and salt anomalies is observed throughout.

The division of the region into the different frontal zones (locations of frontal boundaries presented in Figure 8.2), provides improved insight into the spatial as well as temporal behaviour of AAIW. The evolution of AAIW with time is seen to differ significantly between each zone, with the SAZ having the strongest changes and thus contributing the most to the general impressions for the region of the Southern Ocean south of Africa. However, the PFZ and SACCZ exhibit variations counter to those apparent overall from Figure 8.1. So as better to understand one of the components that may be driving the observed evolution of AAIW, the changes in eddy properties in each frontal zone were also investigated. In this section the results from each zone are discussed and compared, with suggestions on what may be forcing some of the observed changes.

8.4.1 Subantarctic Zone.

The HC and SC budgets and the anomalies for the SAZ exhibit very spikey behaviour. The anomalies (Figure 8.3) change rapidly over a short period of time, indicative of the rapid changes in observed heat and salt observed (Figure 8.4 a and c). These spikes are artefacts of the eddy features that are found within the SAZ. The thickness of the water mass is observed to decrease with time in response to the deepening of the upper isopycnal limit. This observation further highlights the magnitude of change in HC and SC, as even though the vertical extent of AAIW is actually decreasing with time, the heat and salt budgets are seen to increase.

Upon observation of the area belonging to the SAZ in Figure 8.2, large maxima in T and S are observed to frequently re-occur around 42ºS throughout the time series. These are likely the product of eddy features in the area that have already been extensively discussed in previous studies (Swart and Speich, 2010; Dencausse et al. 2011; Arhan et al., 2011). The influence of eddies in this region is furthermore illustrated by both the large amplitudes of HC and SC anomalies and the general highly variable nature of the heat and salt budget curves. Cyclones carry cooler, fresher water, thereby resulting in a drop of HC and SC. While anticyclones, such as intense Agulhas rings, transport warm salty water. It could be hypothesised that the general increase in heat and salt observed in the SAZ may be due to an increase in amplitude and/or frequency of Agulhas rings in the region, thereby providing an injection of warm, saline water. Lutjeharms and Ballegooyen (1988) suggested that the meridional propagation of eddies across the STF is an essential mechanism providing an input of heat to the Southern Ocean. In addition to the influence of elevated advection of subtropical waters into the region via Agulhas Rings eroding the salinity minimum of AAIW, increased evaporation in the South Atlantic Current may also contribute to the augmentation in SC observed.

8.4.2 Polar Frontal Zone.

While both heat and salt anomalies are detected to increase with time in the PFZ, large variations around the trend are observed. Figure 8.5 shows that pre-2009 negative HC and SC anomalies dominate the region, with sizeable positive events after 2010 likely the culprits generating the increasing trend lines. The actual heat and salt budgets (Figure 8.6 a and c) expose that even though both heat and salt anomalies are increasing in magnitude with time, the actual HC only increases by a small amount from 1992 to 2012, while SC is seen to decrease slightly. Changes experienced by AAIW in the PFZ are thus somewhat more complicated than the overall augmentation of temperature and salinity experienced in the SAZ. While anomalies are becoming more extreme in the PFZ, the actual heat and salt content do not exhibit a drastic change.

Upon observation of the alteration in thickness of AAIW, the vertical extent of the water mass is seen to possess a negative trend with the upper isopycnal diving within the water column, and the lower isopycnal rising. While the changes observed in Figure 8.6 b and d are slight, they provide some insight into the contradicting increase in HC and SC anomalies with small and negative changes in the respective actual budgets. The anomalies experienced for AAIW residing within the PFZ are observed to increase in magnitude with time, yet the influence of a decrease in thickness of the water mass results in small net changes in HC and SC budgets. These two mechanisms therefore appear to explain the resultant budget trends. A thinner water mass layer detected within a zone that narrows with time would result in reduced budgets, as these values are calculated as an integral from lower to upper isopycnal depths over all latitudes between the SAF and APF. The positive trend in HC budget designates the magnitude of the heat input experienced due to the increase in anomaly amplitude over the two decades.

8.4.3 Southern ACC Zone.

As the axis of all anomaly plots are set to the same interval, the fluctuations in magnitudes of anomalies within the SACCZ do not appear sizeable relative to the other zones. However the existence and gradient of the negative trend reported in both HC and SC anomalies, and in the actual budgets, must be taken stock of. The rate of change in heat and salt budgets is of comparable magnitude, yet opposite in sign to trends presented for the SAZ. It therefore appears that while the SACCZ experiences fewer extreme events and the amplitude of these phenomena are less sizeable, the net changes experienced are comparable to those detected in the northernmost sector.

The thickness of AAIW is seen to remain stable with time, along with the positions of the isopycnals within the water column. The negative trends in HC and SC therefore indicate an actual drop in T and S values for this region. While it is not immediately clear what could be driving these changes, it could be speculated that a drop in temperature and increase in freshwater of AAIW could be the result of an increase in sea ice, and subsequent elevation of cold and fresh water input via melting. This suggestion, while speculative, may possess some

value, as it is known that the variation of sea ice has important effects on the thermohaline structure of the ocean (Gordon, 1975; Gordon, 1981). An investigation by Zwally et al. (2002) of data spanning from 1979 to 1998, reported an increase in Antarctic sea ice concentration of 15% and an average increase in extent of 0.98 ± 0.37 % per decade. It is hypothesised that much of sea ice growth and retreat is related to wind stress (Gordon, 1975). Perhaps the poleward shift in Southern Hemisphere westerlies south of Africa, discussed in Biastoch et al. (2009), could be influencing sea ice thickness and extent, and consequently also AAIW properties. An increase in sea ice cover is qualitatively consistent with the response of Antarctic sea ice to climate warming due to the stabilising effects of increased snowfall in the Southern Ocean (Zwally et al., 2002).

8.4.4 Possible influence of eddy property changes on AAIW evolution.

The number of anticyclonic eddies detected in the SAZ on a monthly basis far outweighs the frequency of cyclones. In the SAZ, the anticyclonic field is dominated by Agulhas rings originating from the Agulhas Current that carry strong heat and salt signals into the region (eg. Swart and Speich, 2010; Arhan et al., 2011). Cyclones, on the other hand, carry cool, fresher water and are associated with upwelling due to their physical structure. Over the time period, cyclones are observed to become more scarce and their magnitudes less pronounced within the SAZ. The frequency of anticyclones does not change drastically, however a sizeable increase in their measured ADT is detected. The general increase of sea surface heights via the growing ADTôs of eddy features in the SAZ indicates a decrease in feature density within the region. It can be suggested that possibly the increase in dominance of anticyclones, which inject warm saline waters into the SAZ is driving the changes observed in AAIW. These Agulhas rings are deep reaching and thus the signals penetrate to depths within the AAIW layer. As an elevation of heat and salt together are density compensating, the extent of temperature augmentation must outweigh the effects of an input of saline water so as to result in a net increase in ADT.

Within the PFZ, no drastic changes in eddy frequency are evident, however significant increases in ADT are observed. The magnitude of ADT change in this region is larger than

the other two zones investigated. An increase in warm core feature ADT and a drop in cold core eddy magnitude along with the elevated levels of variability observed, correlates with the changes in HC and SC anomalies described in Section 8.2 for the PFZ. The magnitudes of anomalies were observed to increase over time; however the actual HC was only seen to increase slightly along with a small decrease in the SC budget. Elevated anomalies and magnitudes in ADT of these features could be driving pulses of heat and salt injected into the region. It is likely that temperature augmentation dominates the resultant effect, as salt budgets were seen to decrease in the zone along with a decrease in density (ADT increase), which signifies fresher conditions.

For the SACCZ, the magnitudes of cyclones were found to decrease over time as the systems become shallower with a positive trend in ADT. With an absence of anticyclonic features present in this region, it is only from the decrease in extremity of cyclones that one can deduce a decrease in density of turbulent systems occurring in this zone. By pairing this theory with the observed decrease in HC and SC budgets of AAIW detected for the SACCZ in Section 8.2, the logical conclusion is that a decrease in salt is largely driving the rise in density. This decrease in salt may correlate with the sea ice and precipitation changes discussed previously. However, while this hypothesis sparks some interesting questions, without further investigation, no robust conclusions can be drawn.

8.4.5 General impression of AAIW evolution in the southeast Atlantic sector of the Southern Ocean.

The HC and SC anomaly plots indicate a general increase in magnitude of events, thereby presumably leading to elevated heat and salt of AAIW in the region of the ocean south of Africa. However, upon inspection of the behaviour of the water mass within the different frontal zones, a diverse variety of change is exposed. The SAZ is largely affected by eddies, resulting in frequent extreme anticyclonic events and a sizeable general increase in heat and salt despite the subduction of the upper isopycnal thinning the vertical extent of the water mass. Changes in the PFZ are rather complex and complicated to tease apart. The magnitude of anomalies in heat and salt are observed to increase, yet the actual values of these budgets

experience a small positive trend in HC and a marginal negative trend in SC. Here the effects of a decrease in water mass thickness are visible, as even though the magnitude of anticyclone events augmenting heat and salt are seen to increase with time, the opposing effect of a thinning of the water mass vertical and horizontal dimensions results in minor net changes to heat and salt content. The SACCZ exhibits trends completely opposite to those evident for the SAZ. HC and SC anomalies are seen to become more negative over the 20 year period, resulting in a decrease in heat and salt as the thickness and position of the water mass remains largely constant. Mesocale variability is confined to cyclones in this region, which are found to increase in ADT and thus become less dense with time. The forces driving change are therefore hypothesised to be linked to freshwater input from sea ice and precipitation as these are the dominant mechanisms influencing thermohaline changes in the region and that are linked to the effects of global climate change.

The temporal evolution of AAIW in the southeast Atlantic sector of the Southern Ocean is complex, with changes in some zones contrasting variations in others. The AGEM fields have proven very valuable in providing insight into AAIW spatial and temporal variability. The 20 years of AGEM fields provide a tool for the investigation of AAIW behaviour within the ACC, south of Africa, over a sizeable period of time.

9. Summary and Conclusions.

The Atlantic sector of the Southern Ocean is of specific research interest due to the important role this area plays in water mass exchange and transformation. Within the region, waters from the Indian Ocean carried within the Agulhas system interact with those of the South Atlantic and Southern Oceans in a turbulent exchange (Swart and Speich, 2010; Rimaud et el., 2012). This interaction results in high levels of meso- and sub-mesoscale activity, and subsequent mixing. Despite its influence on the global ocean-climate system, however, the southeast Atlantic sector of the Southern Ocean is the least investigated of the three passages to the south of the Southern Hemisphere continents (Legeais et al., 2005). Consequently water mass behaviour and evolution in this region is poorly understood.

Antarctic Intermediate Water (AAIW) plays a vital role in global ocean circulation and climate regulation (Peterson and Stramma, 1991). In the Atlantic sector of the Southern Ocean, AAIW forms part of the returning upper limb of the MOC to the North Atlantic, and is subsequently a major source in the formation of North Atlantic Deep Water (Sloyan and Rintoul, 2001). Recent warming within the water mass has been identified, however, due to the scarcity of data in the southeast Atlantic; the degree of water mass alteration in this area is poorly understood (Banks et al., 2000; Pahnke et al., 2008; Rimaud et al., 2012; Rusciano et al., 2012). In order to obtain improved insight the temporal evolution of AAIW, a time series in needed. This can be obtained through the pairing of a Gravest Empirical Mode (GEM), developed for the Atlantic sector of the Southern Ocean, with satellite altimetry measurements of the region.

The first objective of this study was to develop an improved GEM for the sector of the Southern Ocean south of Africa, building on the work undertaken by Swart et al. (2010) for the GoodHope (GH) line. By uniting the GEM with satellite altimetry to create an Altimetry GEM (AGEM), 20 years of T and S sections relevant for the GH line were attained. Within these thermohaline fields, the AAIW layer was chosen as the water mass of interest to investigate. Using the two decades of generated data, the temporal evolution of AAIW from

1992 to 2012 was examined. This study is designed to answer three key questions; in this section the findings pertaining to each question will be summarized and discussed.

1) **Can a new and improved GEM be created that successfully represents the southeast Atlantic Southern Ocean?**

An upgraded GEM was created for the region via the implementation of various changes and improvements; the most significant being the use of an alternative de-seasoning technique, and the massive augmentation of reference points for the GEM relationships via the use of Argo profile data. Extensive testing was performed to ensure that this GEM was in fact an ñupgradedò version, and that the subsequent results adequately represented the observed fields.

The GEM was found to reproduce the cruise-obtained thermohaline fields remarkably well, capturing on average over 95% of the temperature and 91% of the observed salinity variability over the top 2000dbar of the water column. These percentages of variance captured match well with those reported by the comparable studies of Watts et al. (2001), Sun and Watts (2001), Swart et al. (2010) and Meijers et al. (2011a). The GEM also experienced minimal errors, with a mean RMS error for the upper 2000dbar of $1.65 \pm 2.16 \times 10^{-3}$ ºC for temperature, and $2.69 \pm 2.87 \times 10^{-4}$ for salinity. The sizes of these RMS residuals are at least two orders of magnitude smaller than those reported by similar studies for the Southern Ocean. Watts et al. (2001), who were the first to apply the GEM method to the ACC, obtained a temperature RMS agreement within 0.29º, 0.26º, 0.10º and 0.04ºC at 300, 600, 1000 and 2000dbar respectively. Results from the study undertaken by Meijers et al. (2011a) presented mean RMS residuals of 0.45ºC for temperature and 0.05 for salinity for the water column below 500dbar. The GEM developed by Swart et al. (2010) for the same region of the ocean south of Africa was found to possess an RMS error in the upper 300dbar of 0.54ºC and 0.09 for temperature and salinity respectively. This error was detected to decrease to on average 0.07ºC and 0.02 below the thermocline.

The comparatively minor errors associated with the GEM created in this work are even more impressive in light of the fact that the study domain stretches further north

than that of Swart et al. (2010), to 38ºS versus 40ºS, thereby including a region which experiences high levels of mixing and variability. This convergence of waters in the northern domains of the GH line presents a challenge for the GEM, as multiple thermohaline properties are present along the same stream function coordinate. This obstacle in using the GEM technique to represent the Southern Ocean was also noted by Sun and Watts (2001) where residuals south of Africa were found to be double the size of those in the sector south of Australia. The GEM generated by this work compares very well with results from existing Southern Ocean GEMs, capturing similar percentages of variability, and majorly improving on the magnitude of RMS errors experienced. The changes and improvements that were undertaken to generate an upgraded GEM for this challenging region of the ACC therefore proved to be very successful.

2) **How proficient is the developed AGEM at reproducing observed water properties along the GH line, especially within the AAIW layer?**

The GEM relationships were merged with 20 years of satellite altimetry measurements to create an AGEM, which was subsequently used to generate weekly thermohaline sections for the GH line spanning from 1992 to 2012. The AAIW layer was chosen to be the focus of the investigation, due to both the importance of this water mass for ocean circulation, and because of the lack of understanding of the property changes experienced in the southeast Atlantic Southern Ocean. The AGEM was found to be a very useful and suitable tool for the analysis of AAIW, as the water mass is located within layer of the AGEM where the thermohaline fields are highly accurate. The mean property value differences were found to be very small for AAIW over all latitudes (mean offset for temperature = 0.297ºC; salinity = 0.010). An inexact ADT was identified as largely being the reason for the errors detected, and reducing the Argo data boundaries did not improve the accuracy of the results.

It is important to note, however, that not only are these errors minor but also the advantages of obtaining time evolving T and S fields far outweigh the challenges associated with the use of altimetry. The results presented were highly satisfactory, showing an outstanding agreement of the AGEM temperature and salinity values, heat and salt budgets, and RMS errors with observations belonging to the AAIW layer.

3) How variable is AAIW and what changes has this water mass undergone in the region south of Africa over the past 20 years?

In the region between 38ºS and 52ºS of the GH line, the mean HC and SC anomalies belonging to the AAIW layer were observed to increase from 1992 to 2012. In order to gain insight into the spatial variation of the changes observed, the investigation was carried out separately for the three main frontal zones of the ACC. Within the SAZ a large warming and increase in salinity was observed with positive trends in HC and SC anomalies and budgets. This input of heat and salt may be caused by increased advection of waters from the subtropics, or elevated levels of evaporation in the South Atlantic. The thickness of the water mass was found to decrease with time due to a deepening of the upper isopycnal limit. Alterations within the PFZ of HC and SC anomalies and vertical water mass extent were similar, yet less extreme. However, the actual HC was observed to only increase very slightly over the study period, meanwhile the SC was found to decrease. The results for the SACCZ were rather interesting, exposing an actual decrease in heat and salt budgets, with the rate of change of the same order of magnitude as the positive trend of the SAZ.

So as to better understand one of the influences that may be driving a portion of this change, the change in frequency and ADT of eddy features detected within the study domain between 1992 and 2010 were surveyed. An overall decrease in cold core cyclonic activity and magnitude, combined with an augmentation of warm core anti-cyclonic ADT, indicated an injection of heat and salt into the region. The changes per frontal zone in eddy activity link closely with the evolution of AAIW for each region. This connection exposes a link that has been so far underestimated. Past the point of AAIW subduction south of the APF, the water mass is thought become disconnected from its interaction with the atmosphere (Santoso and England, 2004). However, the deep reaching nature of these turbulent features appears to transfer atmospheric signals to depths reaching the AAIW layer. The water mass therefore appears to undergo transformation via interaction with the mixed layer at latitudes further north than was previously thought to occur.

In conclusion, the generated GEM and AGEM fields were found to successfully represent observations and provide an improvement from the existing established technique. The resultant 20 years of thermohaline sections showed interesting variability within the AAIW layer south of Africa, most notably a large increase in heat and salt content. A portion of the resultant property changes in AAIW may be explained by an increase in dominance and intensity of anticyclones coupled with a decrease in frequency and magnitude of cyclones; thereby indicating elevated inputs of warm, saline water into the region.

The AGEM generated time series has therefore proven to be very valuable and we look forward to further improving the method by extending longitudinally to obtain fields in 4 dimensions (4D), and perhaps by using a different proxy for the northern domain. The sizeable store of Argo data allows for the development of a GEM such as the one created here along multiple lines of longitude, separated for example by 5º. In doing so a 4D GEM for a box south of Africa could be created which would greatly improve understanding of dynamics and water mass exchanges in this important region. Using an alternative proxy for the northern domains where dynamic height does not adequately capture the convergence and interleaving of waters would also further drastically improve the GEM product. Sea water sound speed and current velocity data obtained from Current Pressure Inverted Echo Sounders (CPIES) deployed in the northern sector of the GH transect, for example, could complement the AGEM. These measurements would provide a more appropriate proxy for use in the northern reaches of the domain. However, many CPIES need to be deployed before including this proxy relation in the AGEM technique. This should be partly achieved in the near future within the CLIVAR SAMOC program (see: http://www.aoml.noaa.gov/phod/SAMOC_international/samoc_background1.php).

Many improvements can be implemented to further improve the GEM product, and with time we hope to implement these and utilize the resultant fields to obtain a better understanding of dynamics in the region of the ocean south of Africa. Despite the challenges that exist when using the current AGEM technique developed here, the resultant 20 years of thermohaline data for the Atlantic sector of the Southern Ocean provides unprecedented insight into the evolution of AAIW in this area.

Acknowledgements.

I am extremely grateful to my three supervisors, Professor Sabrina Speich, Dr Sebastiaan Swart, and Dr Isabelle Ansorge for their continued help, guidance and support over the last two years. I have learnt an enormous amount from these academics and truly appreciate all the time and effort they have put in over the duration of my Masterôs. Their devotion to and passion for the science of oceanography greatly inspired me and consequently motivated me to work harder and be truly invested in the research undertaken for this project. I would also like to thank my parents, John Hutchinson and Rosa Scalabrino, for their absolute dedication to proofreading my work, paying it a level of attention that was invaluable. As I had to submit while overseas, Damian Weldon proved to be a true friend, really helping out with the printing and submission of this thesis.

Finally, I would like to acknowledge the South African National Research Foundation, ICEMASA, the South African National Antarctic Programme, and the University of Cape Town for their financial support in the form of bursaries and travel grants over the last two years.

References.

Ansorge, I., Speich, S., Lutjeharms, J., Goni, G., Rautenbach, C.d.W., Froneman, P., Rouault, M. and Garzoli, S. 2005. Monitoring the oceanic flow between Africa and Antarctica: Report of the first GoodHope cruise. *South african journal of science.* 101(1 and 2):29-35.

Arbic, B.K. and Brechner Owens, W. 2001. Climatic Warming of Atlantic Intermediate Waters. *Journal of climate.* 14(20):4091-4108.

Arhan, M., Speich, S., Messager, C., Dencausse, G., Fine, R. and Boye, M. 2011. Anticyclonic and cyclonic eddies of subtropical origin in the subantarctic zone south of Africa. *Journal of geophysical research: Oceans (1978–2012).* 116(C11).

Banks, H.T., Wood, R.A., Gregory, J.M., Johns, T.C. and Jones, G.S. 2000. Are observed decadal changes in intermediate water masses a signature of anthropogenic climate change? *Geophysical research letters.* 27(18):2961-2964.

Biastoch, A., Böning, C.W., Schwarzkopf, F. and Lutjeharms, J. 2009. Increase in Agulhas leakage due to poleward shift of Southern Hemisphere westerlies. *Nature.* 462(7272):495-498.

Boebel, O., Lutjeharms, J., Schmid, C., Zenk, W., Rossby, T. and Barron, C. 2003. The Cape Cauldron: a regime of turbulent inter-ocean exchange. *Deep sea research part II: Topical studies in oceanography.* 50(1):57-86.

Böning, C.W., Dispert, A., Visbeck, M., Rintoul, S. and Schwarzkopf, F. 2008. The response of the Antarctic Circumpolar Current to recent climate change. *Nature geoscience.* 1(12):864-869.

Book, J.W., Wimbush, M., Imawaki, S., Ichikawa, H., Uchida, H. and Kinoshita, H. 2002. Kuroshio temporal and spatial variations south of Japan determined from inverted echo sounder measurements. *Journal of geophysical research.* 107(C9):3121.

David, A. (2012) - Fronts, tourbillons et transferts meridiens dans lôocean Austral au sud de lôAfrique a partir de lôaltimetrie satellitale. Thèse de doctorat de l'Université de Bretagne Occidentale.

Dencausse, G., Arhan, M. and Speich, S. 2010a. Spatio-temporal characteristics of the Agulhas Current retroflection. *Deep sea research part I: Oceanographic research papers.* 57(11):1392-1405.

Dencausse, G., Arhan, M. and Speich, S. 2010b. Routes of Agulhas rings in the southeastern Cape Basin. *Deep sea research part I: Oceanographic research papers.* 57(11):1406-1421.

Ducet, N., Le Traon, P. and Reverdin, G. 2000. Global high-resolution mapping of ocean circulation from TOPEX/Poseidon and ERS-1 and-2. *Journal of geophysical research: Oceans (1978–2012).* 105(C8):19477-19498.

Faure, V., Arhan, M., Speich, S. and Gladyshev, S. 2011. Heat budget of the surface mixed layer south of Africa. *Ocean dynamics.* 61(10):1441-1458.

Feron, R.C., De Ruijter, W.P. and Oskam, D. 1992. Ring shedding in the Agulhas Current system. *Journal of geophysical research.* 97(C6):9467-9477.

Fine, R.A. 1993. Circulation of Antarctic intermediate water in the South Indian Ocean. *Deep sea research part I: Oceanographic research papers.* 40(10):2021-2042.

Garzoli, S.L. and Matano, R. 2011. The South Atlantic and the Atlantic meridional overturning circulation. *Deep sea research part II: Topical studies in oceanography.* 58(17):1837-1847.

Gille, S.T. 2002. Warming of the Southern Ocean Since the 1950s. *Science*, 295: 1275-1277.

Gille, S.T. 2008. Decadal-scale temperature trends in the Southern Hemisphere ocean. *Journal of climate.* 21(18):4749-4765.

Gladyshev, S., Arhan, M., Sokov, A. and Speich, S. 2008. A hydrographic section from South Africa to the southern limit of the Antarctic Circumpolar Current at the Greenwich meridian. *Deep sea research part I: Oceanographic research papers.* 55(10):1284-1303.

Goni, G.J., Garzoli, S.L., Roubicek, A.J., Olson, D.B. and Brown, O.B. 1997. Agulhas ring dynamics from TOPEX/POSEIDON satellite altimeter data. *Journal of marine research.* 55(5):861-883.

Gordon, A. L., and H. Taylor. 1975. Seasonal change of Antarctic sea ice cover. *Science*, 187, 346-347

Gordon, A.L. 1981. Seasonality of Southern Ocean sea ice. *Journal of geophysical research: Oceans (1978–2012).* 86(C5):4193-4197.

Gould, J., Roemmich, D., Wijffels, S., Freeland, H., Ignaszewsky, M., Jianping, X., Pouliquen, S., Desaubies, Y. et al. 2004. Argo profiling floats bring new era of in situ ocean observations. *Eos, transactions american geophysical union.* 85(19):185-191.

Jacobs, S. and Georgi, D. 1977. Observations on the southwest Indian/Antarctic Ocean. *Deep-sea res.* 24:43-84.

Killworth, P.D. and Hughes, C.W. 2002. The Antarctic Circumpolar Current as a free equivalent-barotropic jet. *Journal of marine research.* 60(1):19-45.

Le Traon, P., Nadal, F. and Ducet, N. 1998. An improved mapping method of multisatellite altimeter data. *Journal of atmospheric and oceanic technology.* 15(2):522-534.

Le Traon, P. and Ogor, F. 1998. ERS-1/2 orbit improvement using TOPEX/POSEIDON: The 2 cm challenge. *Journal of geophysical research: Oceans (1978–2012).* 103(C4):8045-8057.

Legeais, J., Speich, S., Arhan, M., Ansorge, I., Fahrbach, E., Garzoli, S. and Klepikov, A. 2005. The baroclinic transport of the Antarctic Circumpolar Current south of Africa. *Geophysical research letters.* 32(24).

Lemke, P. 1992. *WHP cruise summary information: A12.*

Levitus, S., Antonov, J.I., Boyer, T.P. and Stephens, C. 2000. Warming of the world ocean. *Science.* 287(5461):2225-2229.

Lovenduski, N.S. and Ito, T. 2009. The future evolution of the Southern Ocean CO2 sink. *Journal of marine research.* 67(5):597-617.

Lutjeharms, J. 1996. The exchange of water between the South Indian and South Atlantic Oceans. In *The South Atlantic.* Springer. 125-162.

Lutjeharms, J. and Van Ballegooyen, R. 1988. The retroþection of the Agulhas Current. *J.phys.Ocean0gr.* 18:1570-1583.

McCartney, M.S. 1982. The subtropical recirculation of mode waters. *J.mar.res.* 40:427-464.

Meijers, A., Bindoff, N. and Rintoul, S. 2011a. Estimating the four-dimensional structure of the Southern Ocean using satellite altimetry. *Journal of atmospheric and oceanic technology.* 28(4):548-568.

Meijers, A., Bindoff, N. and Rintoul, S. 2011b. Frontal movements and property fluxes: Contributions to heat and freshwater trends in the Southern Ocean. *Journal of geophysical research.* 116(C8):C08024.

Meinen, C.S. 2001. Structure of the North Atlantic Current in stream-coordinates and the circulation in the Newfoundland Basin. *Deep sea research part I: Oceanographic research papers.* 48(7):1553-1580.

Meinen, C.S. and Watts, D.R. 2000. Vertical structure and transport on a transect across the North Atlantic Current near 42 N: Time series and mean. *Journal of geophysical research: Oceans (1978–2012).* 105(C9):21869-21891.

Meredith, M.P. and Hogg, A.M. 2006. Circumpolar response of Southern Ocean eddy activity to a change in the Southern Annular Mode. *Geophysical research letters.* 33(16).

Olbers, D., Gouretski, V., Seiß, G. and Schröter, J. 1992. Hydrographic Atlas of the Southern Ocean, 17 pp. 82 plates, Alfred Wegener Inst. for Polar and Mar. *Res., bremerhaven, germany.*

Orsi, A.H., Whitworth, T. and Nowlin, W.D. 1995. On the meridional extent and fronts of the Antarctic Circumpolar Current. *Deep sea research part I: Oceanographic research papers.* 42(5):641-673.

Pahnke, K., Goldstein, S.L. and Hemming, S.R. 2008. Abrupt changes in Antarctic Intermediate Water circulation over the past 25,000 years. *Nature geoscience.* 1(12):870-874.

Peterson, R.G. and Stramma, L. 1991. Upper-level circulation in the South Atlantic Ocean. *Progress in oceanography.* 26(1):1-73.

Piola, A.R. and Georgi, D.T. 1982. Circumpolar properties of Antarctic intermediate water and Subantarctic Mode Water. *Deep sea research part A.oceanographic research papers.* 29(6):687-711.

Rimaud, J., Speich, S., Blanke, B. and Grima, N. 2012. The exchange of Intermediate Water in the southeast Atlantic: Water mass transformations diagnosed from the Lagrangian analysis of a regional ocean model. *Journal of geophysical research: Oceans (1978–2012).* 117(C8).

Rintoul, S., Donguy, J. and Roemmich, D. 1997. Seasonal evolution of upper ocean thermal structure between Tasmania and Antarctica. *Deep sea research part I: Oceanographic research papers.* 44(7):1185-1202.

Rintoul, S., W Hughes, C. and Olbers, D. 2001. .6 The antarctic circumpolar current system. *International geophysics.* 77:271-XXXVI.

Rintoul, S., Speer, K., Sparrow, M., Meredith, M., Hofmann, E., Fahrbach, E., Summerhayes, C., Worby, A. et al. 2010. Southern Ocean Observing System (SOOS): Rationale and strategy for sustained observations of the Southern Ocean. *Proceedings of OceanObs '09: Sustained ocean observations and information for society.*

Rintoul, S.R., Sokolov, S. and Church, J. 2002. A 6 year record of baroclinic transport variability of the Antarctic Circumpolar Current at 140 E derived from expendable bathythermograph and altimeter measurements. *Journal of geophysical research.* 107(C10):3155.

Rio, M., Schaeffer, P., Moreaux, G., Lemoine, J. and Bronner, E. 2009. A new mean dynamic topography computed over the global ocean from GRACE data, altimetry and in-situ measurements. *Poster communication at OceanObs09 symposium.*

Roether, W., M. Samthein, T. J. Muller, W. Nellen, and D. Sahrhage. 1990. Sudatlantik-zircumpolarstrom, reise nr. 11, 3 Oktober 1989 ï 11 Marz 1990, meteor-ber. 90-2, technical report, Univ. of Hamburg, Hamburg, Germany.

Roemmich, D.H., Davis, R.E., Riser, S.C., Owens, W.B., Molinari, R.L., Garzoli, S.L. and Johnson, G.C. 2003. *The argo project.global ocean observations for understanding and prediction of climate variability.*

Roemmich, D.H., Davis, R.E., Riser, S.C., Owens, W.B., Molinari, R.L., Garzoli, S.L. and Johnson, G.C. 2003. *The argo project.global ocean observations for understanding and prediction of climate variability.*

Roemmich, D., Johnson, G.C., Riser, S., Davis, R., Gilson, J., Owens, W.B., Garzoli, S.L., Schmid, C. et al. 2009. The Argo Program: Observing the global ocean with profiling floats.

Roemmich, D., Riser, S., Davis, R. and Desaubies, Y. 2004. Autonomous profiling floats: Workhorse for broad-scale ocean observations. *Mar.technol.soc.J.* 38(2):21-29.

Rusciano, E., Speich, S. and Ollitrault, M. 2012. Interocean exchanges and the spreading of Antarctic Intermediate Water south of Africa. *Journal of geophysical research: Oceans (1978–2012).* 117(C10).

Santoso, A. and England, M.H. 2004. Antarctic Intermediate Water circulation and variability in a coupled climate model. *Journal of physical oceanography.* 34(10):2160-2179.

Sloyan, B.M. and Rintoul, S.R. 2001. Circulation, Renewal, and Modification of Antarctic Mode and Intermediate Water*. *Journal of physical oceanography.* 31(4):1005-1030.

Sokolov, S., King, B.A., Rintoul, S.R. and Rojas, R.L. 2004. Upper ocean temperature and the baroclinic transport stream function relationship in Drake Passage. *Journal of geophysical research: Oceans (1978–2012).* 109(C5).

Sokolov, S. and Rintoul, S.R. 2002. Structure of Southern Ocean fronts at 140 E. *Journal of marine systems.* 37(1):151-184.

Sokolov, S. and Rintoul, S.R. 2007. Multiple Jets of the Antarctic Circumpolar Current South of Australia*. *Journal of physical oceanography.* 37(5):1394-1412.

Sokolov, S. and Rintoul, S.R. 2009. Circumpolar structure and distribution of the Antarctic Circumpolar Current fronts: 1. Mean circumpolar paths. *Journal of geophysical research: Oceans (1978–2012).* 114(C11).

Speich, S. and Arhan, M. 2007. GOODHOPE/Southern Ocean: A study and monitoring of the Indo-Atlantic connections. *Mercator newsletter, october.* 27:29-41.

Speich, S., Blanke, B. and Cai, W. 2007. Atlantic meridional overturning circulation and the Southern Hemisphere supergyre. *Geophysical research letters.* 34(23):L23614.

Speich, S., and F. Dehairs. 2008. MD166 international polar year BONUS-GoodHope cruise report, technical report, Inst. Fr. de Rech. Pour lôExploit. de la Mer, Brest France

Speich, S., Blanke, B. and Madec, G. 2001. Warm and cold water routes of an OGCM thermohaline conveyor belt. *Geophysical research letters.* 28(2):311-314.

Stommel, H. 1947. Note on the use of TS correlation for dynamic height anomaly computations. *J.mar.res.* 6(2):85-92.

Sun, C. and Watts, D.R. 2001. A circumpolar gravest empirical mode for the Southern Ocean hydrography. *Journal of geophysical research.* 106(C2):2833-2855.

Sun, C. and Watts, D.R. 2002a. A view of ACC fronts in streamfunction space. *Deep sea research part I: Oceanographic research papers.* 49(7):1141-1164.

Sun, C. and Watts, D.R. 2002b. A pulsation mode in the Antarctic Circumpolar Current south of Australia. *Journal of physical oceanography.* 32(5):1479-1495.

Sverdrup, H.U., Johnson, M.W. and Fleming, R.H. 1942. *The oceans: their physics, chemistry, and general biology.* Prentice-Hall New York.

Swart, S. and Speich, S. 2010. An altimetry-based gravest empirical mode south of Africa: 2. Dynamic nature of the Antarctic Circumpolar Current fronts. *Journal of geophysical research: Oceans (1978–2012).* 115(C3).

Swart, S., Speich, S., Ansorge, I.J., Goni, G.J., Gladyshev, S. and Lutjeharms, J.R. 2008. Transport and variability of the Antarctic Circumpolar Current south of Africa. *Journal of geophysical research: Oceans (1978–2012).* 113(C9).

Swart, S., Speich, S., Ansorge, I.J. and Lutjeharms, J.R. 2010. An altimetry-based gravest empirical mode south of Africa: 1. Development and validation. *Journal of geophysical research: Oceans (1978–2012).* 115(C3).

Talley, L. 1996. Antarctic intermediate water in the South Atlantic. In *The South Atlantic.* Springer. 219-238.

Watts, D.R., Sun, C. and Rintoul, S. 2001. A two-dimensional gravest empirical mode determined from hydrographic observations in the Subantarctic Front. *Journal of physical oceanography.* 31(8):2186-2209.

Watts, D.R., Sun, C. and Rintoul, S. 2001. A two-dimensional gravest empirical mode determined from hydrographic observations in the Subantarctic Front. *Journal of physical oceanography.* 31(8):2186-2209.

Whitworth III, T. and Peterson, R. 1985. Volume transport of the Antarctic Circumpolar Current from bottom pressure measurements. *Journal of physical oceanography.* 15(6):810-816.

World Ocean Circulation Experiment. 2002. World Ocean Circulation Experiment, Global data, version 3.0, technical report, Natl. Oceanogr. Data Cent., Silver Spring, Md.

Zwally, H.J., Comiso, J.C., Parkinson, C.L., Cavalieri, D.J. and Gloersen, P. 2002. Variability of Antarctic sea ice 1979ï 1998. *Journal of geophysical research: Oceans (1978–2012).* 107(C5):9-1-9-19.